Supporting Information for

Heteroatom engineering enhancing thermoelectric power factor of molecular junctions

W. Peng, N. Chen, Y. Xie, Assoc. Prof. Y. Li

Key Laboratory of Organic Optoelectronics and Molecular Engineering, Department of Chemistry, Tsinghua University, Beijing 100084, China

E-mail: yuanli_thu@tsinghua.edu.cn.

Assoc. Prof. L. Ma

State Key Laboratory of Metastable Materials Science & Technology and Key Laboratory for Microstructural Material Physics of Hebei Province, School of Science, Yanshan University, Qinhuangdao 066004, China

E-mail: maliang-phy@ysu.edu.cn.

Prof. J. Lü

School of Physics and Wuhan National High Magnetic Field Center, Huazhong University of Science and Technology, Wuhan 430074, China

Wuhan Institute of Quantum Technology, Wuhan 430074, China

E-mail: jtlu@hust.edu.cn.

S1. Synthesis.

General Methods. All reagents and solvents were purchased from commercial sources and used. Manipulations were performed under a normal laboratory atmosphere unless otherwise noted. Nuclear magnetic resonance (NMR) spectra were recorded at ambient temperature using Bruker AVANCE III 400 spectrometers, with working frequencies of 400 MHz for ^{1}H and 100 MHz for ^{13}C, respectively. Chemical shifts are reported in ppm relative to the residual internal non-deuterated solvent signals ($CDCl_3$). The samples were performed with a Waters Synapt G2-Si ESI-Q-TOF High resolution MS system, equipped with a Waters Acquity H class Ultra High Performance Liquid Chromatograph (UHPLC).

Synthesis and Characterization of Compounds

5-iodo-1-pentylthioacetate (I-C_5-SAc) as prepared according to a literature method.[1] 1, 5-diiodopentane (10.00 g, 30.80 mmol) and potassium thioacetate (0.87 g, 7.70 mmol) were added into 300 mL tetrahydrofuran, stirred for 12h at room temperature, followed by removal of the acetone under reduced pressure. The residue was dissolved in diethyl ether, filtered, and washed with DI water. The organic layer was dried over Na_2SO_4, filtered and concentrated after which the raw product was purified with column chromatography with ethyl acetate and hexane (1: 10). Yield: 1.57 g (6.90 mmol) 5-iodo-1-pentylthioacetate (89.0 % yield). ^{1}H NMR (400 MHz, $CDCl_3$) δ 3.18 (t, J = 6.9 Hz, 2H), 2.87 (t, J = 7.2 Hz, 2H), 2.33 (s, 3H), 1.84 (p, J = 7.1 Hz, 2H), 1.64 – 1.56 (m, 2H), 1.52 – 1.44 (m, 2H). ^{13}C NMR (100 MHz, Chloroform-*d*) δ 195.77, 32.87, 30.70, 29.59, 28.80, 28.51, 6.61. HRMS (ESI+): m/z calc for $C_7H_{13}IOS$ [M+H]$^{+}$ 272.9810, found 272.9806.

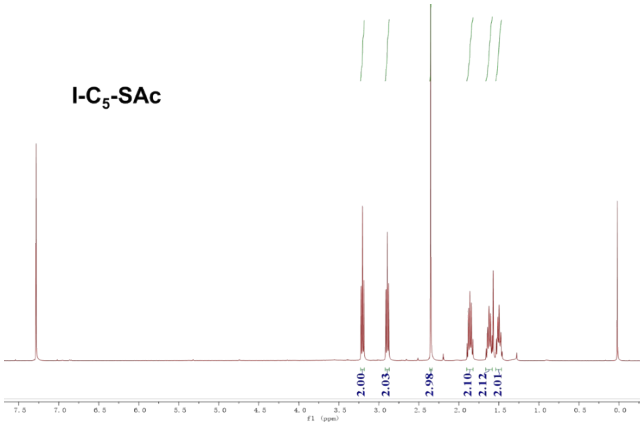

Fig. S1. The ^{1}H-NMR spectrum of compound I-C_5-SAc.

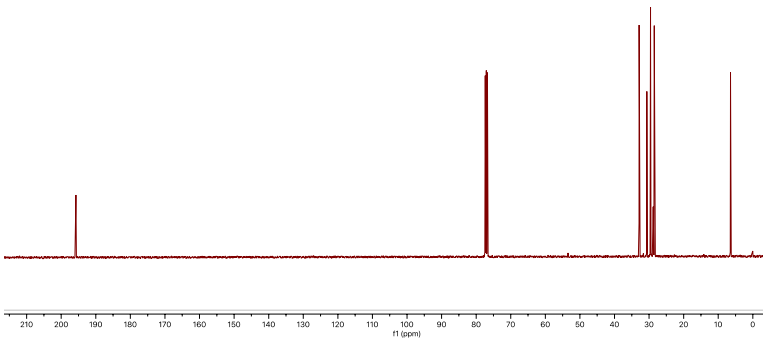

Fig. S2. The ^{13}C-NMR spectrum of compound I-C_5-SAc.

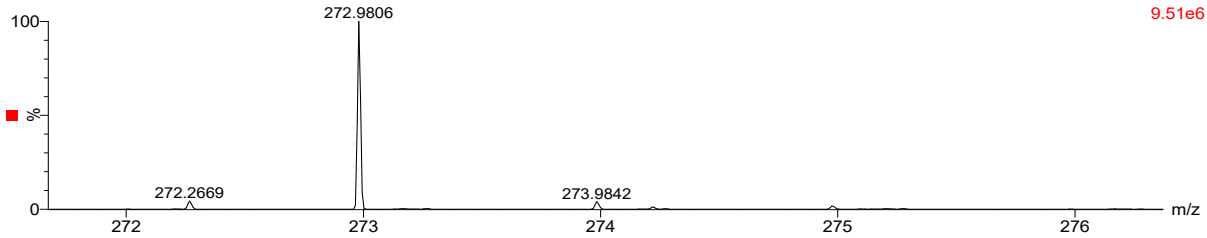

Fig. S3. The HRMS spectrum of compound I-C_5-SAc.

5-iodopentane-1-thiol (HS-C_5-I) was synthesized as follows. 5-iodo-1-pentylthioacetate was dissolved (1.37 g, 6.02 mmol) in 40 mL methanol and degassed for 20 min. Subsequently, 1.5 mL trifluoroacetic acid was added. The solution was refluxed for 5h then cooled down to room temperature. The solvent was removed by rotary evaporator; DCM was used to extract the product. The organic layer was washed with DI water 3 times before dried over anhydrous Na_2SO_4. After filtration and concentration, the raw product was purified by column chromatography with hexane as eluent. Yield: 18 % (0.25 g, 1.08 mmol). ^{1}H NMR (400 MHz, Chloroform-*d*) δ 3.19 (t, *J* = 7.0 Hz, 2H), 2.57 – 2.51 (m, 2H), 1.84 (p, *J* = 7.0 Hz, 2H), 1.68 – 1.60 (m, 2H), 1.54 – 1.47 (m, 2H). ^{13}C NMR (100 MHz, Chloroform-*d*) δ 38.70, 33.07, 29.35, 28.11, 6.57. HRMS (ESI+): m/z calc for $C_5H_{11}IS$ $[M+H]^+$ 228.9548, found 228.9569.

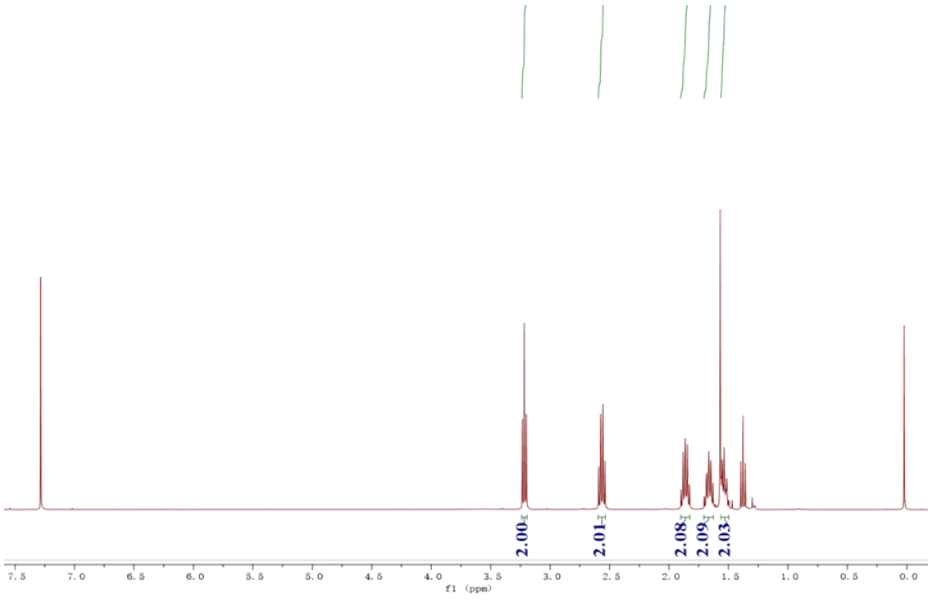

Fig. S4. The ^{1}H-NMR spectrum of compound HS-C_5-I.

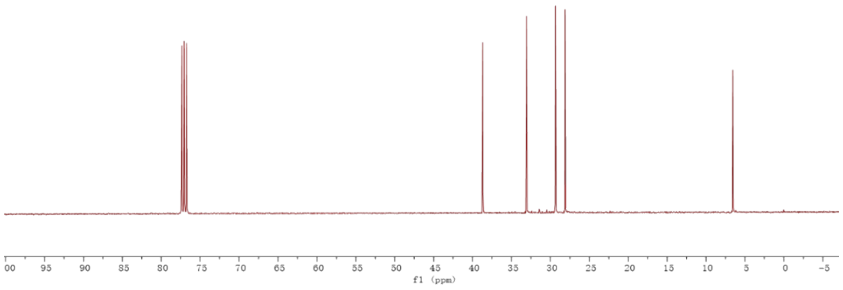

Fig. S5. The ^{13}C-NMR spectrum of compound HS-C_5-I.

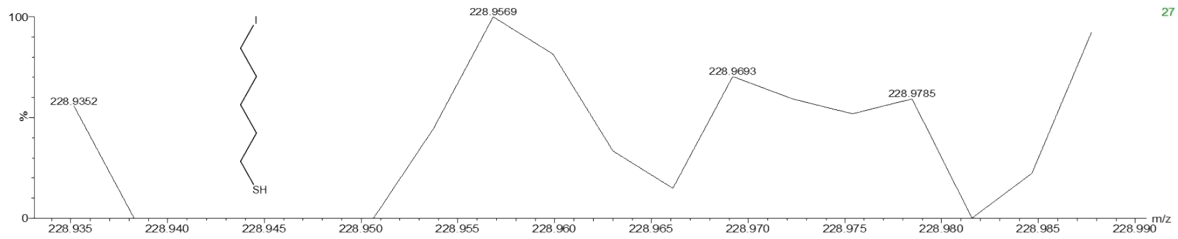

Fig. S6. The HRMS spectrum of compound HS-C_5-I.

***S*-(8-iodooctyl) ethanethioate (I-C_8-SAc)** as prepared as follows.[1] 1,8-diiodooctane (5.00 g, 13.66 mmol) and potassium thioacetate (0.39 g, 3.42 mmol) were added into 200 mL tetrahydrofuran, stirred for 12h at room temperature, followed by removal of the tetrahydrofuran under reduced pressure. The residue was dissolved in diethyl ether, filtered,

and washed with DI water. The organic layer was dried over Na_2SO_4, filtered and concentrated after which the raw product was purified with column chromatography with ethyl acetate and hexane (1: 10). Yield: 0.95 g (3.04 mmol) *S*-(8-iodooctyl) ethanethioate (89.0 % yield). ^{1}H NMR (400 MHz, Chloroform-*d*) δ 3.19 (t, *J* = 7.0 Hz, 2H), 2.87 (t, *J* = 7.3 Hz, 2H), 2.33 (s, 3H), 1.82 (p, *J* = 7.1 Hz, 2H), 1.60 – 1.56 (m, 2H), 1.32 (q, *J* = 6.1, 4.8 Hz, 8H). ^{13}C NMR (100 MHz, Chloroform-*d*) δ 196.03, 33.47, 30.68, 30.40, 29.46, 29.10, 28.88, 28.67, 28.36, 7.26. HRMS (ESI+): m/z calc for $C_{10}H_{19}IOS$ $[M+H]^+$ 315.0274, found 315.0270.

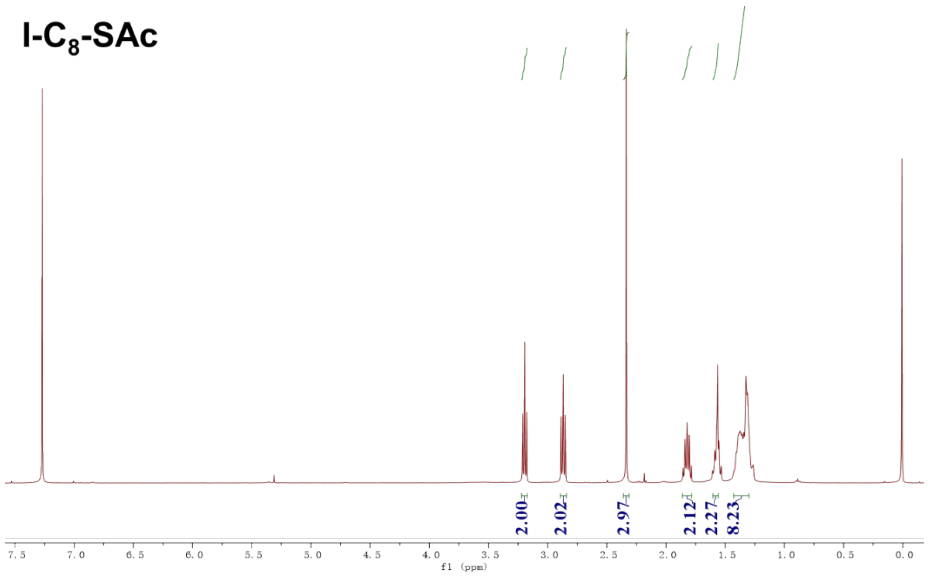

Fig. S7. The ^{1}H-NMR spectrum of compound I-C_8-SAc.

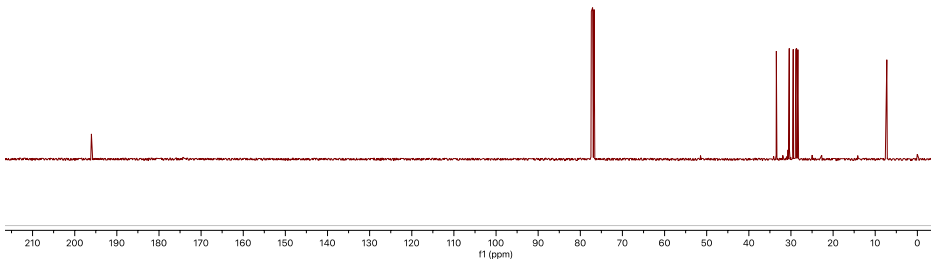

Fig. S8. The ^{13}C spectrum of compound I-C_8-SAc.

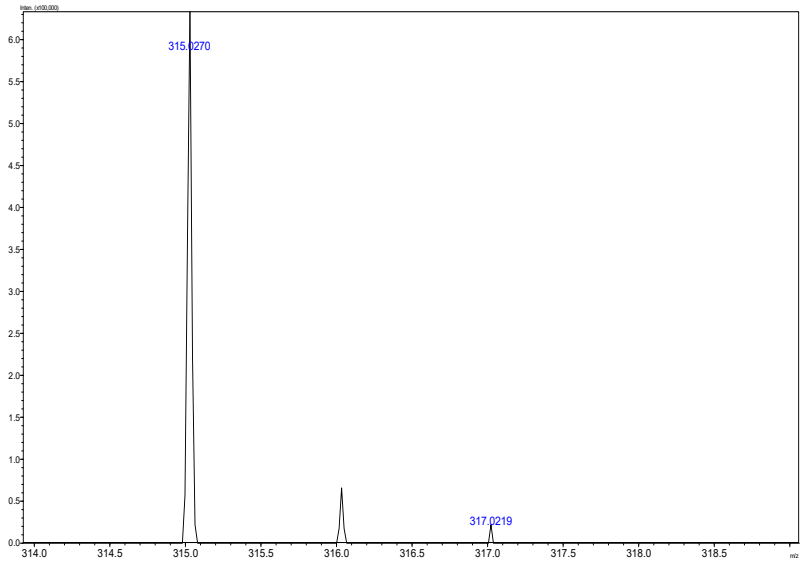

Fig. S9. The HRMS spectrum of compound I-C_8-SAc.

8-iodooctane-1-thiol (HS-C_8-I) was synthesized as follows. *S*-(8-iodooctyl) ethanethioate was dissolved (0.71 g, 2.27 mmol) in 30 mL methanol and degassed for 20 min. Subsequently, 1.0 mL trifluoroacetic acid was added. The solution was refluxed for 5h then cooled down to room temperature. The solvent was removed by rotary evaporator; DCM was used to extract the product. The organic layer was washed with DI water 3 times before dried over anhydrous Na_2SO_4. After filtration and concentration, the raw product was purified by column chromatography with hexane as eluent. Yield: 18 % (0.11 g, 0.41 mmol). ^{1}H NMR (400 MHz, Chloroform-*d*) δ 3.21 (t, *J* = 7.0 Hz, 2H), 2.55 (q, *J* = 7.4 Hz, 2H), 1.84 (p, *J* = 7.1 Hz, 2H), 1.63 (t, *J* = 7.4 Hz, 2H), 1.45 – 1.33 (m, 8H). ^{13}C NMR (100 MHz, Chloroform-*d*) δ 33.96, 33.49, 30.42, 29.66, 28.86, 28.42, 28.25, 24.63, 7.27. HRMS (ESI+): m/z calc for $C_8H_{16}IS$ $[M+H]^+$ 271.0017, found 271.0226.

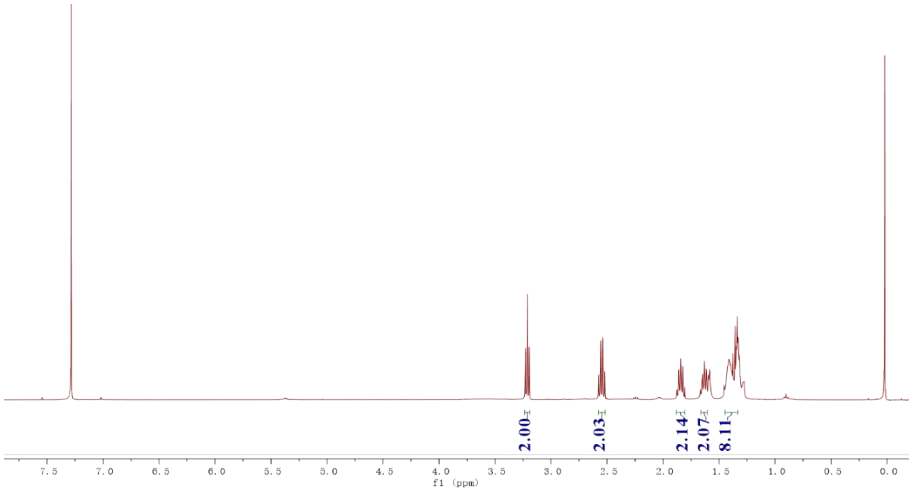

Fig. S10. The ^{1}H-NMR spectrum of compound HS-C_8-I.

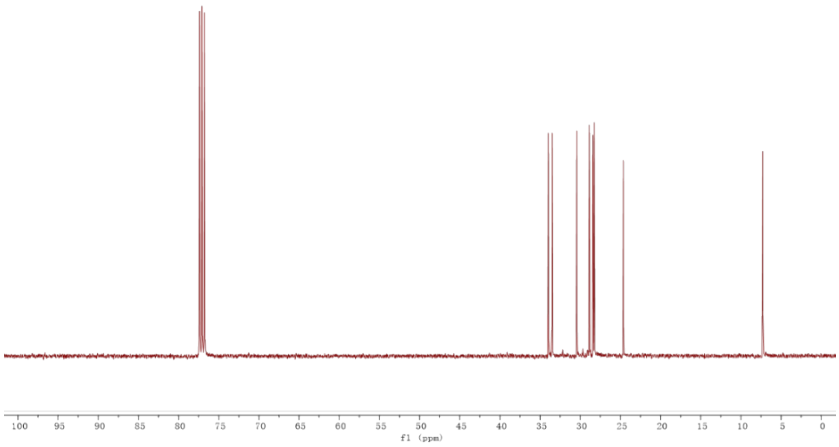

Fig. S11. The ^{13}C spectrum of compound HS-C_8-I.

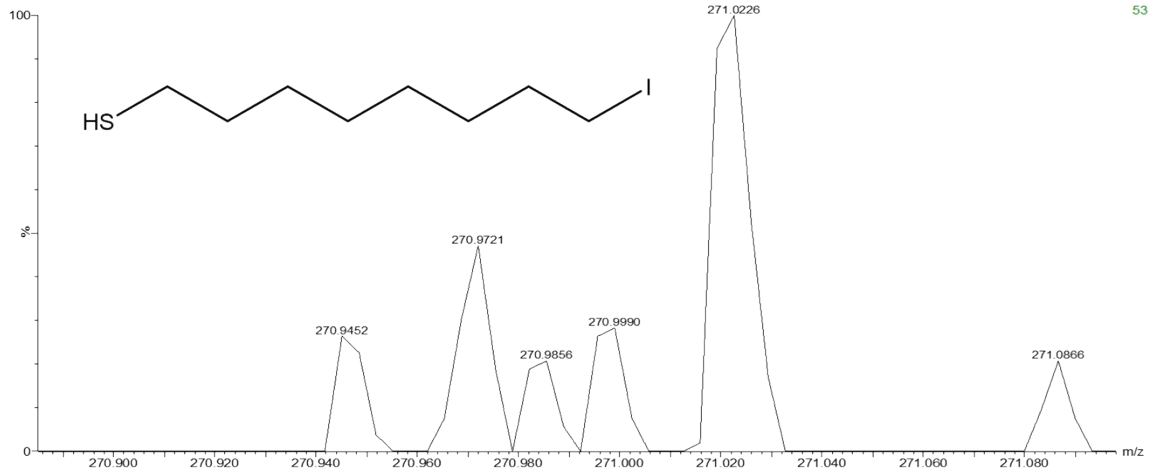

Fig. S12. The HRMS spectrum of compound HS-C_8-I.

1,11-diiodoundecane (I-C_{11}-I) was prepare as follows.[1] 1,11-dibromoundecane (11.80 g, 34.60 mmol) and sodium iodide (15.00 g, 138.00 mmol) were added into 300 mL acetone, refluxed for 5h, cooled down, followed by removal of the acetone under reduced pressure. The residue was dissolved in diethyl ether, filtered, and washed with DI water. The organic layer was dried over Na_2SO_4, filtered and concentrated after which the raw product was purified with column chromatography with hexane. Yield: 12.7 g (31.14 mmol) 1,11-diiodoundecane (90.0 % yield). ^{1}H NMR (400 MHz, Chloroform-*d*) δ 3.20 (td, *J* = 7.1, 1.6 Hz, 4H), 1.88 – 1.79 (m, 4H), 1.39 (q, *J* = 6.8 Hz, 4H), 1.29 (s, 10H).

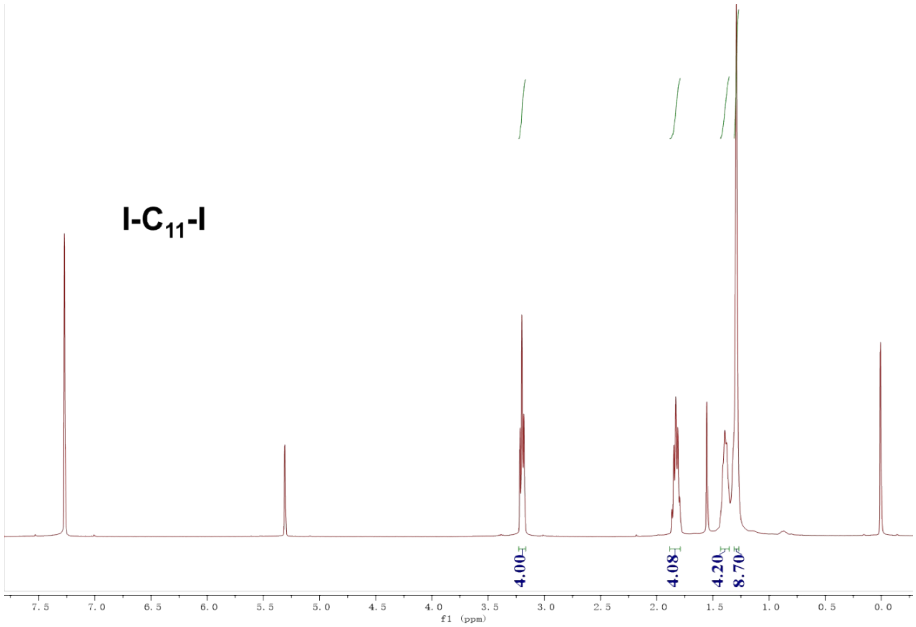

Fig. S13. The ^{1}H-NMR spectrum of compound I-C_{11}-I.

***S*-(11-iodoundecyl) ethanethioate (I-C_{11}-SAc)** was prepared as follows[1]. 1,11-diiodoundecane (17.00 g, 41.7 mmol) and potassium thioacetate (1.20 g, 10.50 mmol) were added into 300 mL tetrahydrofuran, stirred for 12h at room temperature, followed by removal of the tetrahydrofuran under reduced pressure. The residue was dissolved in diethyl ether, filtered, and washed with DI water. The organic layer was dried over Na_2SO_4, filtered and concentrated after which the raw product was purified with column chromatography with dichloromethane and hexane (1: 2). Yield: 3.32 g (9.35 mmol) *S*-(11-iodoundecyl) ethanethioate (89.0 % yield). ^{1}H NMR (400 MHz, Chloroform-*d*) δ 3.21 (t, *J* = 7.0 Hz, 2H),

2.88 (t, J = 7.3 Hz, 2H), 2.34 (s, 3H), 1.84 (p, J = 7.1 Hz, 2H), 1.61 – 1.55 (m, 3H), 1.43 – 1.27 (m, 14H).

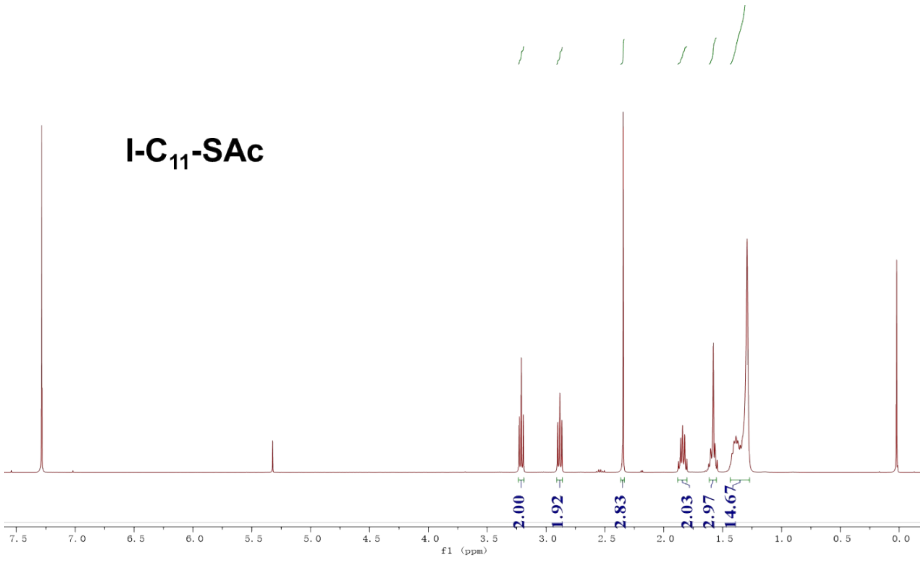

Fig. S14. The ^{1}H-NMR spectrum of compound I-C_{11}-SAc.

11-iodoundecane-1-thiol (HS-C_{11}-I) was prepared as follows. *S*-(11-iodoundecyl) ethanethioate (2.17 g, 6.11 mmol) was dissolved in 50 mL methanol and degassed for 20 min. Subsequently, 4.0 mL trifluoroacetic acid was added. The solution was refluxed for 5h then cooled down to room temperature. The solvent was removed by rotary evaporator; DCM was used to extract the product. The organic layer was washed with DI water 3 times before dried over anhydrous Na_2SO_4. After filtration and concentration, the raw product was purified by column chromatography with dichloromethane and hexane (1: 2) as eluent. Yield: 18 % (0.36 g, 1.10 mmol). ^{1}H NMR (400 MHz, Chloroform-*d*) δ 3.18 (t, J = 7.0 Hz, 2H), 2.51 (q, J = 7.4 Hz, 2H), 1.81 (p, J = 7.1 Hz, 2H), 1.59 (p, J = 7.2 Hz, 2H), 1.37 – 1.24 (m, 14H). ^{13}C NMR (100 MHz, Chloroform-*d*) δ 34.05, 33.57, 30.51, 29.47, 29.40, 29.07, 28.54, 28.38, 24.68, 7.36. HRMS (ESI+): m/z calc for $C_{11}H_{22}IS$ $[M+H]^+$ 313.0487, found 313.0439.

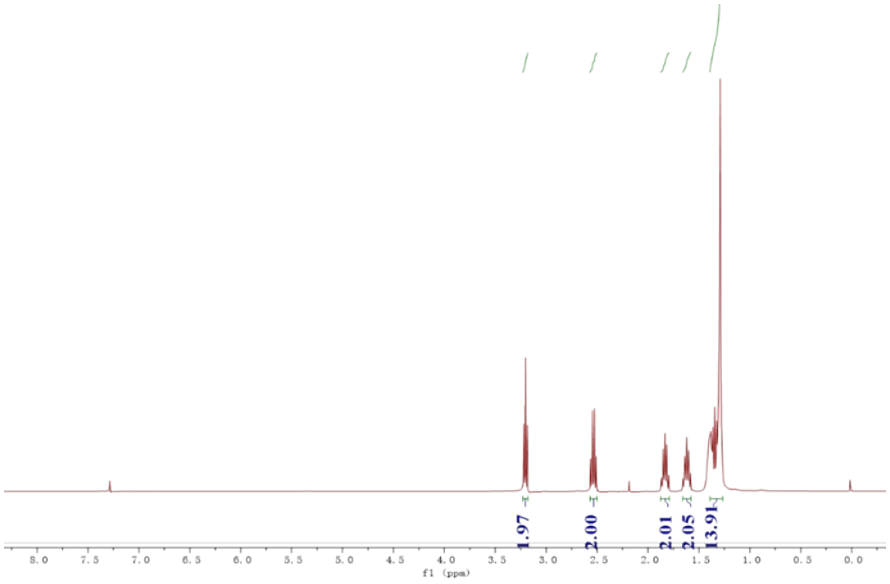

Fig. S15. The ^{1}H-NMR spectrum of compound HS-C_{11}-I.

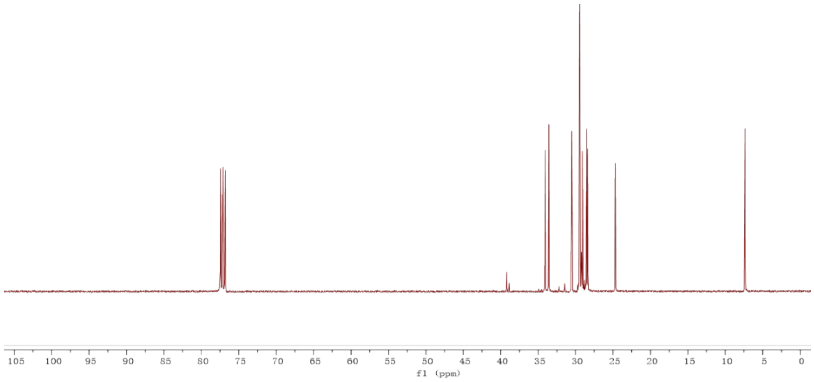

Fig. S16. The ^{13}C-NMR spectrum of compound HS-C_{11}-I.

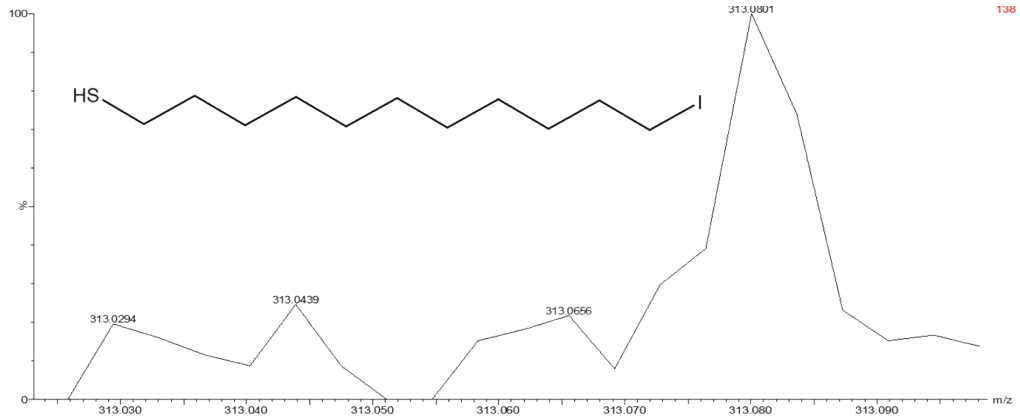

Fig. S17. The HRMS spectrum of compound HS-C_{11}-I.

1,14-dibromotetradecane (Br-C14-Br) was synthesized according to previous reported method.[2] A 50 mL solution of triphenylphosphine (3.93 g, 15 mmol) in anhydrous THF was

added to a stirred solution of N-bromosuccinamide (NBS, 2.67 g, 15 mmol) in 50 mL THF at 0 ˚C. With vigorous stirring, a solution of 1,14-tetradecanediol (1.00 g, 4.34 mmol) in 25 mL THF was slowly added to the mixture of NBS and Ph_3P. The resulting solution was warmed to rt and then heated at 50 ˚C for 3.5 h. The THF was then removed under reduced pressure and the residue crystallized from ethanol to obtain 1.1 g of the product as a white powder (70% yield). ^{1}H NMR (400 MHz, Chloroform-*d*) δ 3.43 (t, *J* = 6.9 Hz, 4H), 1.88 (p, *J* = 6.9 Hz, 4H), 1.44 (q, *J* = 7.0 Hz, 4H), 1.30 (d, *J* = 6.4 Hz, 16H).

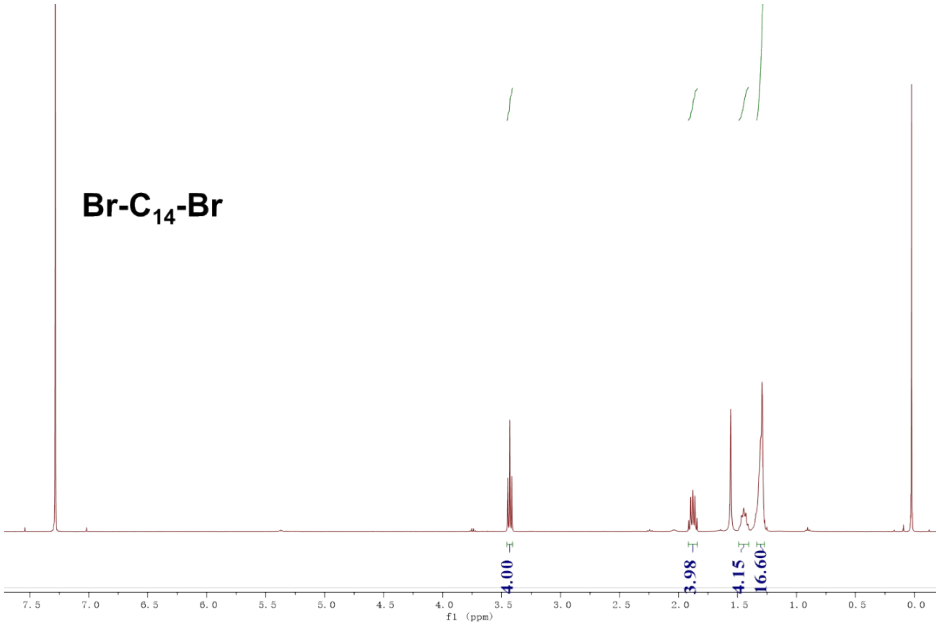

Fig. S18. The ^{1}H-NMR spectrum of compound Br-C_{14}-Br.

1,14-diiodotetradecane (**I-C_{14}-I**) was prepare as follows[1]. 1,14-dibromotetradecane (2.52 g, 7.00 mmol) and sodium iodide (4.00 g, 28.00 mmol) were added into 200 mL acetone, refluxed for 5h, cooled down, followed by removal of the acetone under reduced pressure. The residue was dissolved in diethyl ether, filtered, and washed with DI water. The organic layer was dried over Na_2SO_4, filtered and concentrated after which the raw product was purified with column chromatography with hexane. Yield: 2.84 g (6.30 mmol) 1,14-diiodotetradecane (90.0 % yield). 1H NMR (400 MHz, Chloroform-d) δ 3.20 (t, J = 7.0 Hz, 4H), 1.83 (p, J = 7.1 Hz, 4H), 1.43 – 1.36 (m, 4H), 1.32 – 1.26 (m, 16H).

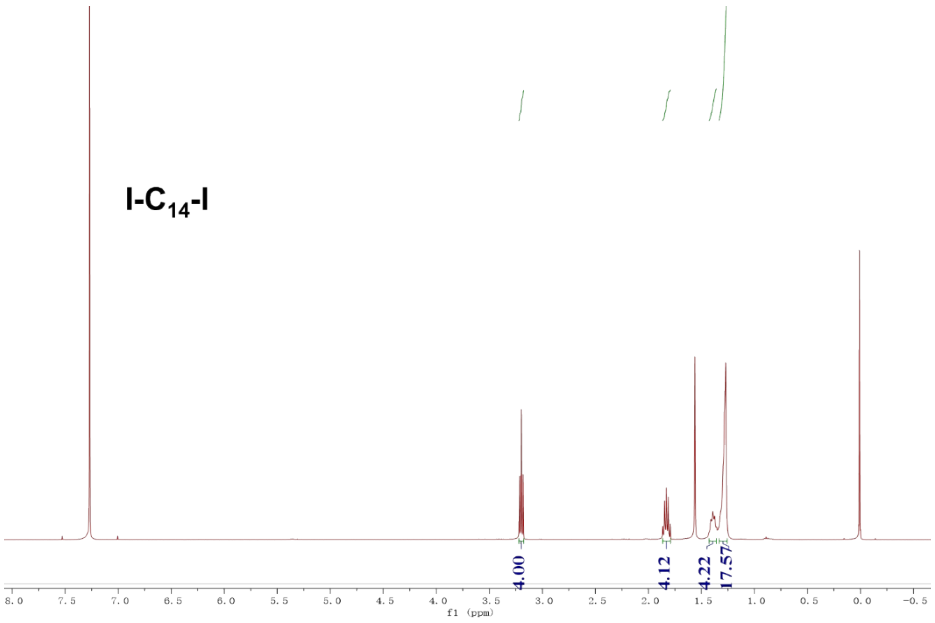

Fig. S19. The ^{1}H-NMR spectrum of compound I-C_{14}-I.

***S*-(14-iodotetradecyl) ethanethioate (I-C_{14}-SAc)** was prepared as follows.[1] 1,14-diiodotetradecane (13.56 g, 30.00 mmol) and potassium thioacetate (1.05 g, 7.50 mmol) were added into 300 mL tetrahydrofuran, stirred for 12h at room temperature, followed by removal of the tetrahydrofuran under reduced pressure. The residue was dissolved in diethyl ether, filtered, and washed with DI water. The organic layer was dried over Na_2SO_4, filtered and concentrated after which the raw product was purified with column chromatography with dichloromethane and hexane (1: 2). Yield: 2.60 g (6.68 mmol) *S*-(14-iodotetradecyl) ethanethioate (89.0 % yield). ^{1}H NMR (400 MHz, Chloroform-*d*) δ 3.21 (t, *J* = 7.0 Hz, 2H), 2.89 (t, *J* = 7.4 Hz, 2H), 2.35 (s, 3H), 1.84 (p, *J* = 7.1 Hz, 2H), 1.61 (d, *J* = 7.0 Hz, 2H), 1.28 (s, 20H).

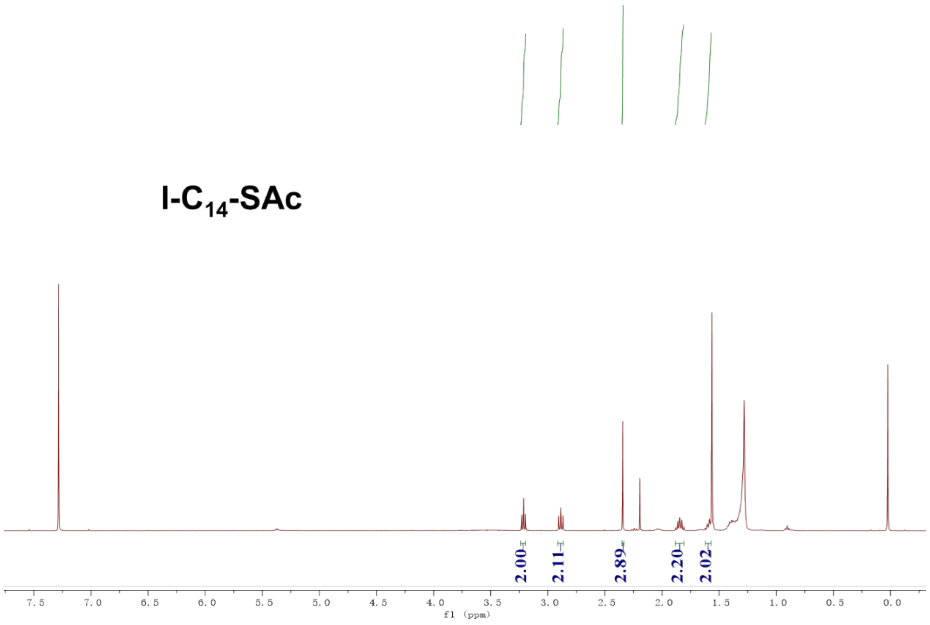

Fig. S20. The ^{1}H-NMR spectrum of compound I-C_{14}-SAc.

14-iodotetradecane-1-thiol (HS-C_{14}-I) was prepared as follows. *S*-(14-iodotetradecyl) ethanethioate (2.08 g, 5.22 mmol) was dissolved in 50 mL methanol and degassed for 20 min. Subsequently, 4.0 mL trifluoroacetic acid was added. The solution was refluxed for 5h then cooled down to room temperature. The solvent was removed by rotary evaporator; DCM was used to extract the product. The organic layer was washed with DI water 3 times before dried over anhydrous Na_2SO_4. After filtration and concentration, the raw product was purified by column chromatography with dichloromethane and hexane (1: 2) as eluent. Yield: 18 % (0.33 g, 0.94 mmol). ^{1}H NMR (400 MHz, Chloroform-*d*) δ 3.21 (t, J = 7.1 Hz, 2H), 2.55 (q, J = 7.4 Hz, 2H), 1.84 (p, J = 7.1 Hz, 2H), 1.63 (t, J = 7.4 Hz, 2H), 1.39 – 1.27 (m, 20H). ^{13}C NMR (100 MHz, Chloroform-*d*) δ 34.10, 33.61, 30.55, 29.65, 29.63, 29.62, 29.58, 29.56, 29.46, 29.12, 28.59, 28.42, 24.70, 7.29. HRMS (ESI+): m/z calc for $C_{14}H_{28}IS$ $[M+H]^+$ 355.0956, found 355.0986.

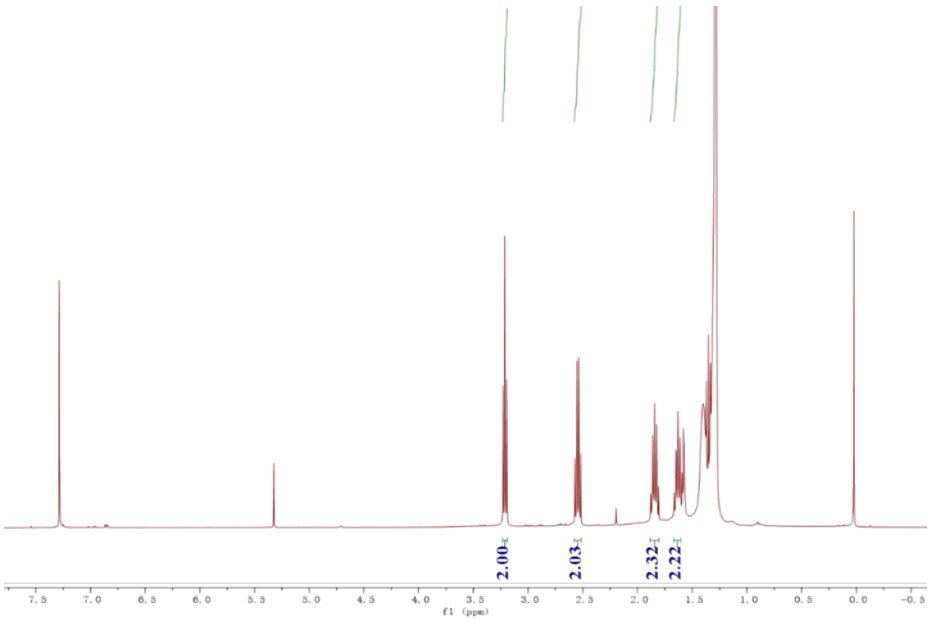

Fig. S21. The ^{1}H-NMR spectrum of compound HS-C_{14}-I.

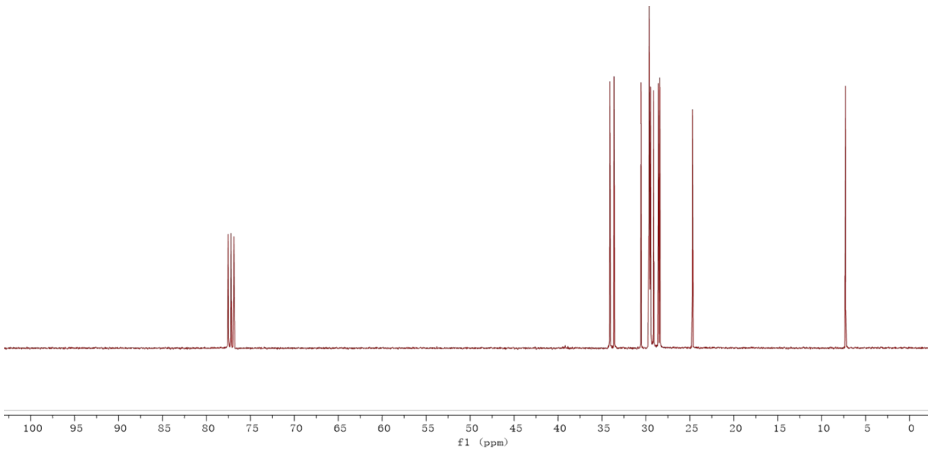

Fig. S22. The ^{13}C-NMR spectrum of compound HS-C_{14}-I.

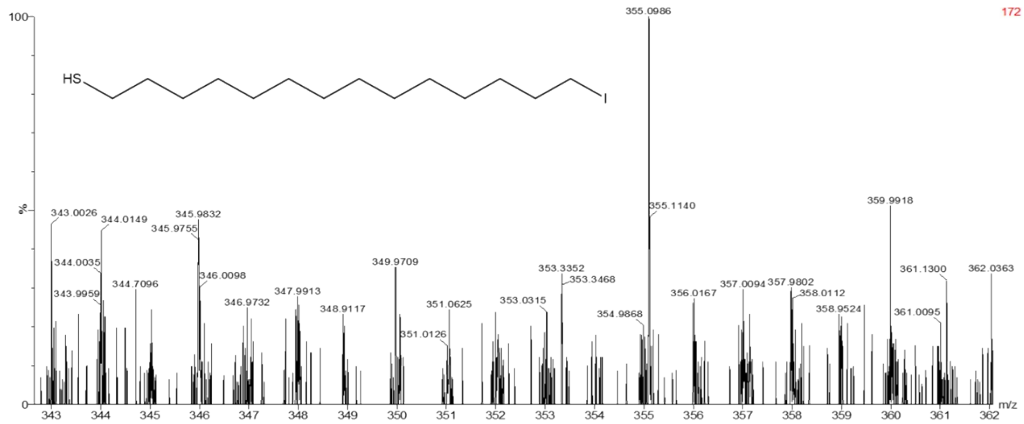

Fig. S23. The HRMS spectrum of compound I-C_{14}-SH.

***S*-(2-(2-ethoxyethoxy)ethyl) ethanethioate ($(C_2O)_2$-C_2-SAc)** was prepared as follows.[1] 1-bromo-2-(2-ethoxyethoxy)ethane (1.97 g, 10.00 mmol) and potassium thioacetate (4.56 g, 40.00 mmol) were added into 300 mL tetrahydrofuran, refluxed for 12h, followed by removal of the tetrahydrofuran under reduced pressure. The residue was dissolved in diethyl ether, filtered, and washed with DI water. The organic layer was dried over Na_2SO_4, filtered and concentrated after which the raw product was purified with column chromatography with dichloromethane and hexane (1:2). Yield: 1.71 g (8.90 mmol) *S*-(2-(2-ethoxyethoxy)ethyl) ethanethioate (89.0 % yield). ^{1}H NMR (400 MHz, Chloroform-*d*) δ 3.66 – 3.59 (m, 6H), 3.54 (t, J = 7.0 Hz, 2H), 3.12 (t, J = 6.5 Hz, 2H), 2.36 (s, 3H), 1.24 (t, J = 7.0 Hz, 3H). ^{13}C NMR (100 MHz, Chloroform-*d*) δ 195.54, 70.35, 69.76, 69.73, 66.67, 30.55, 28.79, 15.14. HRMS (ESI+): m/z calc for $C_8H_{16}O_3S$ $[M+H]^+$ 193.0893, found 193.0890.

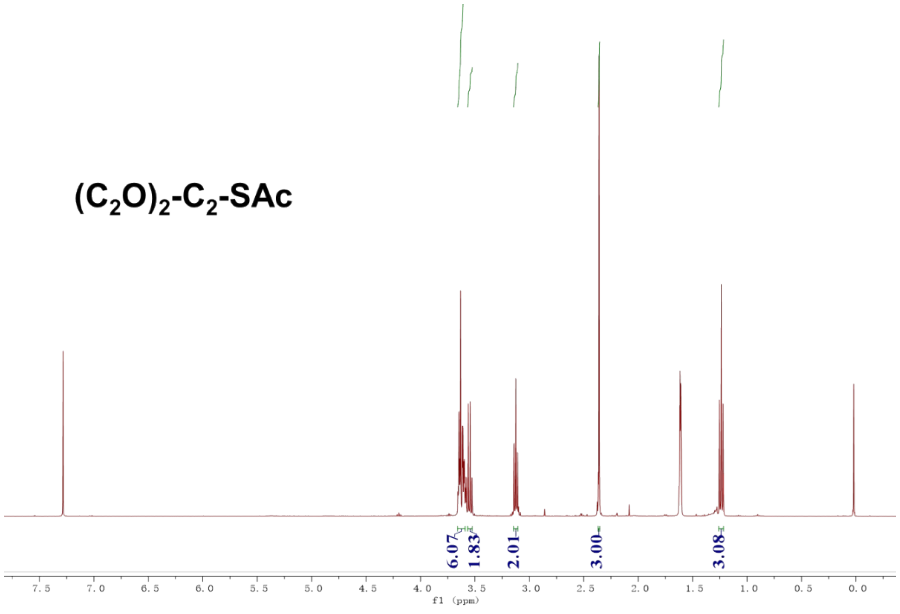

Fig. S24. The ^{1}H-NMR spectrum of compound $(C_2O)_2$-C_2-SAc.

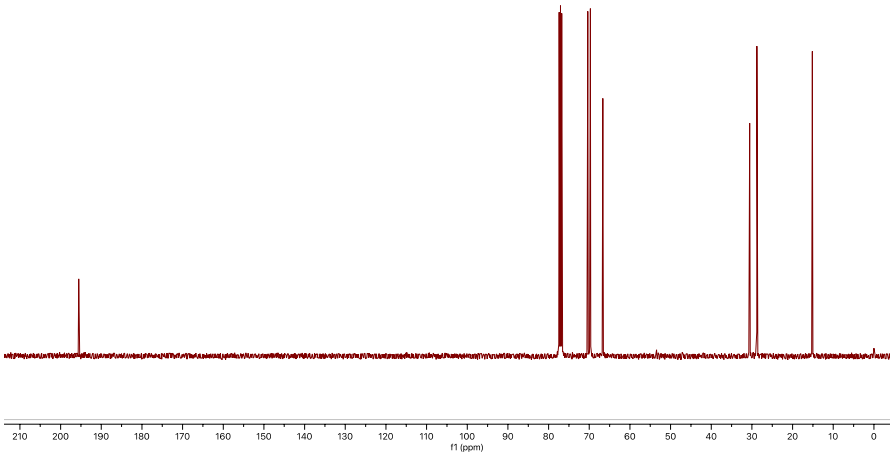

Fig. S25. The ^{13}C-NMR spectrum of compound $(C_2O)_2$-C_2-SAc.

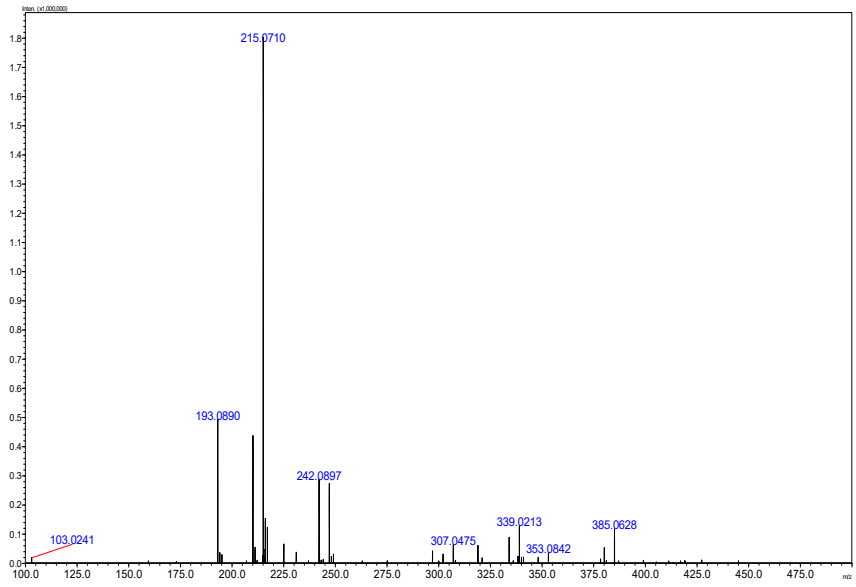

Fig. S26. The HRMS spectrum of compound $(C_2O)_2$-C_2-SAc.

2-(2-ethoxyethoxy)ethane-1-thiol (HS-$(C_2O)_2$-C_2) was prepared as follows. *S*-(2-(2-ethoxyethoxy)ethyl) ethanethioate (1.05 g, 7.00 mmol) was dissolved in 50 mL methanol and degassed for 20 min. Subsequently, 4.0 mL trifluoroacetic acid was added. The solution was refluxed for 5h then cooled down to room temperature. The solvent was removed by rotary evaporator; DCM was used to extract the product. The organic layer was washed with DI water 3 times before dried over anhydrous Na_2SO_4. After filtration and concentration, the raw product was purified by column chromatography with dichloromethane and hexane (1: 2) as eluent.

Yield: 18 % (0.19 g, 1.26 mmol). ^{1}H NMR (400 MHz, Chloroform-*d*) δ 3.67 – 3.61 (m, 6H), 3.56 (q, *J* = 7.0 Hz, 2H), 2.73 (q, *J* = 8.2, 6.5 Hz, 2H), 1.24 (t, *J* = 7.0 Hz, 3H). ^{13}C NMR (100 MHz, Chloroform-*d*) δ 72.93, 70.31, 69.74, 66.67, 24.22, 15.15. HRMS (ESI+): m/z calc for $C_6H_{14}O_2S$ $[M+H]^+$ 149.0636, found 149.0643.

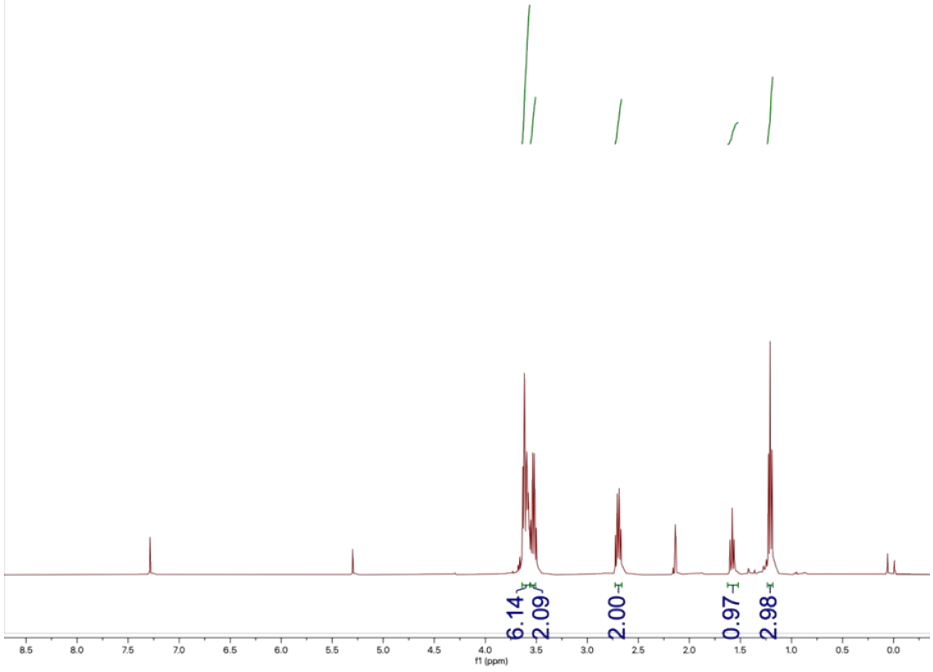

Fig. S27. The ^{1}H-NMR spectrum of compound HS-$(C_2O)_2$-C_2.

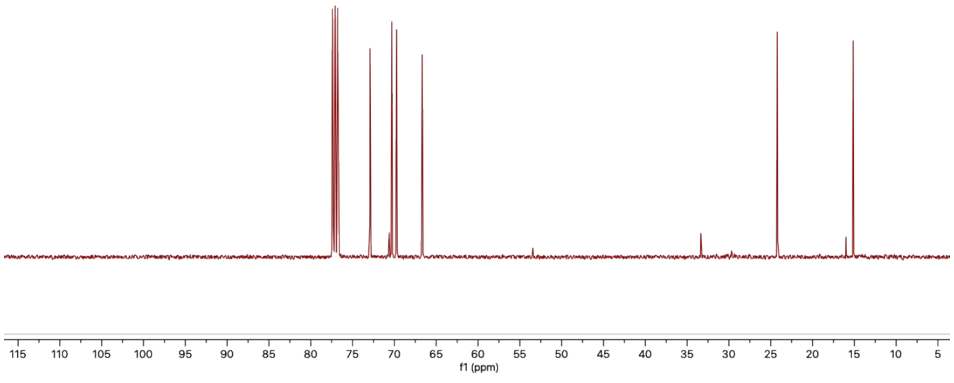

Fig. S28. The ^{13}C-NMR spectrum of compound HS-$(C_2O)_2$-C_2.

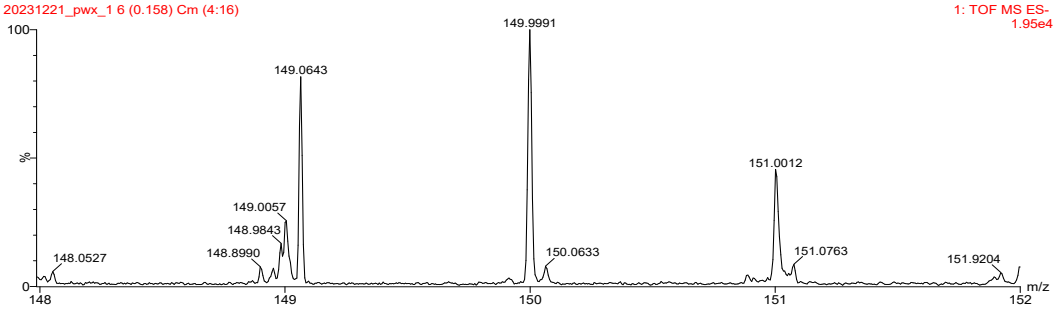

Fig. S29. The HRMS spectrum of compound HS-$(C_2O)_2$-C_2.

2-(2-(2-ethoxyethoxy)ethoxy)ethyl 4-methylbenzenesulfonate ($(C_2O)_3$-C_2-OTs) was prepared as follows.[3] In a 250 mL round-bottomed flask, triethylene glycol monoethyl ether (5.00 mL, 28.60 mmol) was dissolved in triethylamine (20 mL, 144.00 mmol), and the mixture was cooled to 0 °C. After addition of *para*-toluenesulfonyl chloride (6.00 g, 31.40 mmol), the mixture was allowed to warm slowly to room temperature and stirred for further 5 h. Subsequently, the reaction mixture was carefully added to a stirred mixture of concentrated hydrochloric acid (30 mL) and crushed ice (40 g). The mixture was extracted three times with diethyl ether (100 mL), and the combined organic phases were washed successively with brine (100 mL) and a saturated solution of sodium hydrogen carbonate. The organic phases were dried with $MgSO_4$ and filtered, and the solvents were removed under reduced pressure. Clear, colorless oil. Yield: 8.54 g (90 %). ^{1}H NMR (400 MHz, Chloroform-*d*) δ 7.84 – 7.81 (m, 2H), 7.36 (d, J = 8.1 Hz, 2H), 4.21 – 4.17 (m, 2H), 3.71 (dd, J = 5.6, 4.2 Hz, 2H), 3.65 – 3.57 (m, 8H), 3.54 (q, J = 7.0 Hz, 2H), 2.47 (s, 3H), 1.23 (t, J = 7.0 Hz, 3H).

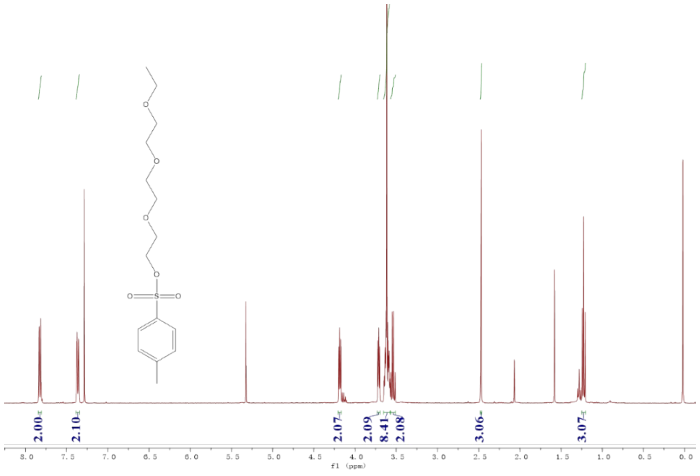

Fig. S30. The ^{1}H-NMR spectrum of compound $(C_2O)_3$-C_2-OTs.

***S*-(2-(2-(2-ethoxyethoxy)ethoxy)ethyl) ethanethioate ($(C_2O)_3$-C_2-SAc)** was prepared as follows.[4] 2-(2-(2-ethoxyethoxy)ethoxy)ethyl 4-methylbenzenesulfonate (3.32 g, 10.00 mmol) and potassium thioacetate (4.56 g, 40.00 mmol) were added into 300 mL tetrahydrofuran, refluxed for 12h, followed by removal of the tetrahydrofuran under reduced pressure. The residue was dissolved in diethyl ether, filtered, and washed with DI water. The organic layer was dried over Na_2SO_4, filtered and concentrated after which the raw product was purified with column chromatography with dichloromethane and hexane (1:2). Yield: 2.10 g (8.90 mmol) *S*-(2-(2-(2-ethoxyethoxy)ethoxy)ethyl) ethanethioate (89.0 % yield). ^{1}H NMR (400 MHz, Chloroform-*d*) δ 3.69 – 3.60 (m, 10H), 3.55 (q, J = 7.0 Hz, 2H), 3.12 (t, J = 6.5 Hz, 2H), 2.36 (s, 3H), 1.23 (t, J = 7.0 Hz, 3H). ^{13}C NMR (100 MHz, Chloroform-*d*) δ 195.42, 70.69, 70.51, 70.31, 69.79, 69.73, 66.59, 30.50, 28.82, 15.12. HRMS (ESI+): m/z calc for $C_{10}H_{20}O_4S$ $[M+H]^+$ 237.1155 found 237.1154.

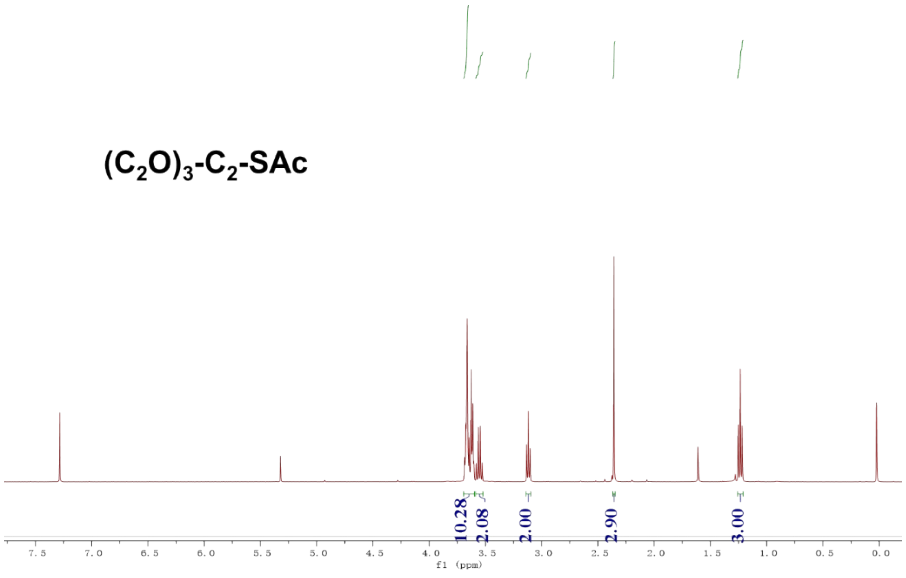

Fig. S31. The ^{1}H-NMR spectrum of compound $(C_2O)_3$-C_2-SAc.

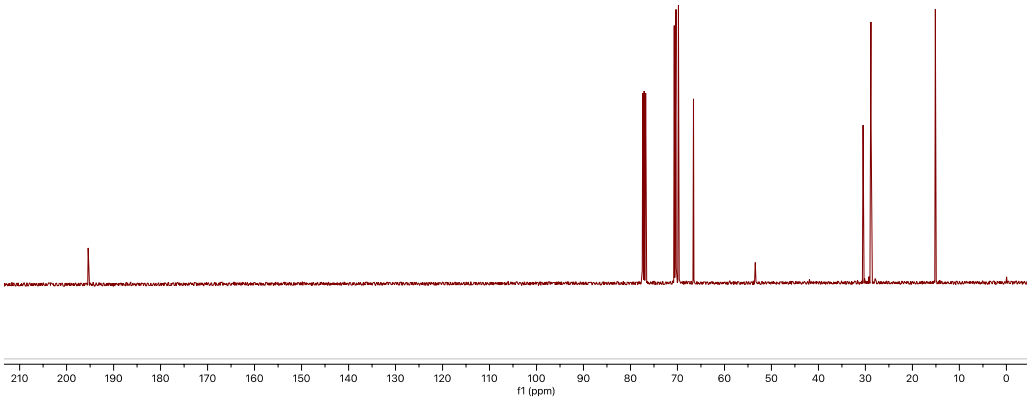

Fig. S32. The ^{13}C-NMR spectrum of compound $(C_2O)_3$-C_2-SAc.

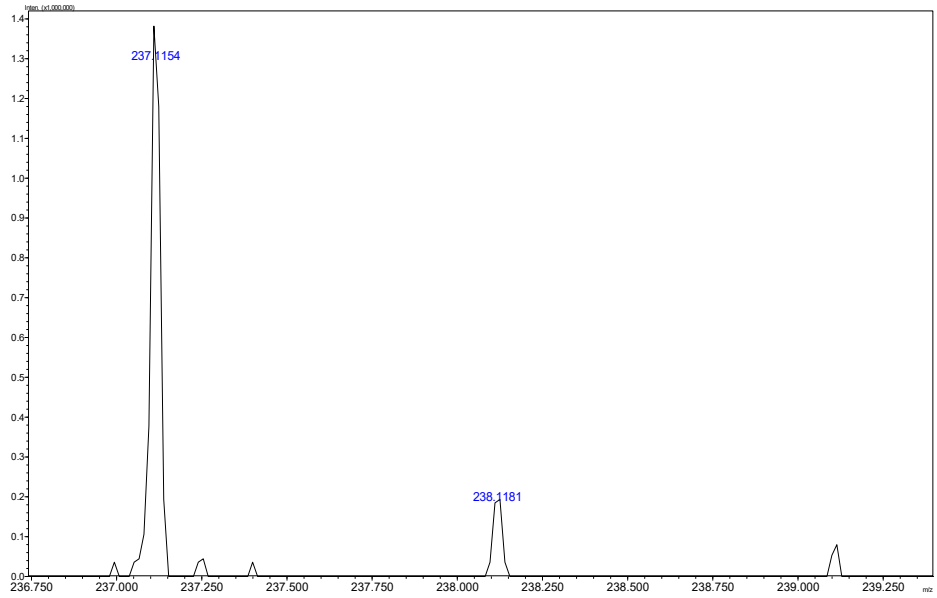

Fig. S33. The HRMS spectrum of compound $(C_2O)_3$-C_2-SAc.

2-(2-(2-ethoxyethoxy)ethoxy)ethane-1-thiol (HS-$(C_2O)_3$-C_2) was prepared as follows.[5] *S*-(2-(2-(2-ethoxyethoxy)ethoxy)ethyl) ethanethioate (1.00 g, 4.24 mmol) was dissolved in dry THF (50 mL) and added dropwise to a stirring slurry of $LiAlH_4$ (0.64 g; 16.96 mmol) in THF (16.96 mL) at 0 °C. The reaction was stirred at room temperature for 6 h under nitrogen. The reaction was then quenched at 0 °C with water (25 mL, previously degassed), and was acidified

with 1 M HCl solution (previously degassed). The mixture was then extracted with Et_2O (3 × 100 mL). The combined organic phases were washed with water (1 × 100 mL) and brine (1 × 100 mL), dried over $MgSO_4$, filtered, and evaporated to dryness. The crude thiol product was purified by column chromatography on silica gel (hexanes). Yield: 0.76 g (3.90 mmol) 2-(2-(2-ethoxyethoxy)ethoxy)ethane-1-thiol (92.0 % yield). ^{1}H NMR (400 MHz, Chloroform-*d*) δ 3.69 – 3.60 (m, 10H), 3.54 (q, *J* = 7.0 Hz, 2H), 2.71 (dt, *J* = 8.2, 6.4 Hz, 2H), 1.60 (t, *J* = 8.2 Hz, 1H), 1.22 (t, *J* = 7.0 Hz, 3H). ^{13}C NMR (100 MHz, Chloroform-*d*) δ 72.74, 70.58, 70.42, 70.10, 69.72, 66.44, 24.14, 15.08. HRMS (ESI+): m/z calc for $C_8H_{19}O_3S$ $[M+H]^+$ 195.1055, found 195.1054.

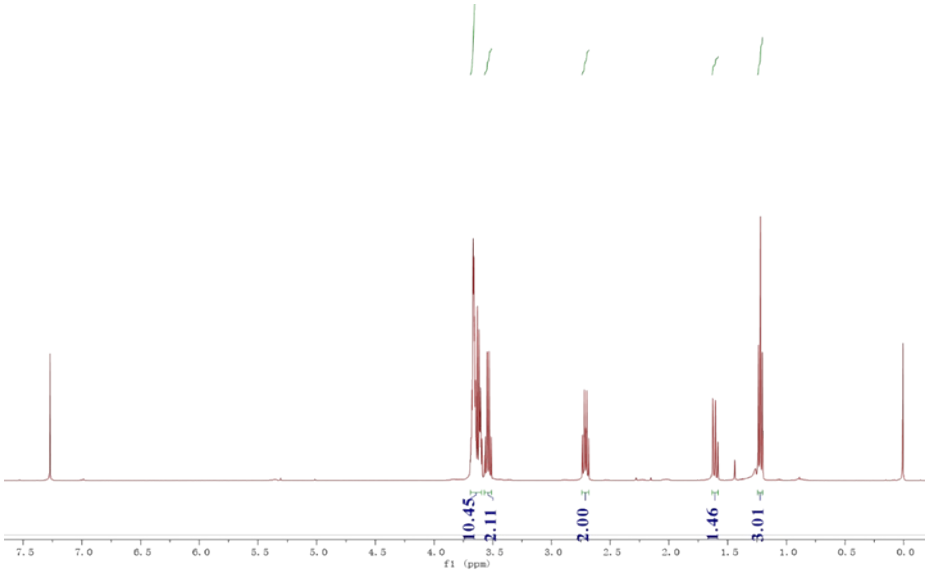

Fig. S34. The ^{1}H-NMR spectrum of compound HS-$(C_2O)_3$-C_2.

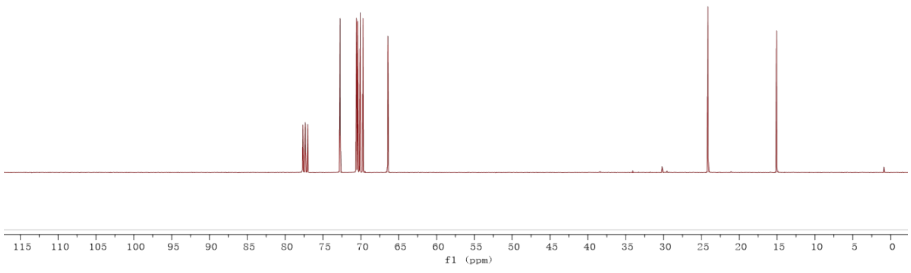

Fig. S35. The ^{13}C-NMR spectrum of compound HS-$(C_2O)_3$-C_2.

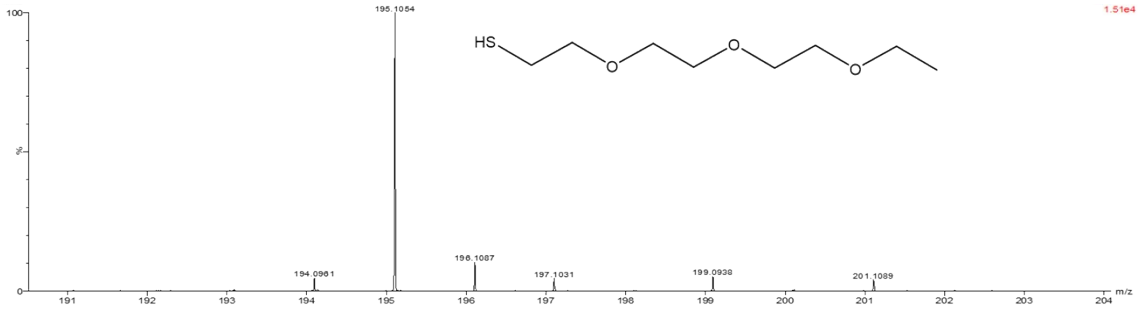

Fig. S36. The HRMS spectrum of compound HS-$(C_2O)_3$-C_2.

3,6,9,12-tetraoxatetradecan-1-ol ($(C_2O)_4$-C_2-OH) was prepared as follows[6]. A suspension of 60% NaH in mineral oil (1 g, 25.23 mmol) was washed with anhydrous hexane (10 mL) and suspended in freshly distilled THF (30 mL). Then, tetraethylene glycol (4 mL, 22.94 mmol) was added to the above suspension and the reaction mixture was refluxed for 1 h. After the mixture was cooled to 0 °C using an ice bath, bromoethane (0.88 mL, 11.47 mmol) was added slowly, and the reaction mixture was kept at 0 °C for 1 h. The solvent was evaporated under a vacuum, ice water was added, and then, the aqueous solution was extracted twice with $CHCl_3$. The combined extract was washed with brine, dried over anhydrous Na_2SO_4, and concentrated to yield the crude compound. After silica gel chromatography (4% CH_3OH in $CHCl_3$ as eluting solvent), 3,6,9,12-tetraoxatetradecan-1-ol was obtained (650 mg, as a colorless oil, 25.5% yield). ^{1}H NMR (400 MHz, Chloroform-*d*) δ 3.74 – 3.57 (m, 16H), 3.52 (q, J = 7.0 Hz, 2H), 1.21 (t, J = 7.0 Hz, 3H).

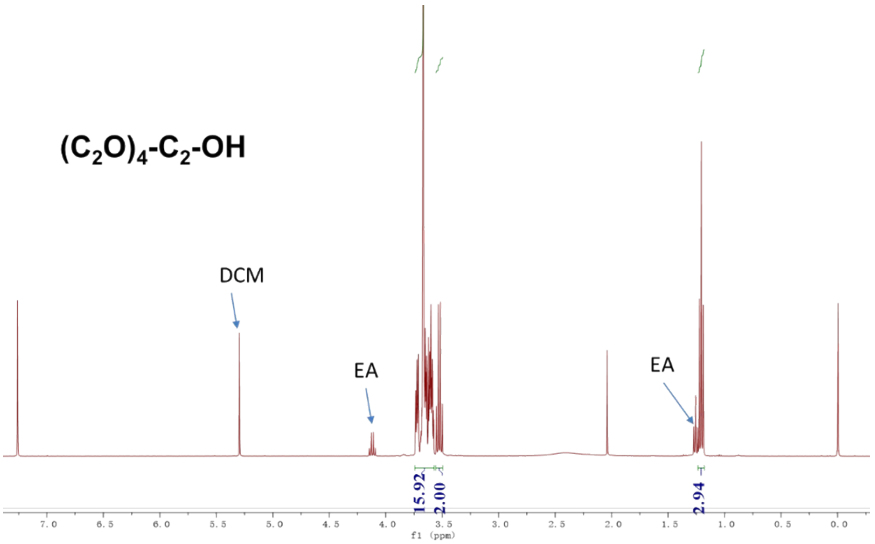

Fig. S37. The ^{1}H-NMR spectrum of compound $(C_2O)_4$-C_2-OH.

3,6,9,12-tetraoxatetradecyl 4-methylbenzenesulfonate ($(C_2O)_4$-C_2-OTs) was prepared as follows.[3] In a 250 mL round-bottomed flask, 3,6,9,12-tetraoxatetradecan-1-ol (18.00 g, 81.01 mmol) was dissolved in triethylamine (56.64 mL, 407.52 mmol), and the mixture was cooled to 0 °C. After addition of *para*-toluenesulfonyl chloride (16.98 g, 88.86 mmol), the mixture was allowed to warm slowly to room temperature and stirred for further 5 h. Subsequently, the reaction mixture was carefully added to a stirred mixture of concentrated hydrochloric acid (50 mL) and crushed ice (80 g). The mixture was extracted three times with diethyl ether (200 mL), and the combined organic phases were washed successively with brine (200 mL) and a saturated solution of sodium hydrogen carbonate. The organic phases were dried with $MgSO_4$ and filtered, and the solvents were removed under reduced pressure. Clear, colorless oil. Yield: 27.4 g (90 %). ^{1}H NMR (400 MHz, Chloroform-*d*) δ 7.83 – 7.77 (m, 2H), 7.37 – 7.31 (m, 2H), 4.18 – 4.14 (m, 2H), 3.70 – 3.67 (m, 2H), 3.65 – 3.57 (m, 12H), 3.55 – 3.49 (m, 2H), 2.45 (s, 3H), 1.20 (t, J = 7.0 Hz, 3H).

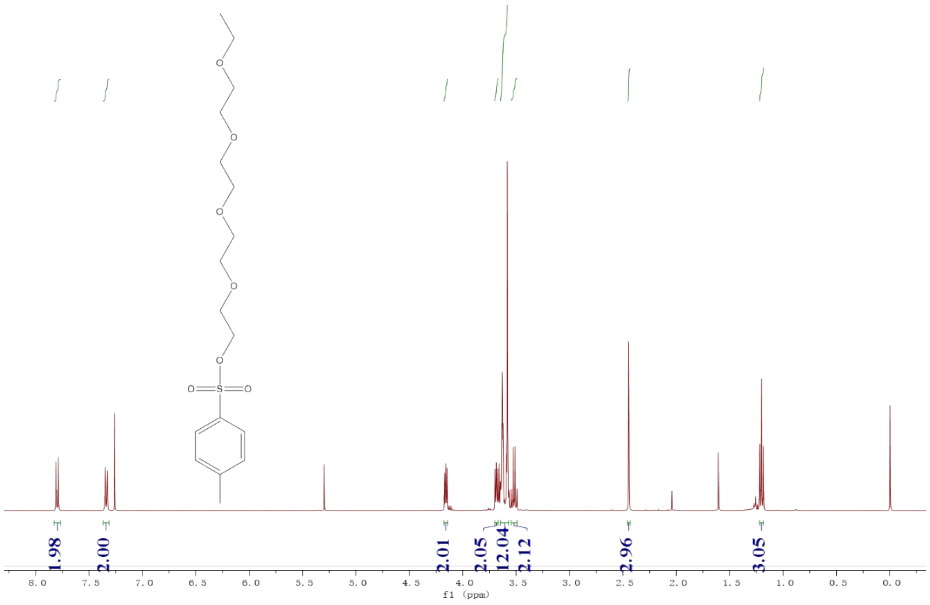

Fig. S38. The ^{1}H-NMR spectrum of compound $(C_2O)_4$-C_2-OTs.

***S*-(3,6,9,12-tetraoxatetradecyl) ethanethioate ($(C_2O)_4$-C_2-SAc)** was prepared as follows.[4] 3,6,9,12-tetraoxatetradecyl 4-methylbenzenesulfonate (10.00 g, 26.60 mmol) and potassium thioacetate (12.13 g, 106.40 mmol) were added into 400 mL tetrahydrofuran, refluxed for 12h,

followed by removal of the tetrahydrofuran under reduced pressure. The residue was dissolved in diethyl ether, filtered, and washed with DI water. The organic layer was dried over Na_2SO_4, filtered and concentrated after which the raw product was purified with column chromatography with dichloromethane and hexane (1:2). Yield: 6.63 g (23.67 mmol) *S*-(3,6,9,12-tetraoxatetradecyl) ethanethioate (89.0 % yield). ^{1}H NMR (400 MHz, Chloroform-*d*) δ 3.66 – 3.57 (m, 14H), 3.53 (q, *J* = 7.0 Hz, 2H), 3.09 (t, *J* = 6.5 Hz, 2H), 2.33 (s, 3H), 1.21 (t, *J* = 7.0 Hz, 3H). ^{13}C NMR (100 MHz, Chloroform-*d*) δ 195.38, 70.64, 70.61, 70.57, 70.48, 70.29, 69.79, 69.72, 66.56, 30.49, 28.81, 15.12. HRMS (ESI+): m/z calc for $C_{12}H_{24}O_5S$ [M+H]$^+$ 281.1417, found 281.1417.

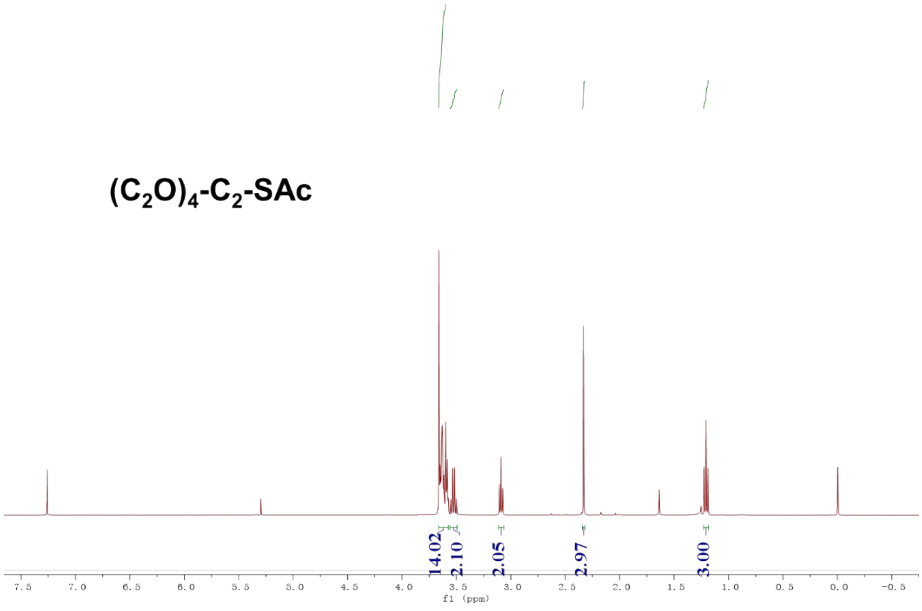

Fig. S39. The ^{1}H-NMR spectrum of compound $(C_2O)_4$-C_2-SAc.

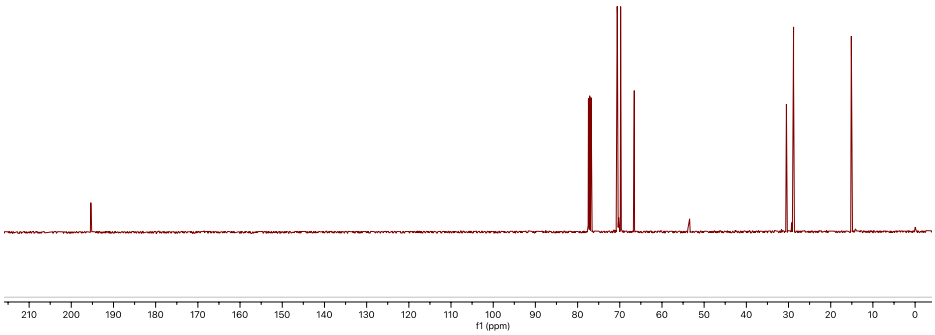

Fig. S40. The ^{13}C-NMR spectrum of compound $(C_2O)_4$-C_2-SAc.

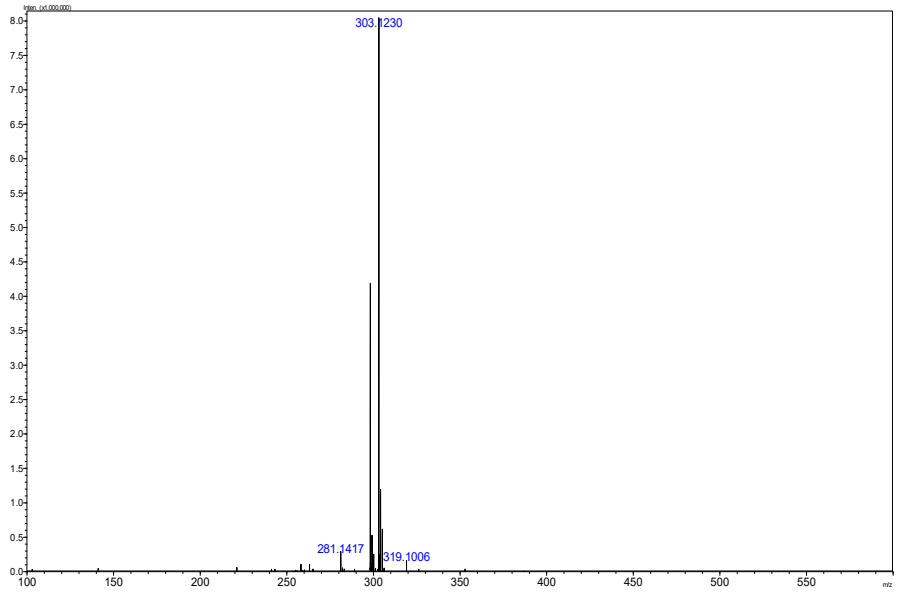

Fig. S41. The HRMS spectrum of compound $(C_2O)_4$-C_2-SAc.

3,6,9,12-tetraoxatetradecane-1-thiol (HS-$(C_2O)_4$-C_2) was prepared as follows.[5] *S*-(3,6,9,12-tetraoxatetradecyl) ethanethioate (1.00 g, 3.57 mmol) was dissolved in dry THF (40 mL) and added dropwise to a stirring slurry of $LiAlH_4$ (0.54 g; 14.28 mmol) in THF (14.3 mL) at 0 °C. The reaction was stirred at room temperature for 6 h under nitrogen. The reaction was then quenched at 0 °C with water (25 mL, previously degassed), and was acidified with 1 M HCl solution (previously degassed). The mixture was then extracted with Et_2O (3 × 100 mL). The combined organic phases were washed with water (1 × 100 mL) and brine

(1 × 100 mL), dried over $MgSO_4$, filtered, and evaporated to dryness. The crude thiol product was purified by column chromatography on silica gel (hexanes). Yield: 0.78 g (3.28 mmol) 3,6,9,12-tetraoxatetradecane-1-thiol (92.0 % yield). ^{1}H NMR (400 MHz, Chloroform-*d*) δ 3.71 – 3.60 (m, 14H), 3.58 – 3.52 (m, 2H), 2.72 (dt, *J* = 8.3, 6.5 Hz, 2H), 1.23 (t, *J* = 7.0 Hz, 3H). ^{13}C NMR (100 MHz, Chloroform-*d*) δ 72.76, 70.57, 70.53, 70.51, 70.43, 70.12, 69.73, 66.46, 24.16, 15.10. HRMS (ESI+): m/z calc for $C_{10}H_{23}O_4S$ $[M+H]^+$ 239.1317, found 239.1325.

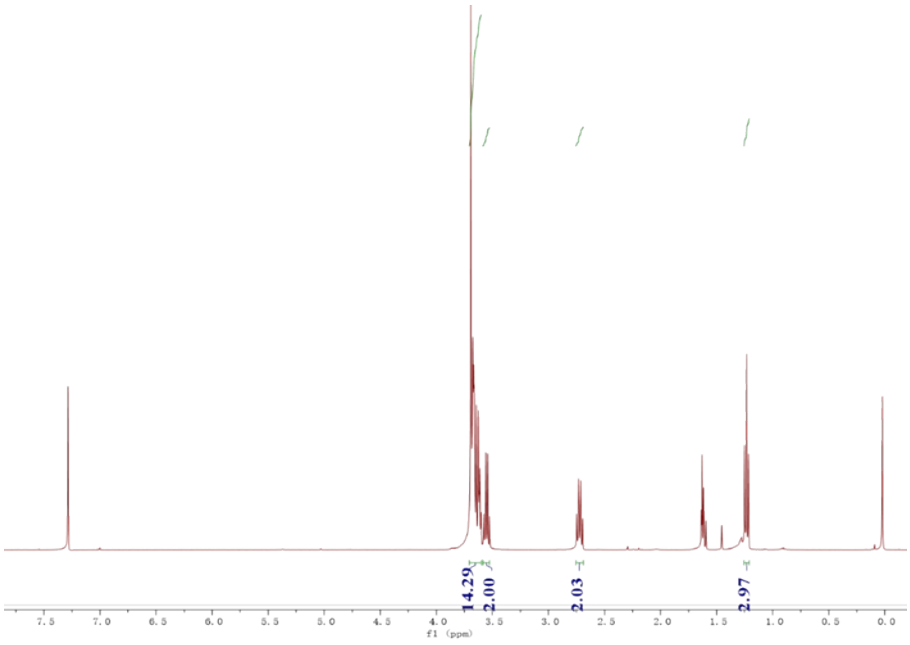

Fig. S42. The ^{1}H-NMR spectrum of compound HS-$(C_2O)_4$-C_2.

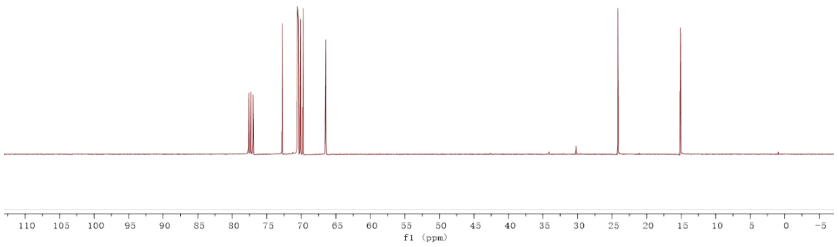

Fig. S43. The ^{13}C-NMR spectrum of compound HS-$(C_2O)_4$-C_2.

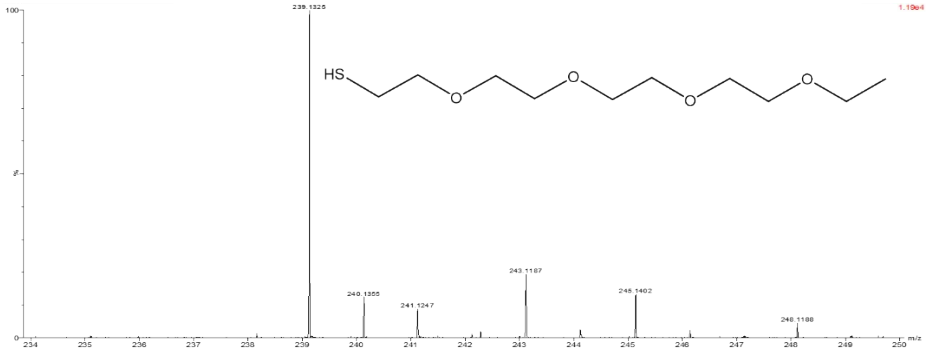

Fig. S44. The HRMS spectrum of compound HS-$(C_2O)_4$-C_2.

1-iodo-2-(2-iodoethoxy)ethane (I-C_2O-C_2-I) was prepared as follows.[7] To a stirred solution of 2-chloroethyl ether (14.30 g, 100.00 mmol) in acetone (200.00 mL) was added powder NaI (65.00 g, 433.6 mmol). The resulting clear yellow solution was heated as reflux for 48h. Then, cooled, filtered through a plug of celite and concentrated to give yellow liquid. This was taken up in ether (200 mL) washed with water (50 mL) and 10% aq. $NaHSO_3$ (20 mL), dried ($NaHSO_4$), filtered. The crude thiol product was purified by column chromatography on silica gel (hexanes). Yield: 26.65 g (82.00 mmol) 1-iodo-2-(2-iodoethoxy)ethane (82.0 % yield). ^{1}H NMR (400 MHz, Chloroform-*d*) δ 3.79 (dd, *J* = 7.4, 6.2 Hz, 4H), 3.29 (t, *J* = 6.8 Hz, 4H).

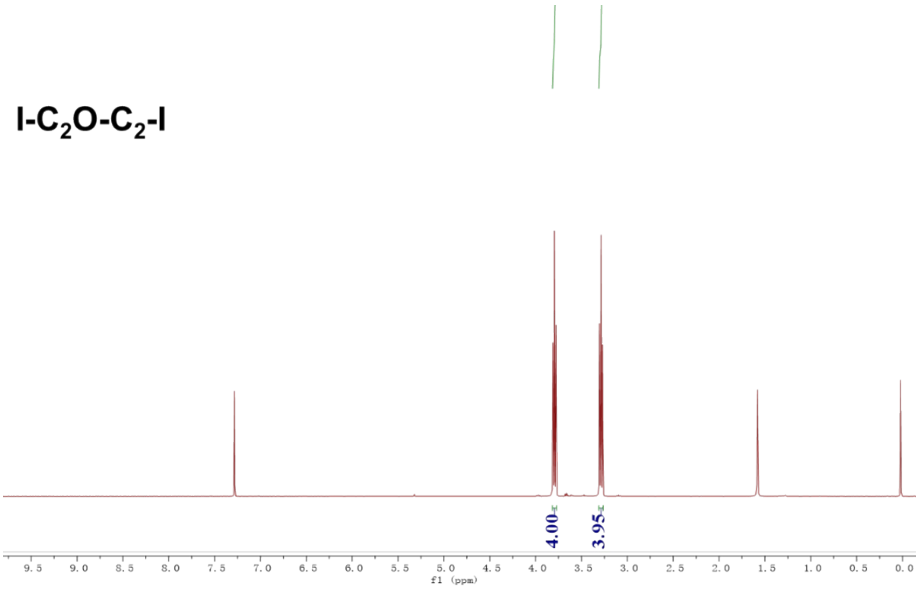

Fig. S45. The ^{1}H-NMR spectrum of compound I-C_2O-C_2-I.

***S*-(2-(2-iodoethoxy)ethyl) ethanethioate (I-C_2O-C_2-SAc)** was prepared as follows similar to the previous work reported.[1] 1-iodo-2-(2-iodoethoxy)ethane (14.80 g, 45.40 mmol) and

potassium thioacetate (1.30 g, 11.34 mmol) were added into 200 mL tetrahydrofuran, stirred for 12h at room temperature, followed by removal of the tetrahydrofuran under reduced pressure. The residue was dissolved in diethyl ether, filtered, and washed with DI water. The organic layer was dried over Na_2SO_4, filtered and concentrated after which the raw product was purified with column chromatography with ethyl acetate and hexane (1: 10). Yield: 2.77 g (10.09 mmol) *S*-(2-(2-iodoethoxy)ethyl) ethanethioate (89.0 % yield). 1H NMR (400 MHz, Chloroform-d) δ 3.78 – 3.72 (m, 2H), 3.64 (td, J = 6.4, 1.7 Hz, 2H), 3.29 – 3.24 (m, 2H), 3.12 (td, J = 6.4, 1.7 Hz, 2H), 2.37 (d, J = 1.8 Hz, 3H). ^{13}C NMR (100 MHz, Chloroform-*d*) δ 195.38, 71.50, 69.29, 30.61, 28.87, 2.70. HRMS (ESI+): m/z calc for $C_6H_{11}O_2SI$ $[M+H]^+$ 274.9603, found 274.9607.

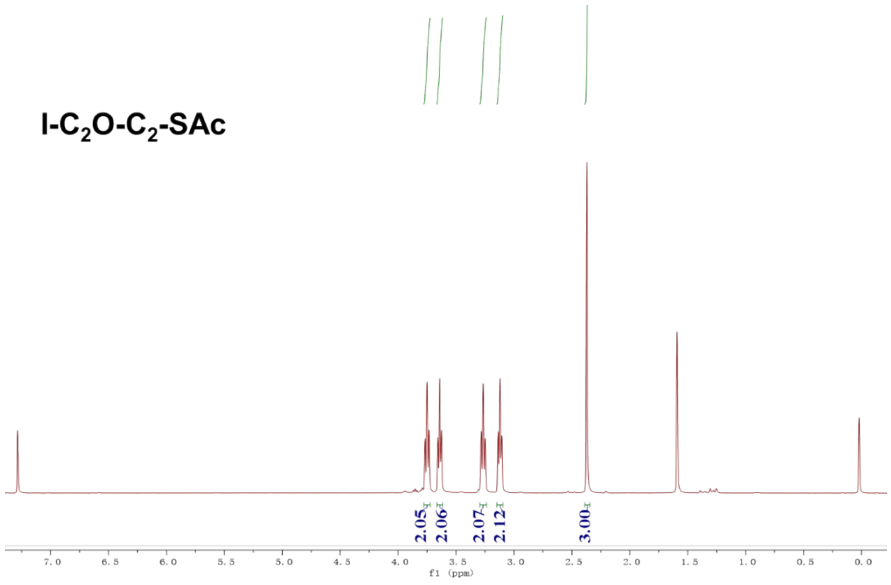

Fig. S46. The ^1H-NMR spectrum of compound I-C_2O-C_2-SAc.

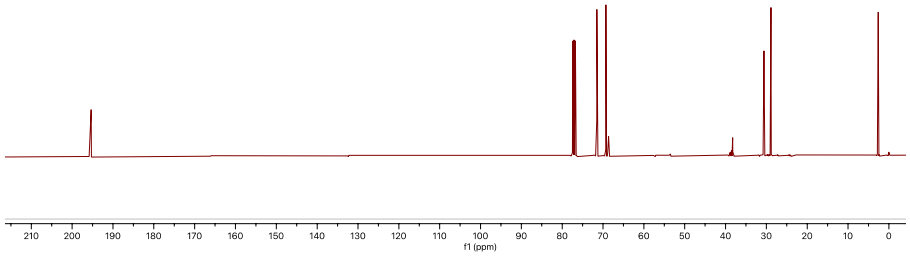

Fig. S47. The ^{13}C NMR spectrum of compound I-C_2O-C_2-SAc.

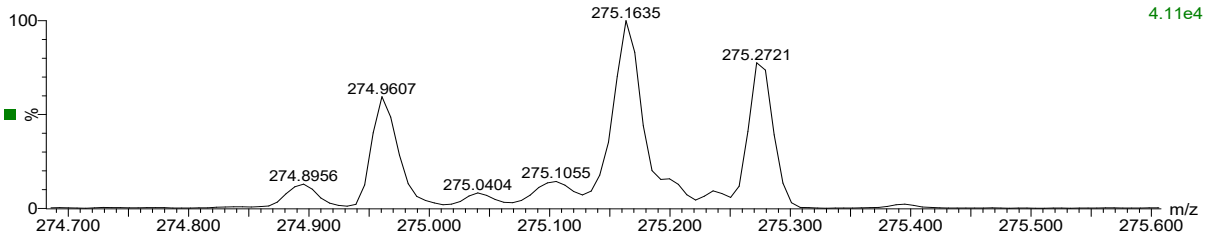

Fig. S48. The HRMS spectrum of compound I-C_2O-C_2-SAc.

2-(2-iodoethoxy)ethane-1-thiol (HS-C_2O-C_2-I) was prepared as follows. *S*-(2-(2-iodoethoxy)ethyl) ethanethioate (1.17 g, 4.27 mmol) was dissolved in 50 mL methanol and degassed for 20 min. Subsequently, 3.0 mL trifluoroacetic acid was added. The solution was refluxed for 5h then cooled down to room temperature. The solvent was removed by rotary evaporator; DCM was used to extract the product. The organic layer was washed with DI water 3 times before dried over anhydrous Na_2SO_4. After filtration and concentration, the raw product was purified by column chromatography with hexane as eluent. Yield: 18 % (0.18 g, 0.77 mmol). ^{1}H NMR (400 MHz, Chloroform-*d*) δ 3.75 (t, *J* = 6.7 Hz, 2H), 3.65 (t, *J* = 6.3 Hz, 2H), 3.28 (t, *J* = 6.7 Hz, 2H), 2.72 (q, *J* = 8.2, 6.3 Hz, 2H), 1.66 (t, *J* = 8.2 Hz, 1H). ^{13}C NMR (100 MHz, Chloroform-*d*) δ 72.32, 71.34, 24.46, 3.21. HRMS (ESI+): m/z calc for C_4H_8OSI [M+H]$^+$ 230.9341, found 230.9356.

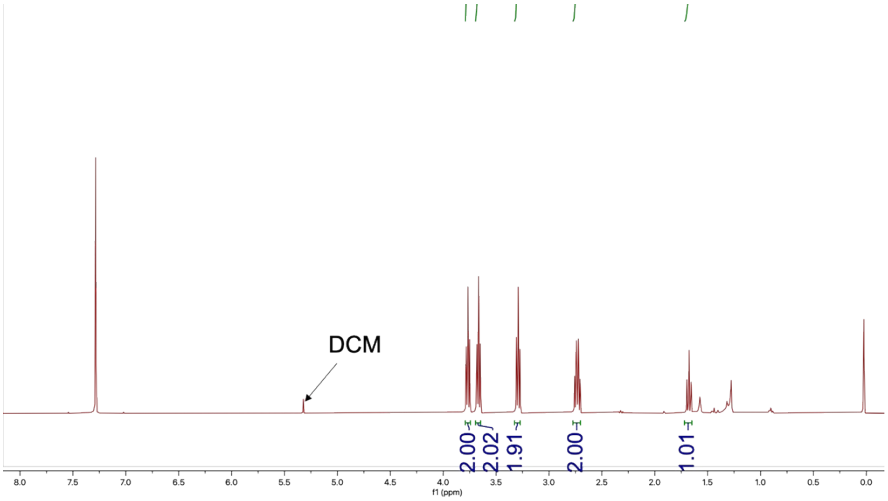

Fig. S49. The ^{1}H-NMR spectrum of compound HS-C_2O-C_2-I.

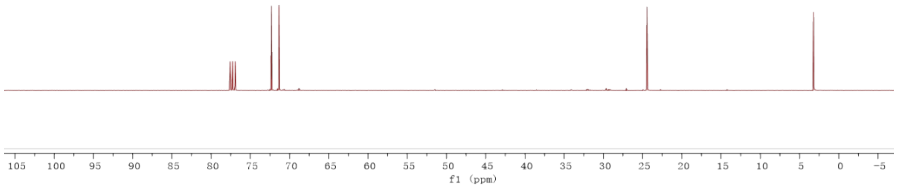

409

410 **Fig. S50.** The ^{13}C-NMR spectrum of compound HS-C_2O-C_2-I.

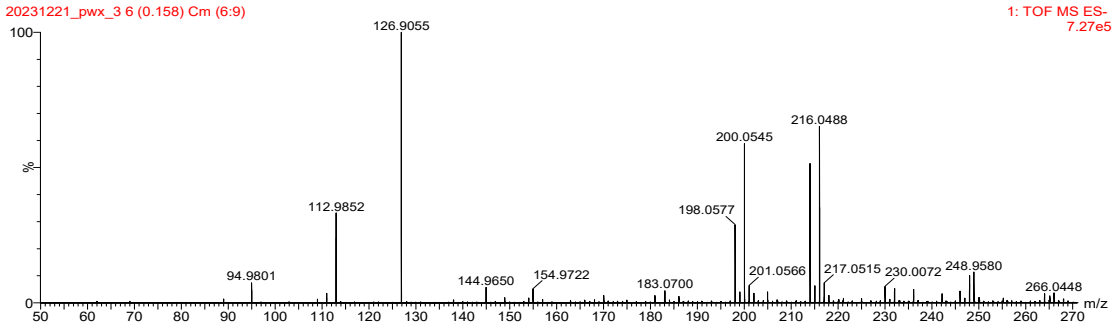

411

412 **Fig. S51.** The HRMS spectrum of compound HS-C_2O-C_2-I.

413

414 **1,2-bis(2-iodoethoxy)ethane (I-(C_2O)$_2$-C_2-I)** was prepared as follows.[7] To a stirred solution
415 of 1,2-bis(2-chloroethoxy)ethane (18.70 g, 100.00 mmol) in acetone (200.00 mL) was added
416 powder NaI (65.00 g, 433.6 mmol). The resulting clear yellow solution was heated as reflux
417 for 48h. Then, cooled, filtered through a plug of celite and concentrated to give yellow liquid.
418 This was taken up in ether (200 mL) washed with water (50 mL) and 10% aq. $NaHSO_3$ (20
419 mL), dried ($NaHSO_4$), filtered. The crude thiol product was purified by column
420 chromatography on silica gel (hexanes). Yield: 30.26 g (82.00 mmol) 1,2-bis(2-iodoethoxy)
421 ethane (82.0 % yield). 1H NMR (400 MHz, Chloroform-d) δ 3.78 (t, J = 6.8 Hz, 4H), 3.69 (s,
422 4H), 3.28 (t, J = 6.8 Hz, 4H).

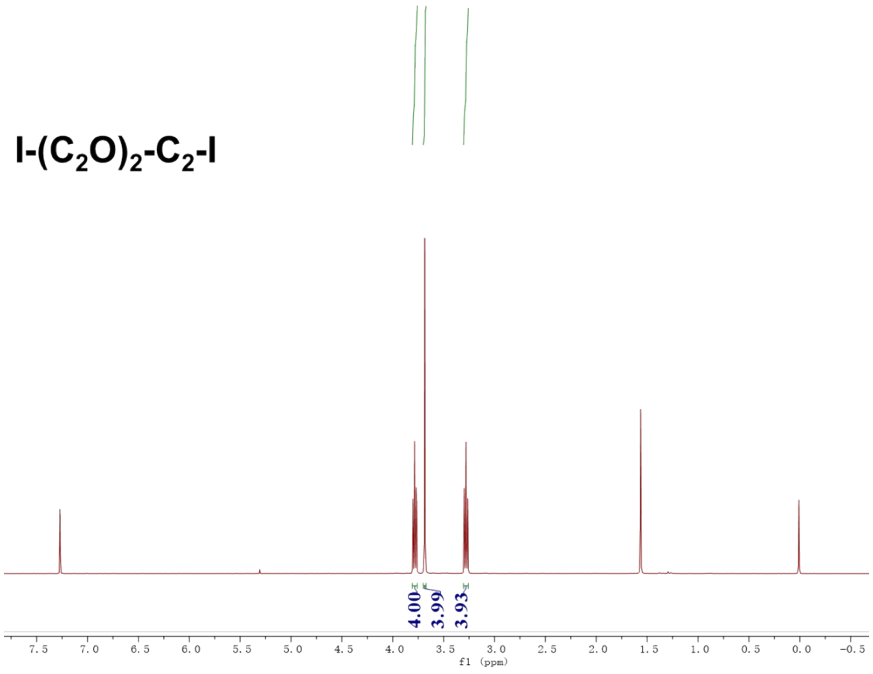

Fig. S52. The ^{1}H-NMR spectrum of compound I-$(C_2O)_2$-C_2-I.

***S*-(2-(2-(2-iodoethoxy)ethoxy)ethyl) ethanethioate (I-$(C_2O)_2$-C_2-SAc)** was prepared as follows.[1] 1,2-bis(2-iodoethoxy)ethane (24.62 g, 66.72 mmol) and potassium thioacetate (1.90 g, 16.68 mmol) were added into 200 mL tetrahydrofuran, stirred for 12h at room temperature, followed by removal of the tetrahydrofuran under reduced pressure. The residue was dissolved in diethyl ether, filtered, and washed with DI water. The organic layer was dried over Na_2SO_4, filtered and concentrated after which the raw product was purified with column chromatography with dichloromethane and hexane (1: 10). Yield: 4.72 g (14.85 mmol) *S*-(2-(2-(2-iodoethoxy)ethoxy)ethyl) ethanethioate (89.0 % yield). ^{1}H NMR (400 MHz, Chloroform-*d*) δ 3.78 (t, *J* = 6.9 Hz, 2H), 3.67 (m, *J* = 4.6, 2.8, 1.4 Hz, 4H), 3.65 – 3.62 (m, 2H), 3.29 (t, *J* = 7.3, 6.5 Hz, 2H), 3.12 (t, *J* = 6.4 Hz, 2H), 2.36 (s, 3H). ^{13}C NMR (100 MHz, Chloroform-*d*) δ 195.42, 72.00, 70.32, 70.14, 69.82, 30.59, 28.86, 2.90. HRMS (ESI+): m/z calc for $C_8H_{15}O_3SI$ $[M+H]^+$ 318.9859, found 318.9850. HRMS (ESI+): m/z calc for $C_8H_{15}O_3SI$ $[M+H]^+$ 318.9859, found 318.9850.

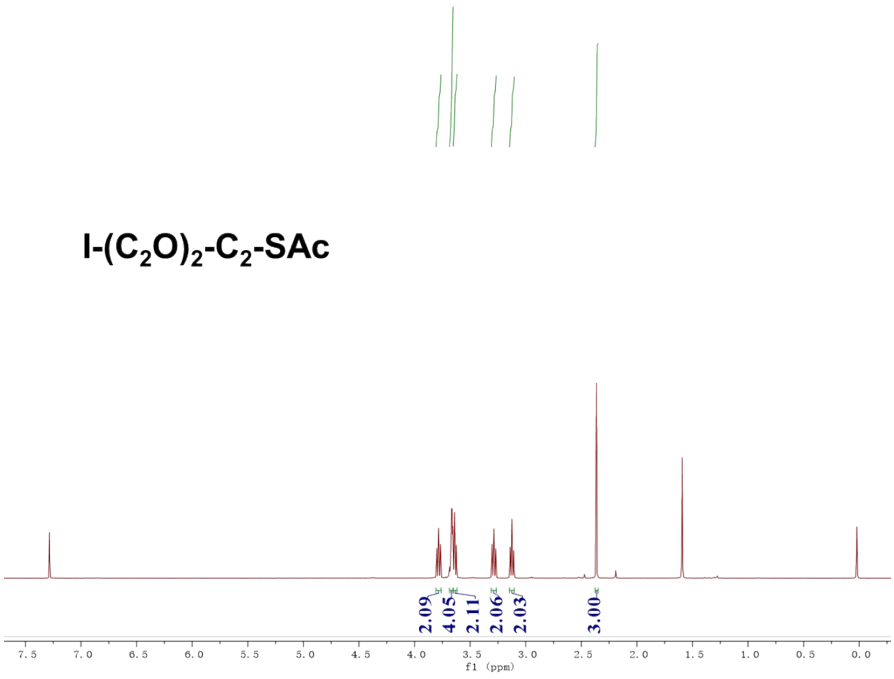

439

440 **Fig. S53.** The ^{1}H-NMR spectrum of compound I-$(C_2O)_2$-C_2-SAc.

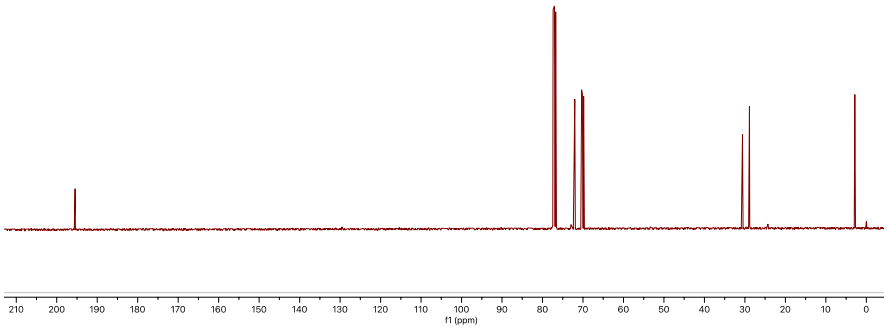

441

442 **Fig. S54.** The ^{13}C-NMR spectrum of compound I-$(C_2O)_2$-C_2-SAc.

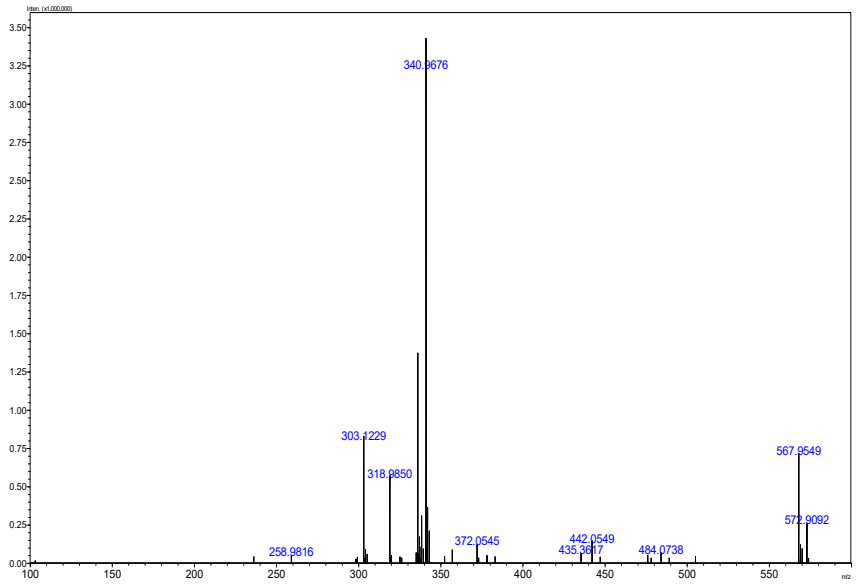

Fig. S55. The HRMS spectrum of compound I-$(C_2O)_2$-C_2-SAc.

2-(2-(2-iodoethoxy)ethoxy)ethane-1-thiol (HS-$(C_2O)_2$-C_2-I) was prepared as follows. *S*-(2-(2-(2-iodoethoxy)ethoxy)ethyl) ethanethioate (0.83 g, 2.61 mmol) was dissolved in 30 mL methanol and degassed for 20 min. Subsequently, 3.0 mL trifluoroacetic acid was added. The solution was refluxed for 5h then cooled down to room temperature. The solvent was removed by rotary evaporator; DCM was used to extract the product. The organic layer was washed with DI water 3 times before dried over anhydrous Na_2SO_4. After filtration and concentration, the raw product was purified by column chromatography with hexane as eluent. Yield: 18 % (0.13 g, 0.47 mmol). ^{1}H NMR (400 MHz, Chloroform-*d*) δ 3.78 (t, *J* = 6.9 Hz, 2H), 3.67 (m, *J* = 5.7, 3.2, 1.5 Hz, 4H), 3.64 (d, *J* = 6.5 Hz, 2H), 3.28 (t, *J* = 6.9 Hz, 2H), 2.72 (q, *J* = 8.2, 6.4 Hz, 2H). ^{13}C NMR (100 MHz, Chloroform-*d*) δ 72.96, 71.99, 70.23, 70.17, 24.31, 2.92. HRMS (ESI+): m/z calc for $C_6H_{14}O_2SI$ $[M+H]^+$ 276.9759, found 276.9762.

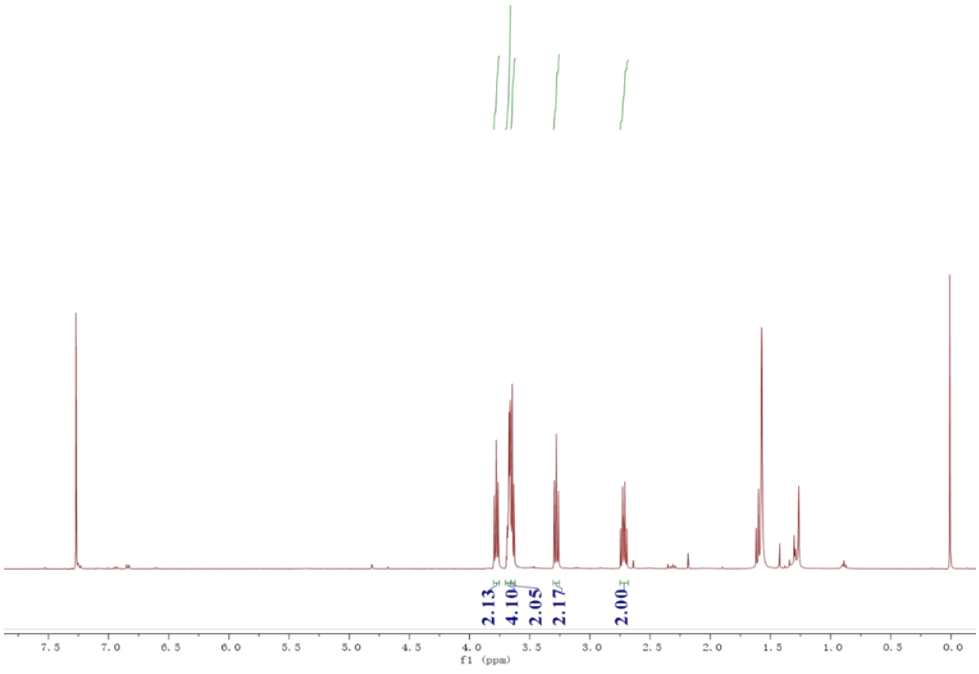

Fig. S56. The ^{1}H-NMR spectrum of compound HS-$(C_2O)_2$-C_2-I.

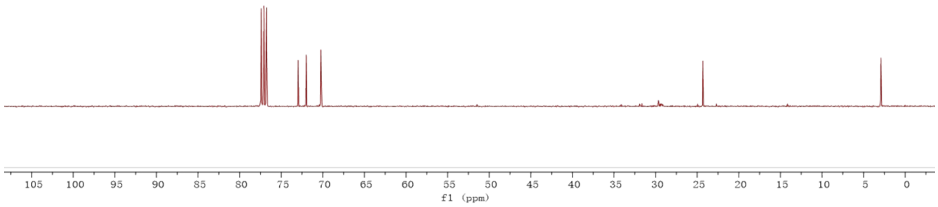

Fig. S57. The ^{13}C-NMR spectrum of compound HS-$(C_2O)_2$-C_2-I.

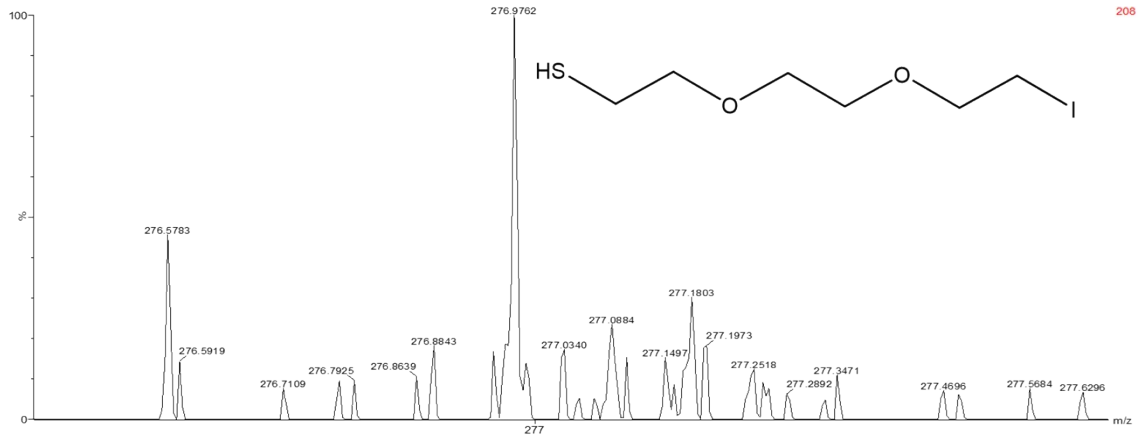

Fig. S58. The HRMS spectrum of compound HS-$(C_2O)_2$-C_2-I.

1-iodo-2-(2-(2-(2-iodoethoxy)ethoxy)ethoxy)ethane (I-$(C_2O)_3$-C_2-I) was prepared as follows.[7] To a stirred solution of 1-chloro-2-(2-(2-(2-chloroethoxy)ethoxy)ethoxy)ethane

(10.00 g, 43.29 mmol) in acetone (200.00 mL) was added powder NaI (25.97 g, 173.16 mmol). The resulting clear yellow solution was heated as reflux for 48h. Then, cooled, filtered through a plug of celite and concentrated to give yellow liquid. This was taken up in ether (200 mL) washed with water (50 mL) and 10% aq. $NaHSO_3$ (20 mL), dried ($NaHSO_4$), filtered. The crude thiol product was purified by column chromatography on silica gel (hexanes). Yield: 14.70 g, 35.49 mmol, 82.0 %. ^{1}H NMR (400 MHz, Chloroform-*d*) δ 3.77 (t, *J* = 6.9 Hz, 4H), 3.68 (s, 8H), 3.28 (t, *J* = 6.9 Hz, 4H).

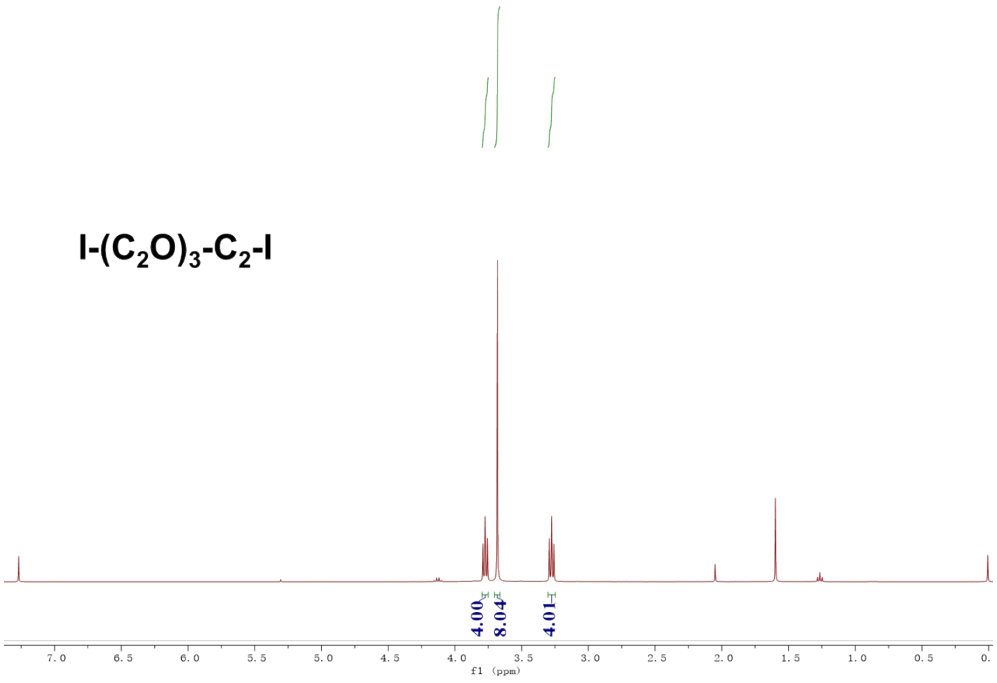

Fig. S59. The ^{1}H-NMR spectrum of compound I-$(C_2O)_3$-C_2-I.

***S*-(2-(2-(2-(2-chloroethoxy)ethoxy)ethoxy)ethyl) ethanethioate (I-$(C_2O)_3$-C_2-SAc)** was prepared as follows similar to the previous work reported.[1] 1-iodo-2-(2-(2-(2-iodoethoxy)ethoxy)ethoxy)ethane (17.94 g, 43.33 mmol) and potassium thioacetate (1.24 g, 10.83 mmol) were added into 200 mL tetrahydrofuran, stirred for 12h at room temperature, followed by removal of the tetrahydrofuran under reduced pressure. The residue was dissolved in diethyl ether, filtered, and washed with DI water. The organic layer was dried over Na_2SO_4, filtered and concentrated after which the raw product was purified with column chromatography with dichloromethane and hexane (1: 10). Yield: 3.49 g (9.64 mmol, 89.0 % yield). ^{1}H NMR (400 MHz, Chloroform-*d*) δ 3.78 (t, *J* = 7.4, 6.5 Hz, 2H), 3.70 – 3.65 (m, 8H),

3.64 – 3.61 (m, 2H), 3.29 (t, J = 7.3, 6.5 Hz, 2H), 3.12 (t, J = 6.5 Hz, 2H), 2.36 (s, 3H). ^{13}C NMR (100 MHz, Chloroform-*d*) δ 195.42, 71.98, 70.65, 70.61, 70.33, 70.25, 69.77, 30.58, 28.86, 2.97. HRMS (ESI+): m/z calc for $C_{10}H_{19}O_4SI$ $[M+Na]^+$ 384.9941, found 384.9940.

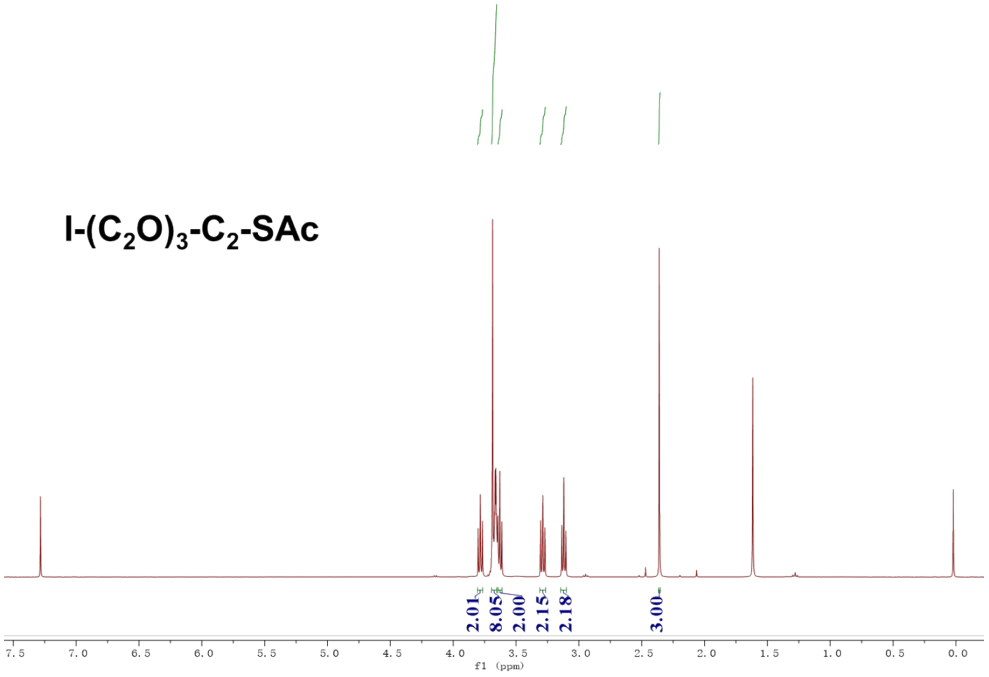

Fig. S60. The ^{1}H-NMR spectrum of compound I-$(C_2O)_3$-C_2-SAc.

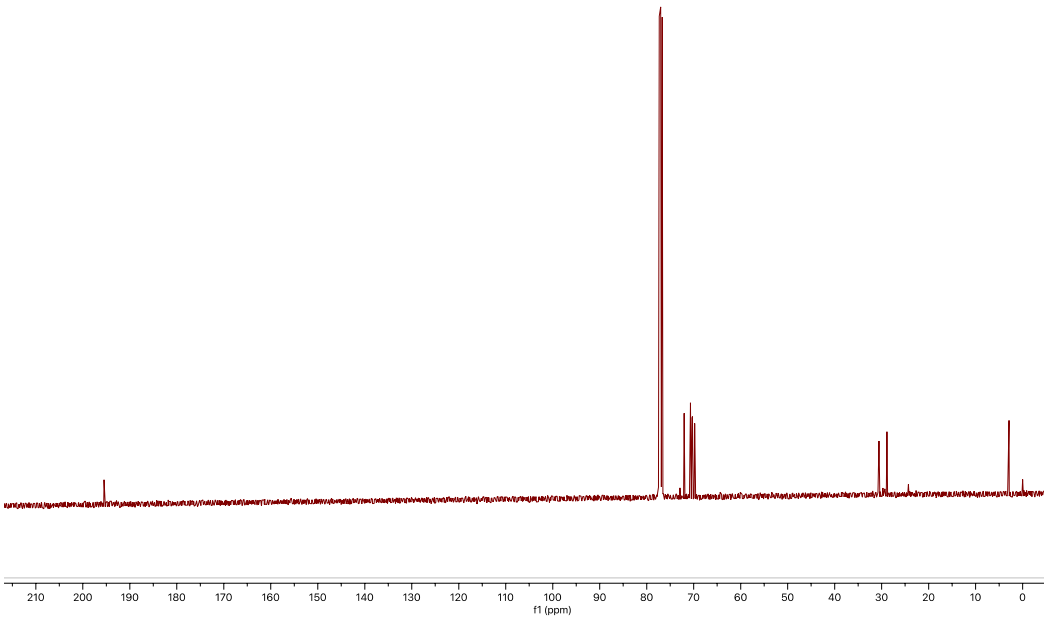

Fig. S61. The ^{13}C-NMR spectrum of compound I-$(C_2O)_3$-C_2-SAc.

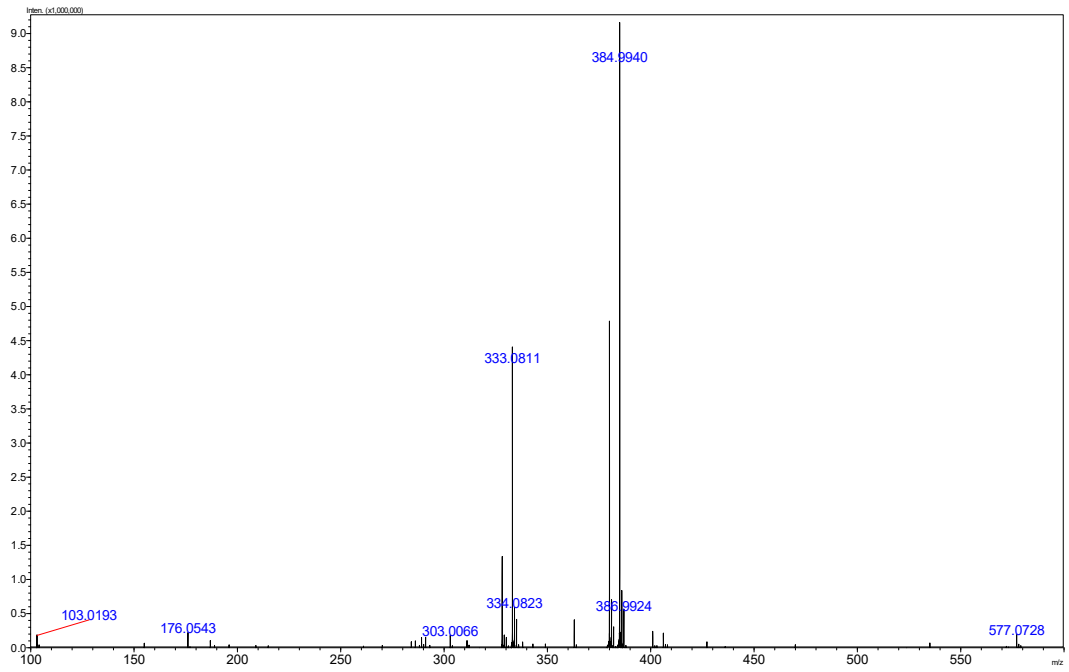

Fig. S62. The HRMS spectrum of compound I-$(C_2O)_3$-C_2-SAc.

2-(2-(2-(2-iodoethoxy)ethoxy)ethoxy)ethane-1-thiol (I-$(C_2O)_3$-C_2-SH) was prepared as follows. *S*-(2-(2-(2-(2-chloroethoxy)ethoxy)ethoxy)ethyl) ethanethioate (1.08 g, 2.98 mmol) was dissolved in 30 mL methanol and degassed for 20 min. Subsequently, 4.0 mL trifluoroacetic acid was added. The solution was refluxed for 5h then cooled down to room temperature. The solvent was removed by rotary evaporator; DCM was used to extract the product. The organic layer was washed with DI water 3 times before dried over anhydrous Na_2SO_4. After filtration and concentration, the raw product was purified by column chromatography with hexane as eluent. Yield: 18 % (0.17 g, 0.54 mmol). ^{1}H NMR (400 MHz, Chloroform-*d*) δ 3.81 – 3.77 (t, 2H), 3.71 – 3.67 (m, 8H), 3.66 – 3.63 (t, 2H), 3.29 (t, J = 7.4, 6.4 Hz, 2H), 2.73 (q, J = 8.2, 6.4 Hz, 2H). ^{13}C NMR (100 MHz, Chloroform-*d*) δ 72.91, 72.00, 70.71, 70.67, 70.65, 70.27, 24.32, 2.95. HRMS (ESI+): m/z calc for $C_8H_{18}O_3SI$ $[M+H]^+$ 321.0021, found 321.0023.

509 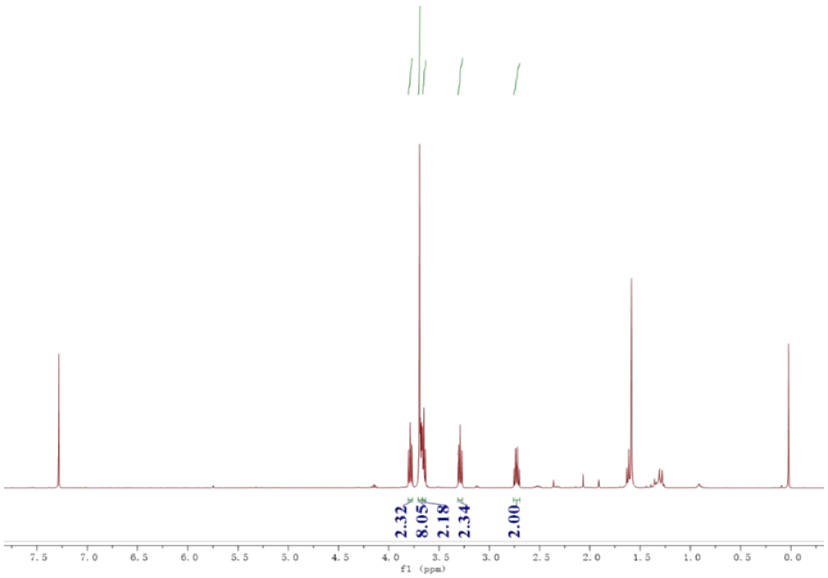

510 **Fig. S63.** The ^{1}H-NMR spectrum of compound HS-$(C_2O)_3$-C_2-I.

511 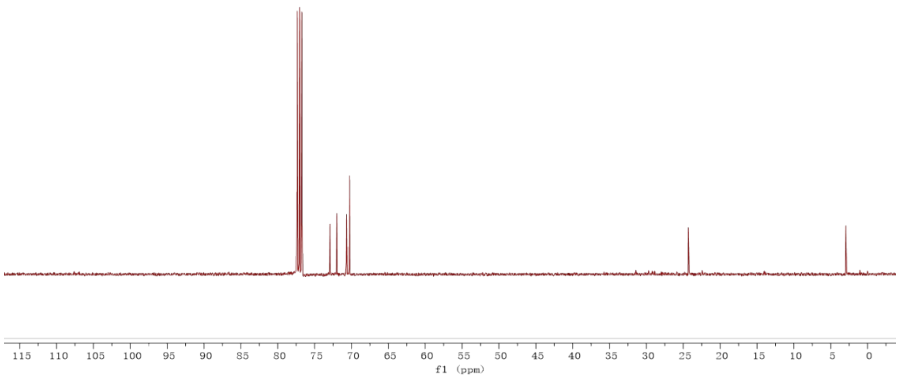

512 **Fig. S64.** The ^{13}C-NMR spectrum of compound HS-$(C_2O)_3$-C_2-I.

513

514 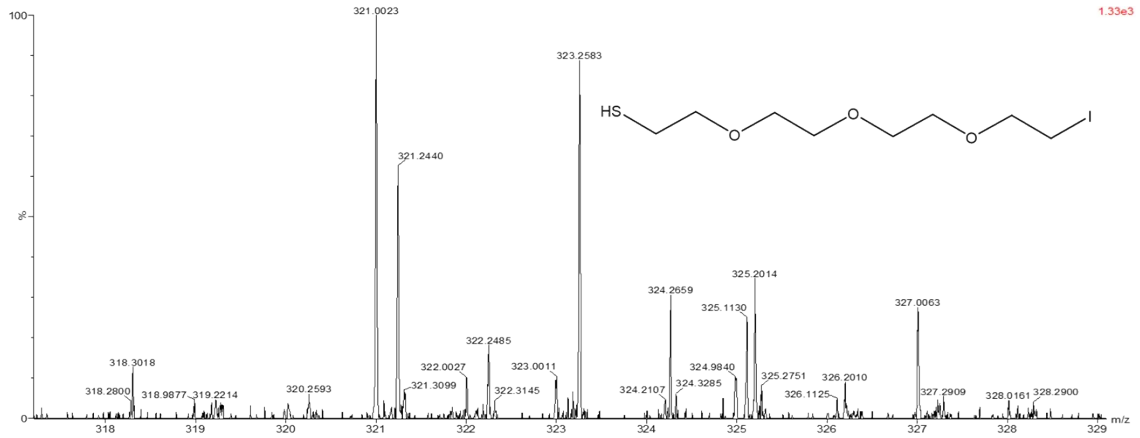

515 **Fig. S65.** The HRMS spectrum of compound HS-$(C_2O)_3$-C_2-I.

516

517 **1,14-diiodo-3,6,9,12-tetraoxatetradecane (I-$(C_2O)_4$-C_2-I)** was prepared as follows.[8] To a

stirred solution of 3,6,9,12-tetraoxatetradecane-1,14-diyl bis(4-methylbenzenesulfonate) (10.00 g, 18.32 mmol) in acetone (200.00 mL) was added powder NaI (10.98 g, 73.26 mmol). The resulting clear yellow solution was heated as reflux for 48h. Then, cooled, filtered through a plug of celite and concentrated to give yellow liquid. This was taken up in ether (200 mL) washed with water (50 mL) and 10% aq. $NaHSO_3$ (20 mL), dried ($NaHSO_4$), filtered. The crude thiol product was purified by column chromatography on silica gel (hexanes). Yield: 6.68 g, 15.02 mmol, 82.0 %. ^{1}H NMR (400 MHz, Chloroform-*d*) δ 3.78 (t, *J* = 7.3, 6.6 Hz, 4H), 3.69 (s, *J* = 1.9 Hz, 12H), 3.29 (t, *J* = 6.9 Hz, 4H).

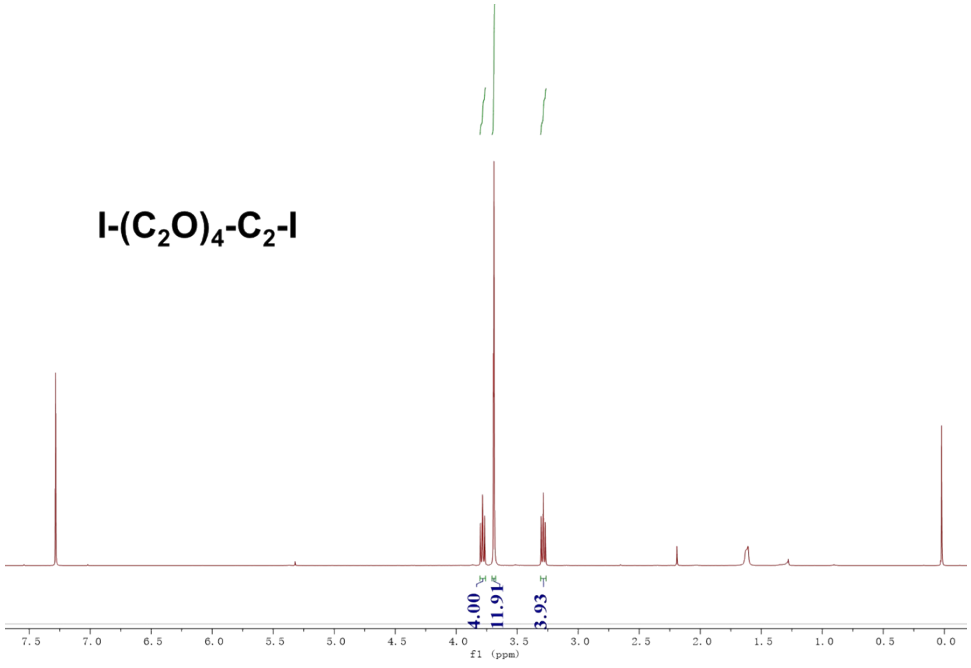

Fig. S66. The ^{1}H-NMR spectrum of compound I-$(C_2O)_4$-C_2-I.

***S*-(14-iodo-3,6,9,12-tetraoxatetradecyl) ethanethioate (I-$(C_2O)_4$-C_2-SAc)** was prepared as follows similar to the previous work reported.[1] 1,14-diiodo-3,6,9,12-tetraoxatetradecane (6.68 g, 15.02 mmol) and potassium thioacetate (0.43 g, 3.76 mmol) were added into 100 mL tetrahydrofuran, stirred for 12h at room temperature, followed by removal of the tetrahydrofuran under reduced pressure. The residue was dissolved in diethyl ether, filtered, and washed with DI water. The organic layer was dried over Na_2SO_4, filtered and concentrated after which the raw product was purified with column chromatography with dichloromethane and hexane (1: 10). Yield: 1.26 g (3.35 mmol, 89.0 % yield). ^{1}H NMR (400 MHz,

Chloroform-*d*) δ 3.78 (t, *J* = 6.9 Hz, 2H), 3.70 – 3.65 (m, 12H), 3.62 (t, *J* = 6.4 Hz, 2H), 3.29 (t, *J* = 6.9 Hz, 2H), 3.12 (t, *J* = 6.5 Hz, 2H), 2.36 (s, 3H). ^{13}C NMR (100 MHz, Chloroform-*d*) δ 195.41, 71.98, 70.68, 70.66, 70.61, 70.53, 70.33, 70.24, 69.76, 30.56, 28.85, 2.94. HRMS (ESI+): m/z calc for $C_{12}H_{23}O_5SI$ $[M+Na]^+$ 429.0203, found 429.0202.

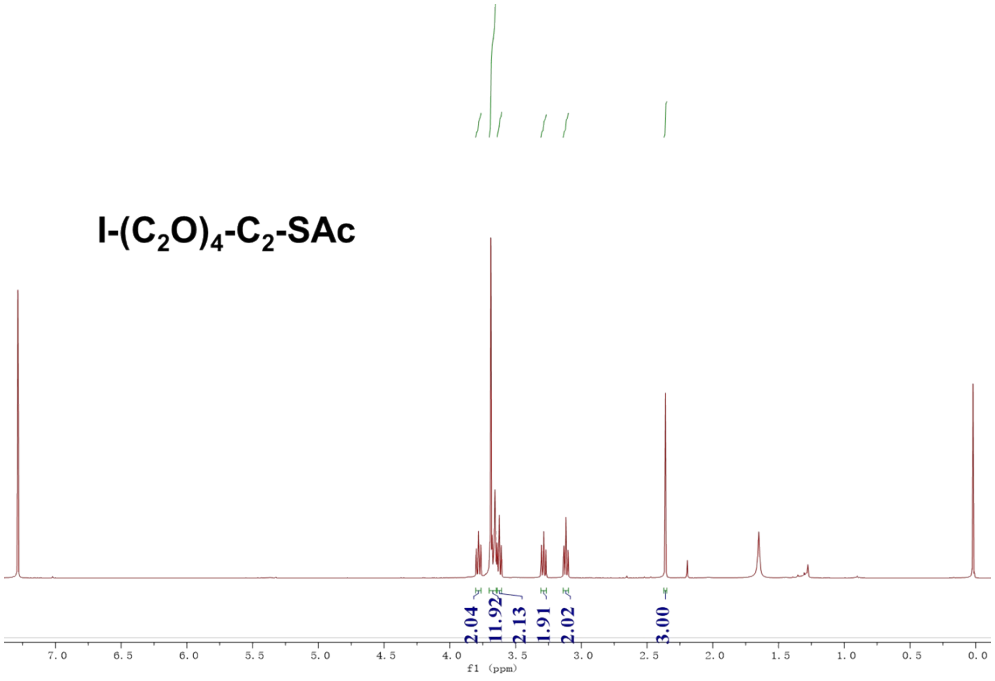

Fig. S67. The ^{1}H-NMR spectrum of compound I-$(C_2O)_4$-C_2-SAc.

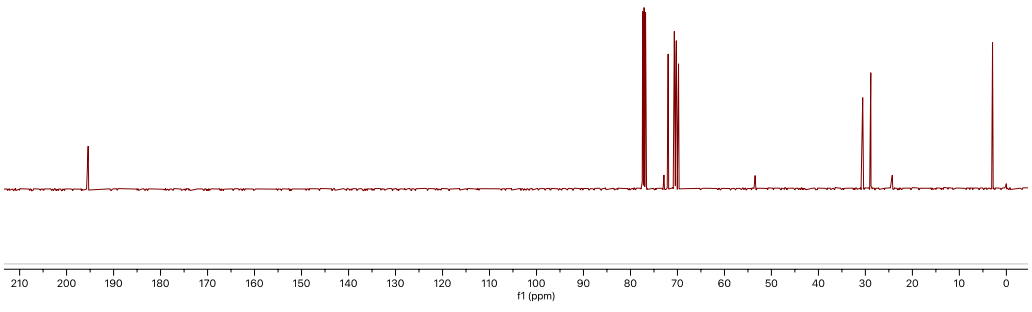

Fig. S68. The ^{13}C-NMR spectrum of compound I-$(C_2O)_4$-C_2-SAc.

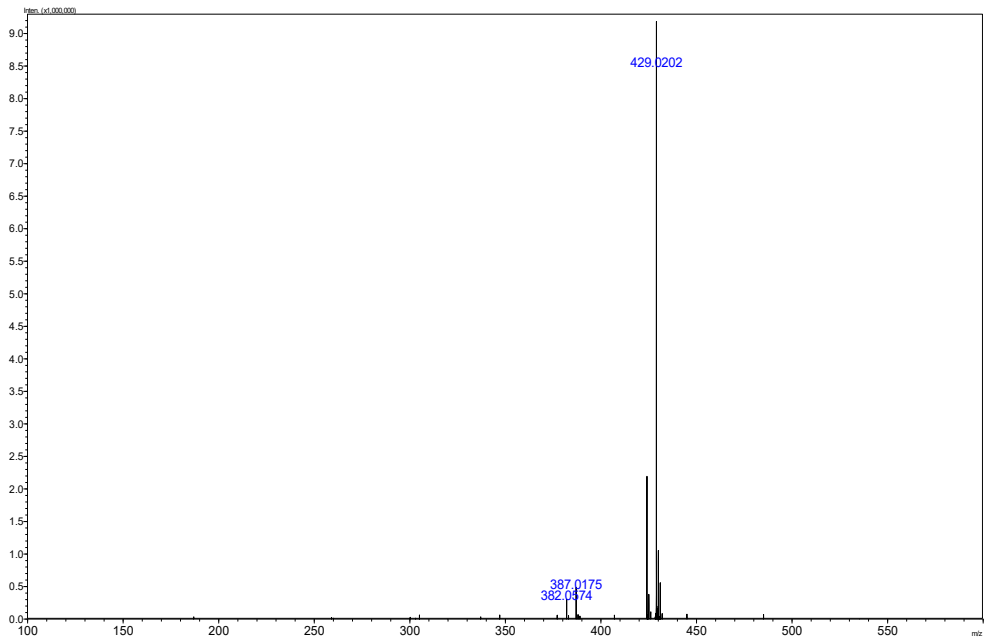

Fig. S69. The HRMS spectrum of compound I-$(C_2O)_4$-C_2-SAc.

14-iodo-3,6,9,12-tetraoxatetradecane-1-thiol (I-$(C_2O)_4$-C_2-SH) was prepared as follows. *S*-*S*-(14-iodo-3,6,9,12-tetraoxatetradecyl) ethanethioate (1.26 g, 3.35 mmol) was dissolved in 30 mL methanol and degassed for 20 min. Subsequently, 4.0 mL trifluoroacetic acid was added. The solution was refluxed for 5h then cooled down to room temperature. The solvent was removed by rotary evaporator; DCM was used to extract the product. The organic layer was washed with DI water 3 times before dried over anhydrous Na_2SO_4. After filtration and concentration, the raw product was purified by column chromatography with hexane as eluent. Yield: 18 % (0.22 g, 0.60 mmol). ^{1}H NMR (400 MHz, Chloroform-*d*) δ 3.78 – 3.75 (t, 2H), 3.67 (m, *J* = 7.0, 2.1 Hz, 12H), 3.62 (t, *J* = 6.4 Hz, 2H), 3.28 (t, *J* = 6.9 Hz, 2H), 2.71 (q, *J* = 8.2, 6.4 Hz, 2H). ^{13}C NMR (100 MHz, Chloroform-*d*) δ 72.87, 71.97, 70.70, 70.66, 70.62, 70.56, 70.25, 70.23, 24.30, 3.01. HRMS (ESI+): m/z calc for $C_{10}H_{22}O_4SI$ $[M+H]^+$ 365.0283, found 365.0259.

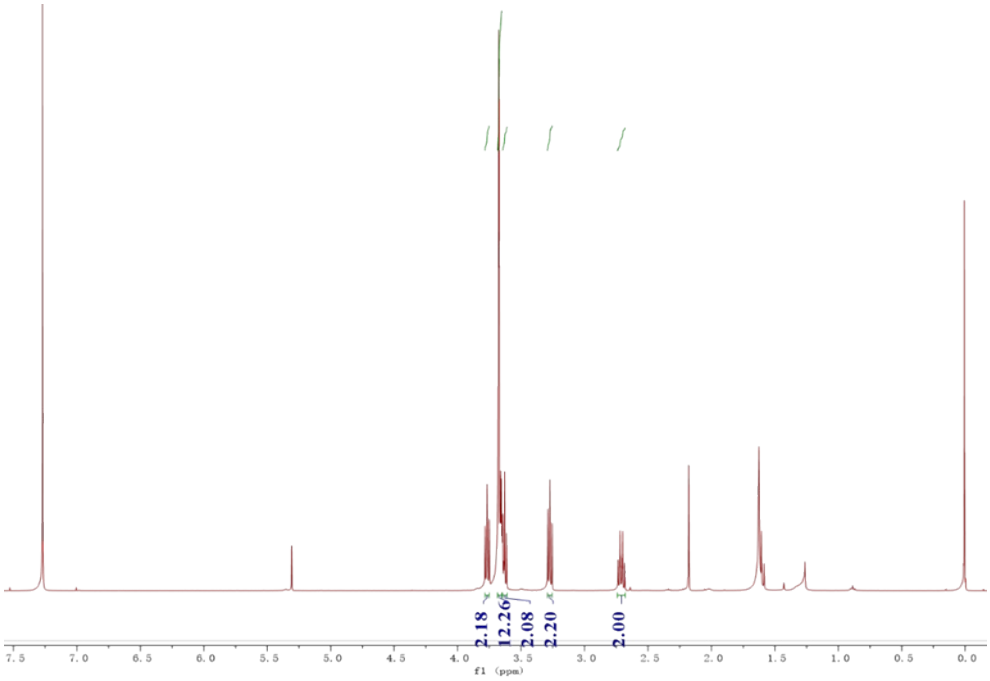

Fig. S70. The ^{1}H-NMR spectrum of compound HS-$(C_2O)_4$-C_2-I.

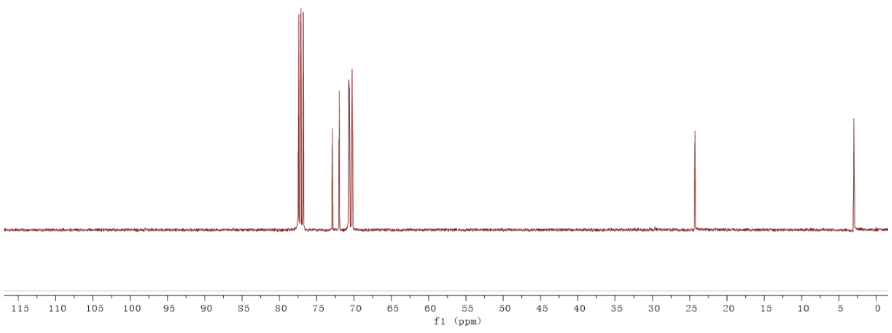

Fig. S71. The ^{13}C-NMR spectrum of compound HS-$(C_2O)_4$-C_2-I.

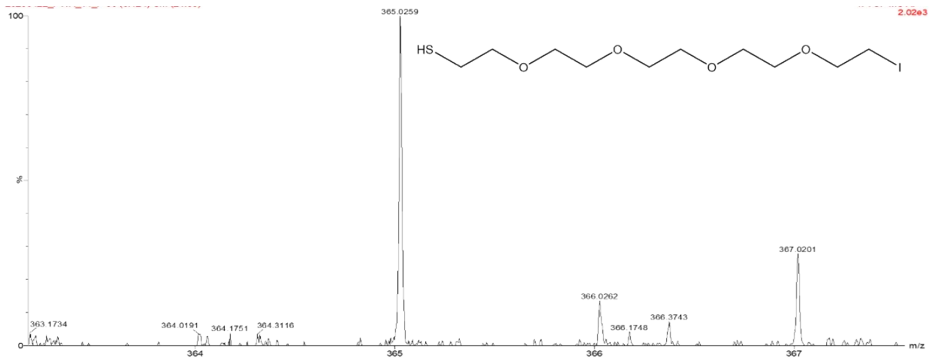

Fig. S72. The HRMS spectrum of compound HS-$(C_2O)_4$-C_2-I.

S2. SAMs preparations

Template-stripped Au surfaces (Au^{TS}). Au^{TS} substrates were prepared as our previous works

reported. [9-11] Firstly, Au (a purity of 99.999% from Dimu Materials, Inc (China)) film with thickness of ~200 nm was thermally deposited on the surface of clean Si (100) wafers (KYKY-400, Zhongke Ke Yi, China), which natively possesses a SiO_2 layer under the base pressure of 2×10^{-5} Pa. In this process, the evaporation rate was primarily set as 0.2 Å/s at the first 50nm and then ~1 Å/s for the rest 150 nm. Secondly, the ultrasonically cleaned glass slides (1.5 × 1.5 cm^2) were dried in a stream of N_2 gas, followed by cleaned by a plasma of air for 5 mins at a pressure of 100 Pa. The slides were stuck on the Au substrate through photo-curable optical adhesive (Norland, No. 61). Thirdly, to cure the optical adhesive, the substrates were placed in a 100 Watt UV lamp at a distance of approximately 60 cm from the light source for about 1 hour. Before preparation of SAMs, the slides with a layer of Au were lift-off by a razor blade.

SAMs preparation. To assembled SAMs, the Au^{TS} substrates were placed in degassed 1 mM ethanolic solutions of the targeted molecules overnight under the protection of inert nitrogen environment. After that, ethanol (AR grade) was utilized to remove the undensely packed molecules, like the physisorbed one, a stream of dry N_2 was used to gently dried the surface of SAMs, and conducted electrical measurements with minutes to avoid the degradation of Au-S covalent interactions as well as surface contaminations.

S3. Sample Characterizations.

X-ray Photoelectron Spectroscopy (XPS) Measurements. XPS was utilized to detect the quality and supermolecular molecular structures of the SAMs composed of the saturated molecules with instruments located in National Center of Electron Spectroscopy in Beijing. The Thermo Scientific K-Alpha XPS system was used as the incident X-ray beam with energy of 1486.6 eV. We collected the high-resolution XPS spectra of S 2*p*, C 1*s*, I 4*f*, O 1*s*. It is worth noted that the peaks of high-resolution XPS spectra of C 1*s* and O 1*s* may originated from the impurities absorbed on the surface of the SAMs in atmosphere. Therefore, detailed analysis of the compositional ratio of C and O for all SAMs seems to have little significance.

To further analyze the chemical environments of each element, the least-square peak fit with a pseudo-Voigt function (a linear combination of Lorentzian (30%) and Gaussian (70%)

functions)[12] was utilized to fit the XPS spectra with Avantage software, and the sloping background was modelled using a smart background correction.

Ultraviolet Photoelectron Spectroscopy (UPS) Measurements. UPS was carried out to characterize the work function (WF) and the location of HOMO with instrument installed in the Thermo Scientific K-Alpha XPS system. The photon energy at 21.22 eV and -10 V bias was utilized to the samples to probe the valence band. The fermi edge of Au was regarded as the reference for all the UPS spectra.

As reported before [1, 13, 14], the S 2*p* spectra could incorporate the chemically adsorbed components (~162 eV), physical adsorbed components (~163 eV) and adsorption at defect sites (~161 eV). As for the I 3*d* XPS spectra that showed two signals in Fig. S74 and S76, other groups have also made these observations. [1, 15] They argued that the origin of these peaks is not clear, which has been attributed to the radiation damage or the formation of metal-I bonds. Hence, the I 3*d* spectra were mainly used to verify the detection of I element in the SAMs with the terminal I atom substitution. Besides, we also carried out the UPS characterizations for the prepared SAMs (Fig.s S77-S80 and Tables S1-S4), from which it could be seen that there is no significant difference in the energy offset (δE_{ME}) for these SAMs, indicating that the SAMs have similar coverage and structure on the bottom electrode.

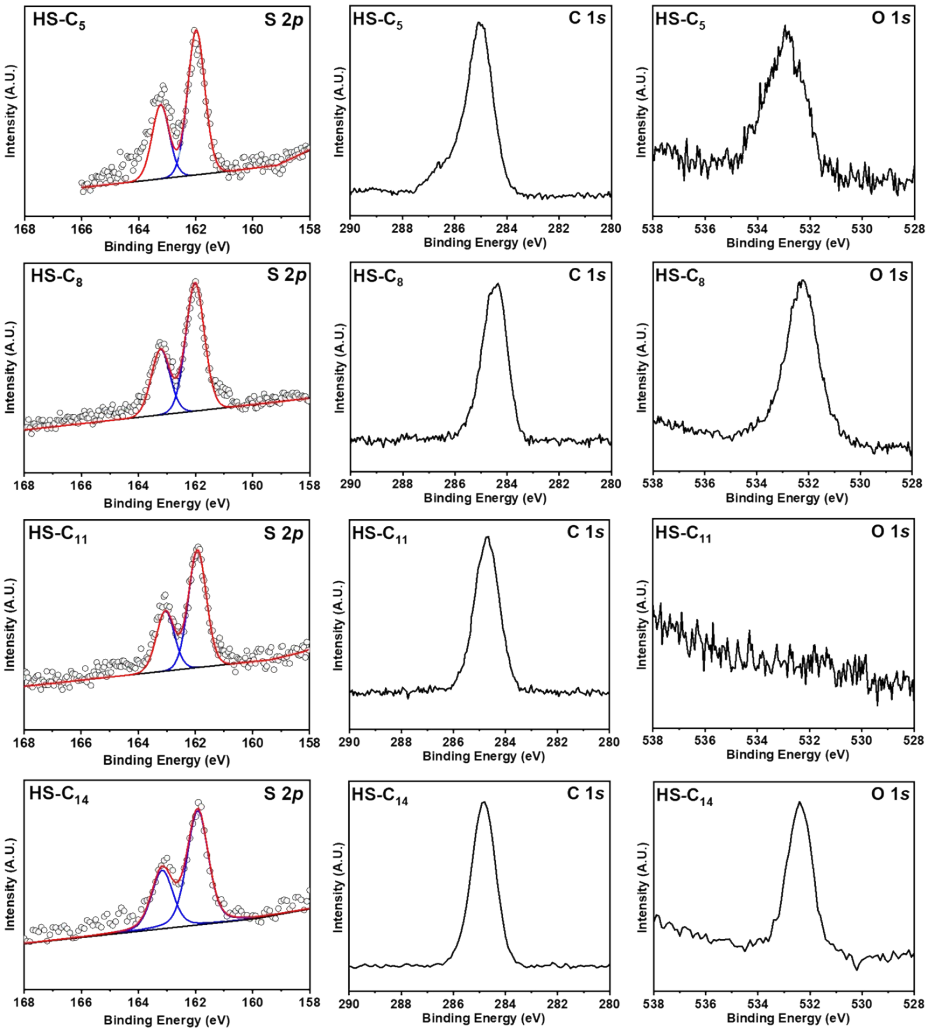

Fig. S73. The high resolution XPS S 2*p*, C 1*s* and O1*s* spectra for Au-SC_5, Au-SC_8, Au-SC_{11} and Au-SC_{14}.

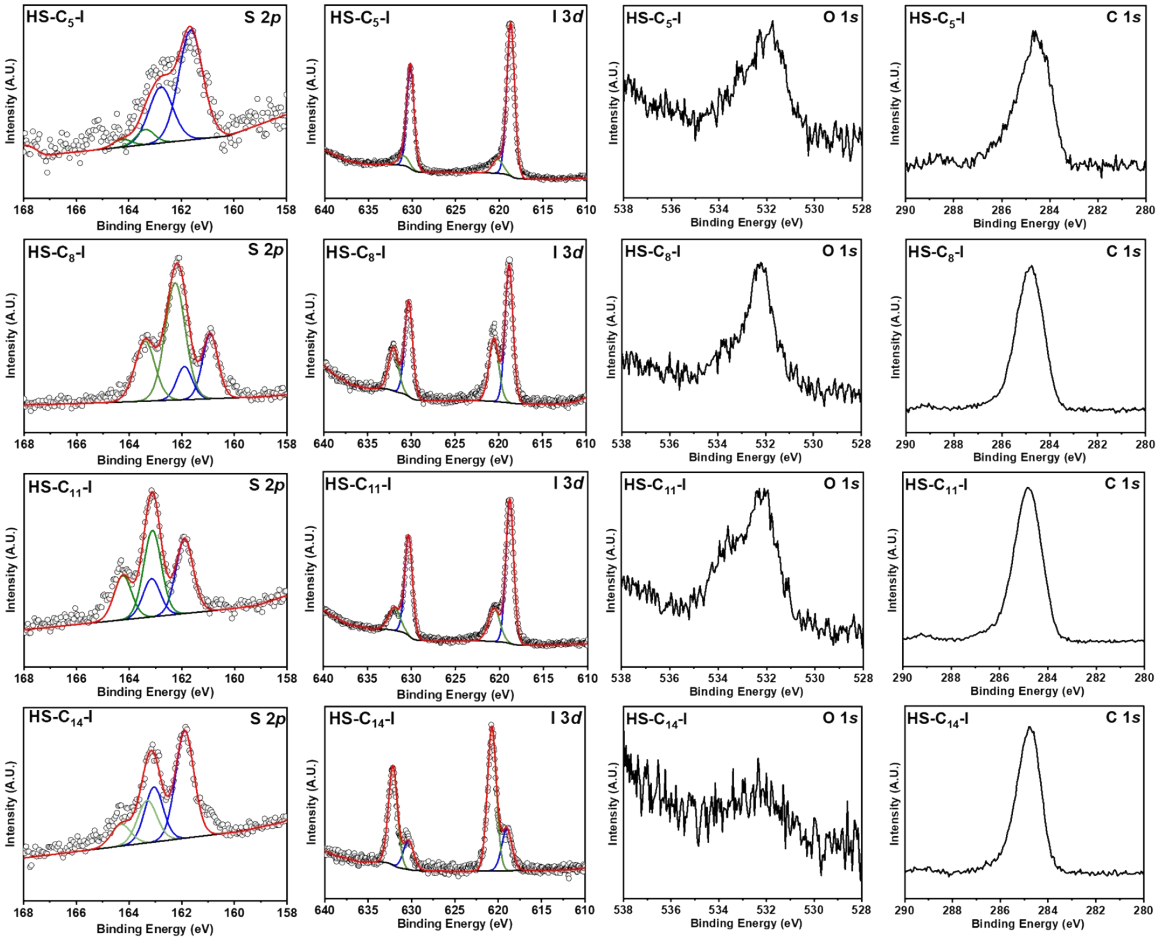

Fig. S74. The high resolution XPS S 2*p*, C 1*s* and O1*s* spectra for Au-SC_5-I, Au-SC_8-I, Au-SC_{11}-I and Au-SC_{14}-I.

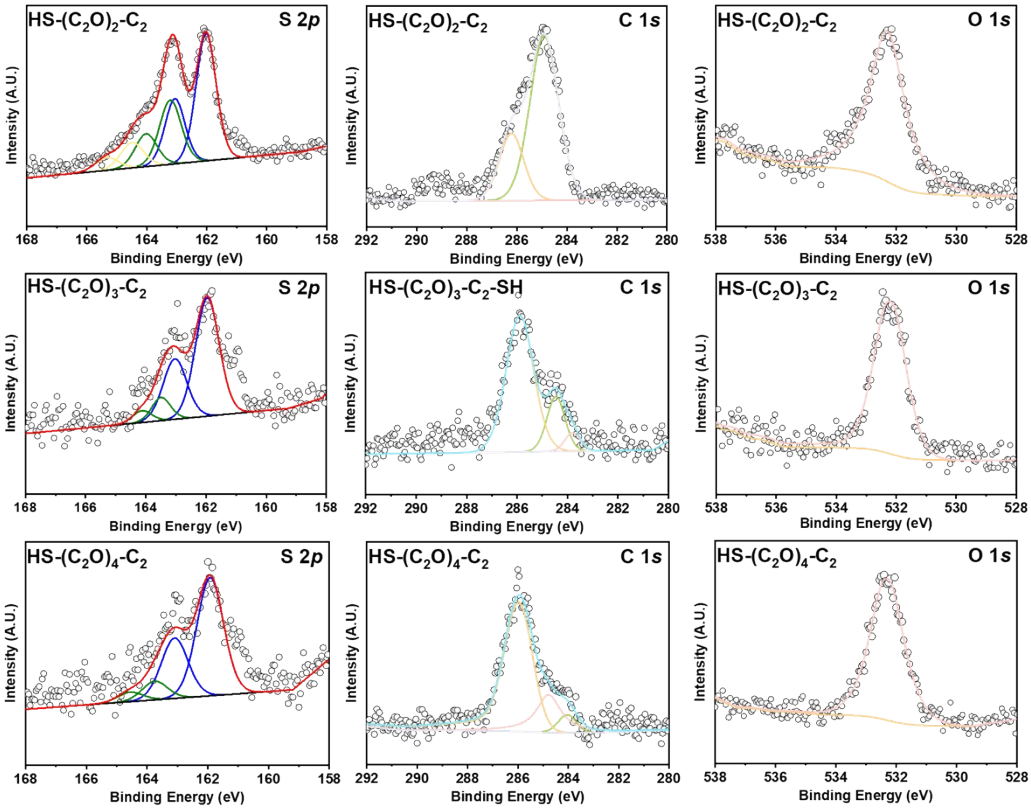

Fig. S75. The high resolution XPS S 2*p*, C 1*s* and O1*s* spectra for Au-S$(C_2O)_2$-C_2, Au-S$(C_2O)_3$-C_2 and Au-S$(C_2O)_4$-C_2.

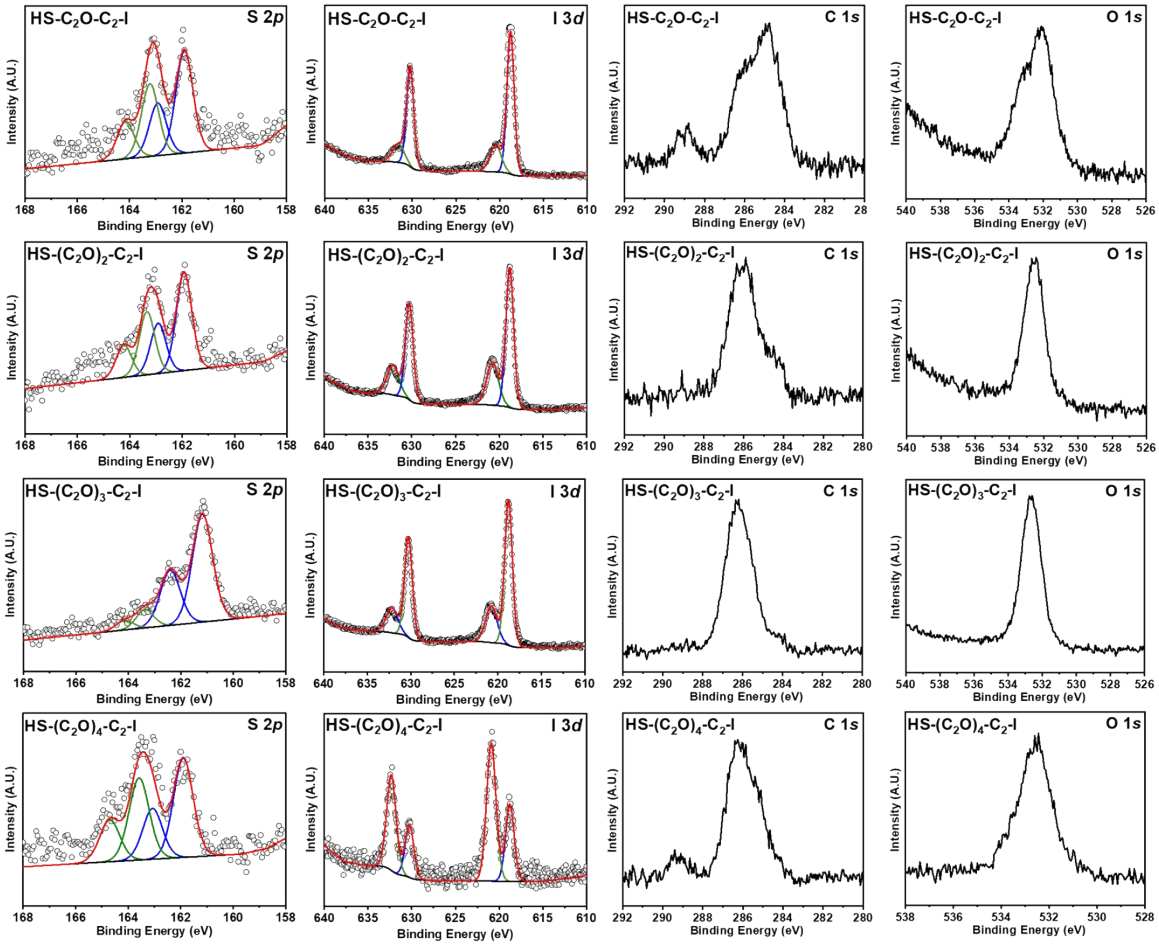

628

629 **Fig. S76.** The high resolution XPS S 2*p*, C 1*s* and O1*s* spectra for Au-SC_2O-C_2-I, Au-

630 $S(C_2O)_2$-C_2-I, Au-$S(C_2O)_3$-C_2-I and Au-$S(C_2O)_4$-C_2-I.

631

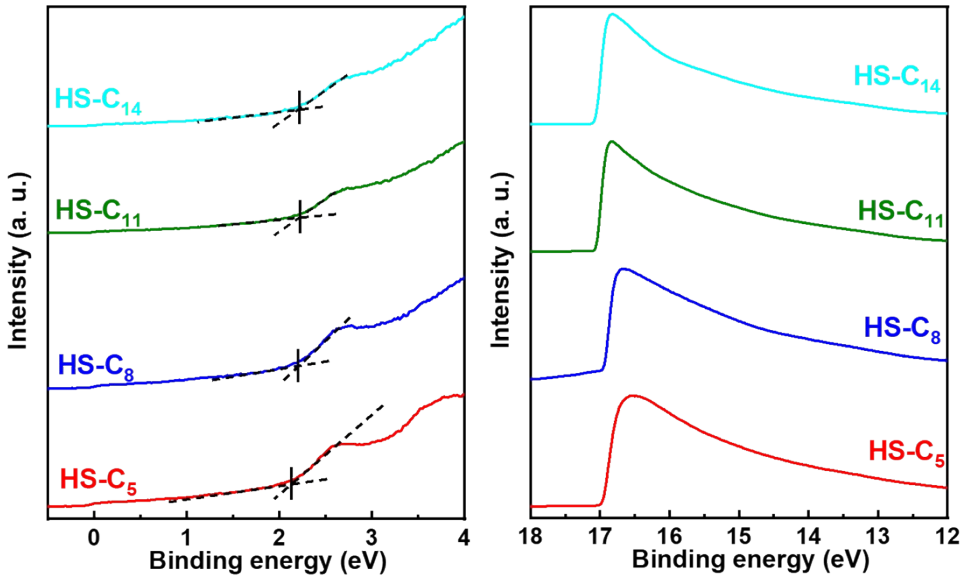

632

633 **Fig. S77.** Secondary cutoff and valence band spectra of the HOMO peak for Au-SC_5, Au-SC_8,

634 Au-SC_{11} and Au-SC_{14}. determined by UPS.

Table S1. Properties of the studied SAMs obtained by UPS

Molecules	δE_{ME} (eV)	$E_{\text{cut off}}$ (eV)	WF (eV)	E_{HOMO} (eV)
HS-C_5	2.10	17.00	4.22	-6.32
HS-C_8	2.17	16.96	4.26	-6.43
HS-C_{11}	2.13	17.06	4.16	-6.29
HS-C_{14}	2.13	17.09	4.13	-6.26

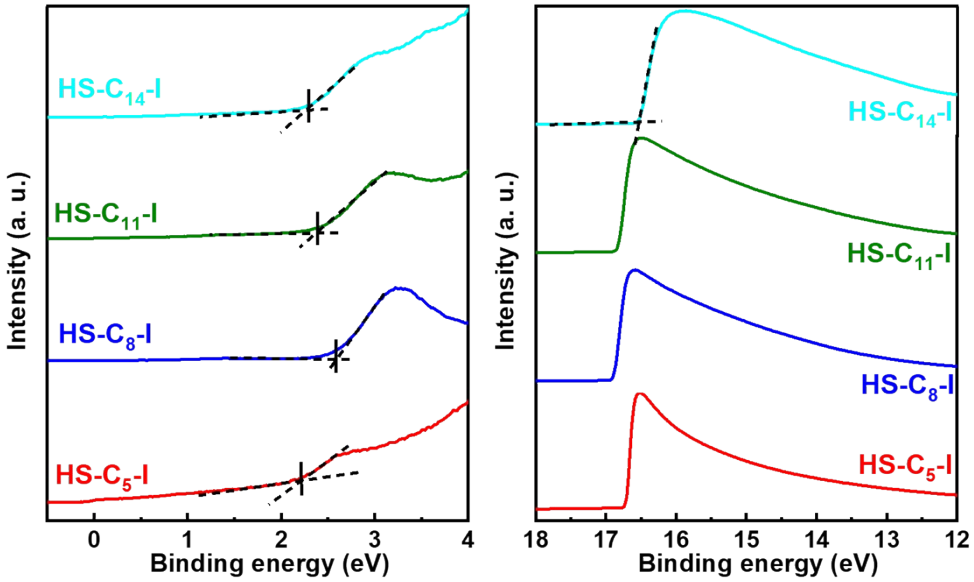

Fig. S78. Secondary cutoff and valence band spectra of the HOMO peak for Au-SC_5-I, Au-SC_8-I, Au-SC_{11}-I and Au-SC_{14}-I. determined by UPS.

Table S2. Properties of the studied SAMs obtained by UPS

Molecules	δE_{ME} (eV)	$E_{\text{cut off}}$ (eV)	WF (eV)	E_{HOMO} (eV)
HS-C_5-I	2.11	16.75	4.47	-6.58
HS-C_8-I	2.57	16.87	4.35	-6.92
HS-C_{11}-I	2.38	16.82	4.40	-6.78
HS-C_{14}-I	2.28	16.53	4.69	-6.97

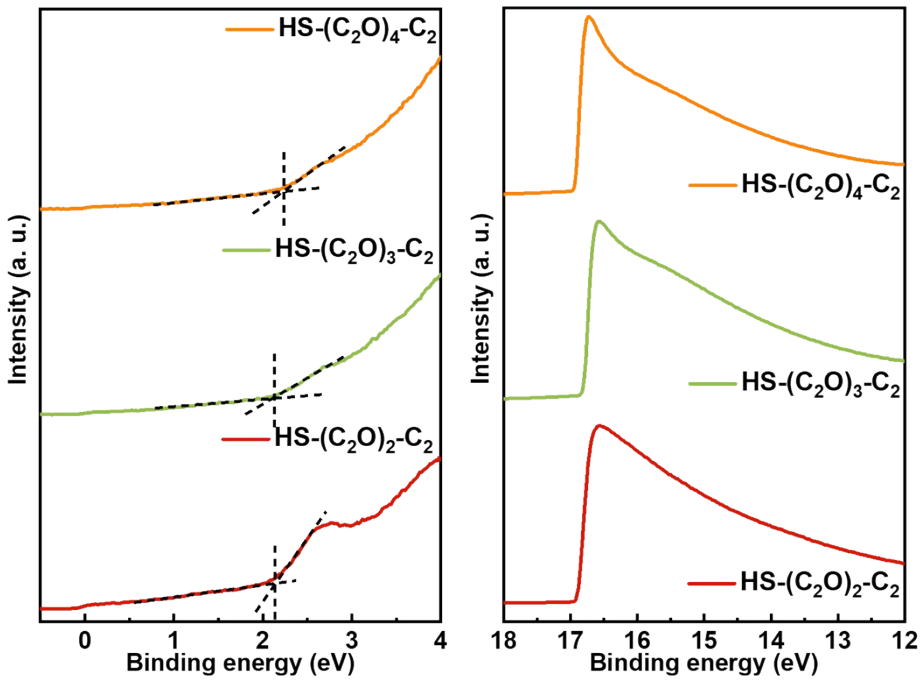

644

645 **Fig. S79.** Secondary cutoff and valence band spectra of the HOMO peak for Au-S$(C_2O)_2$-C_2,

646 Au-S$(C_2O)_3$-C_2 and Au-S$(C_2O)_4$-C_2 determined by UPS.

647

648 **Table S3.** Properties of the studied SAMs obtained by UPS

Molecules	δE_{ME} (eV)	$E_{\text{cut off}}$ (eV)	WF (eV)	E_{HOMO} (eV)
HS-$(C_2O)_2$-C_2	2.13	16.92	4.30	-6.43
HS-$(C_2O)_3$-C_2	2.09	16.82	4.40	-6.49
HS-$(C_2O)_4$-C_2	2.22	16.94	4.28	-6.50

649

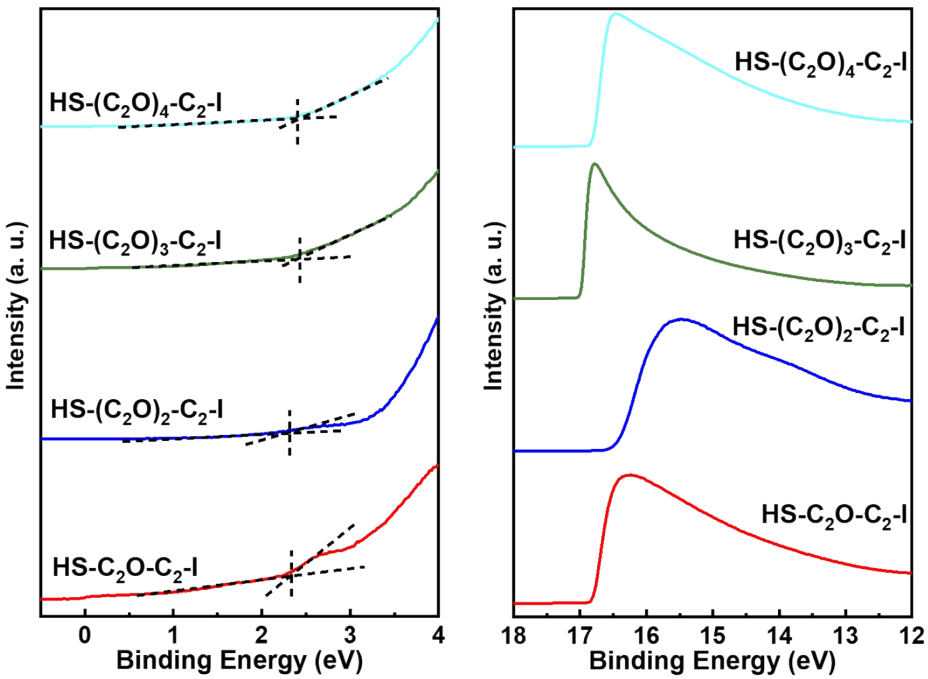

Fig. S80. Secondary cutoff and valence band spectra of the HOMO peak for Au-SC_2O-C_2-I, Au-$S(C_2O)_2$-C_2-I, Au-$S(C_2O)_3$-C_2-I and Au-$S(C_2O)_4$-C_2-I determined by UPS.

Table S4. Properties of the studied SAMs obtained by UPS

Molecules	δE_{ME} (eV)	$E_{\text{cut off}}$ (eV)	WF (eV)	E_{HOMO} (eV)
HS-C_2O-C_2-I	2.22	16.84	4.38	-6.60
HS-$(C_2O)_2$-C_2-I	2.31	16.52	4.70	-7.01
HS-$(C_2O)_3$-C_2-I	2.42	17.00	4.22	-6.64
HS-$(C_2O)_4$-C_2-I	2.40	16.80	4.42	-6.82

S4. Electrical conductance measurements and analysis.

According to our previous work, [9, 10] the cone-shaped tips of Ga_2O_3/EGaIn was contacted with SAMs to form molecular junctions. One of the most important components of the EGaIn junction setup is the micromanipulator (Leica) equipped with a 10-μL glass syringe (Hamilton, 1701RNR) with a metal needle (Hamilton, conical shape 26s) from which the cone-shaped Ga_2O_3/EGaIn top-electrodes are suspended. The drift of this micromanipulator is small (1 nm / h) and it can move the top electrode at a precision of 10 nm precision in the z direction and up to 10 cm in the x direction. The micromanipulator is mounted on an M6 threaded aluminum

breadboard board, along with a USB camera (Edmund Optics, EO-3112C color USB camera) on the a XYZ translation stage with zoom magnification of 4: 1 and 2.5-10 times (Edmund Optics, VZM 100DI) to image and determine the diameter of computer nodes on the screen. The system can magnify a node with a typical diameter of 20 μm by up to 400 times. In order to ensure good electrical contact, a copper wire is welded to the microneedle of the syringe that was attached to the instrument with an alligator clips. A micro-positioner (Crest innovation, S-725PLM) is used to hold the tip of the tungsten probe that is penetrated the SAM and formed direct electrical contact with the Au^{TS} substrate. The entire setup is placed in an aluminum box on an optical table (Zolix) that dampened the vibrations. The cameras, piezoelectric and source gauges are connected to external computers and controlled by LabView. To measure the conductance of the SAMs, the bottom electrode was grounded and the top electrode of Ga_2O_3/EGaIn tip was biased using a sub-femtoamp source meter (Keithley 6430) and shielding cable. To prepare a new cone-shaped tip of Ga_2O_3/EGaIn, the syringe was positioned near a bare Au^{TS} substrate. We squeeze out a small drop of EGaIn so that it remains attached to the tip of the syringe needle, then it was made contact with a freshly prepared sacrificial surface. By slowly lifting the microneedle from Ga_2O_3/EGaIn towards z direction, the Ga_2O_3/EGaIn drop deformed and formed two head-to-head connectors. Finally, the two cones separated, resulting in a cone-shaped tip of Ga_2O_3/EGaIn suspended on a miniature needle and another standing on the Au^{TS} surface. The sacrificial Au^{TS} surface are discarded in favor of Au^{TS} surface that support interested SAMs. The conical-shaped Ga_2O_3/EGaIn is about 10 to 20 microns in diameter, depending on the speed at which the tiny needle is pulled from the Ga_2O_3/EGaIn droplet. The final step, with the camera trained on the node, is to make contact with the SAMs via the conical tip of Ga_2O_3/EGaIn to fabricate the molecular junctions.

During the electrical conductance measurements, the Au^{TS} bottom electrode was grounded and the EGaIn electrode was biased from 0V → +0.5 V → 0V → -0.5 V → 0V, with a step size of 50 mV and a delay of 0.1 s. We collected at least three samples to obtain ≥20 junctions, each with 20-24 $J(V)$ traces, which contains a total of ~480 $J(V)$ traces for each type of SAM. Then, the histograms of $\log_{10}|J|$ were plotted for each bias and fitted Gaussians to the histograms to

obtain the log-mean (μ_{log}) of the values of J and their log standard-deviations (σ_{log}).

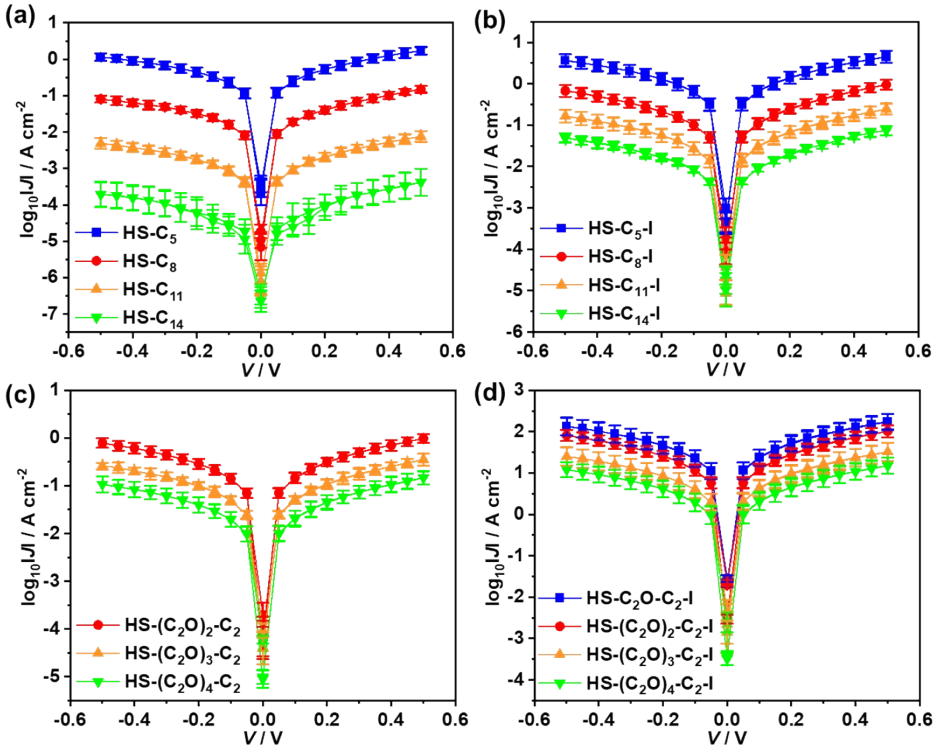

Fig. S81. Average plots of the $\log_{10}|J|-V$ of (a) HS-C_n (n = 5, 8, 10, 11), (b) HS-C_n-I (n = 5, 8, 10, 11), (c) HS-$(C_2O)_m$-C_2 (m = 2, 3, 4), (d) HS-$(C_2O)_m$-C_2-I (m = 1, 2, 3, 4).

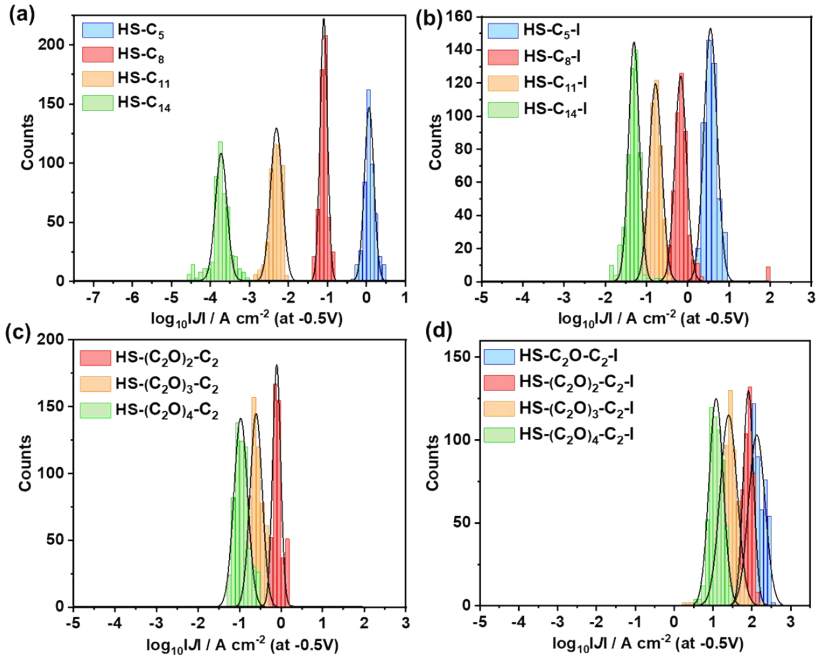

Fig. S82. The histograms of $\log_{10}|J|$ at -0.5V with Gaussian fits for (a) HS-C_n (n = 5, 8, 10, 11), (b) HS-C_n-I (n = 5, 8, 10, 11), (c) HS-$(C_2O)_m$-C_2 (m = 2, 3, 4), (d) HS-$(C_2O)_m$-C_2-I (m =

1, 2, 3, 4).

S5. Thermoelectrical measurements and determination of PF for the molecular junctions. The processes of obtaining the *S* of molecular junctions were followed by our previous work. [11] Based on the "EGaIn" junction setup, we introduce a polyimide (PI) film embedded with multiple heating resistors to heat the bottom electrode generating temperature difference (ΔT = 2.0 K, 3.5 K, 5.0 K) across the molecular junctions as shown in Fig. S83a and S83b. Molecules were assembled on the Au^{TS} electrodes and the conical shaped tips of EGaIn were used to conformally contact the top-surface of the SAMs eventually forming molecular thermoelectric junctions. When the Au^{TS} electrode was heated, *S* of the SAMs, according to Seebeck effect, can be determined by measuring the thermoelectric voltage (ΔV) across the junction and deducing the relationship between ΔV and Seebeck coefficient. The values of ΔV for the SAMs at applied ΔT were obtained by the voltmeter (2182A Nanovoltmeter, Keithley Inc., USA). The temperature of the Au^{TS} electrode and the end of the metal needle (Hamilton, conical shape 26s) were monitored by thermal couple with a detection limit of 0.01K, simultaneously, from which we can roughly extracted the ΔT across the molecular junction induced by the PI film. Typical thermoelectric-voltage traces of the Au^{TS}-S-C_2O-C_2-I//Ga_2O_3/EGaIn junctions at different ΔT are shown in Fig. S83c. Wherein, V_1 refers to the initial voltage across a junction without ΔT (the magnitude of V_1 originated from chemical potential difference at the SAM/electrode interface at room temperature (RT)), the average of V_1 ($<V_1>$) and its standard deviation could be obtained over ~50 s test duration (rate of data acquisition: 10 data points of voltage per second) with a Gaussian fit.

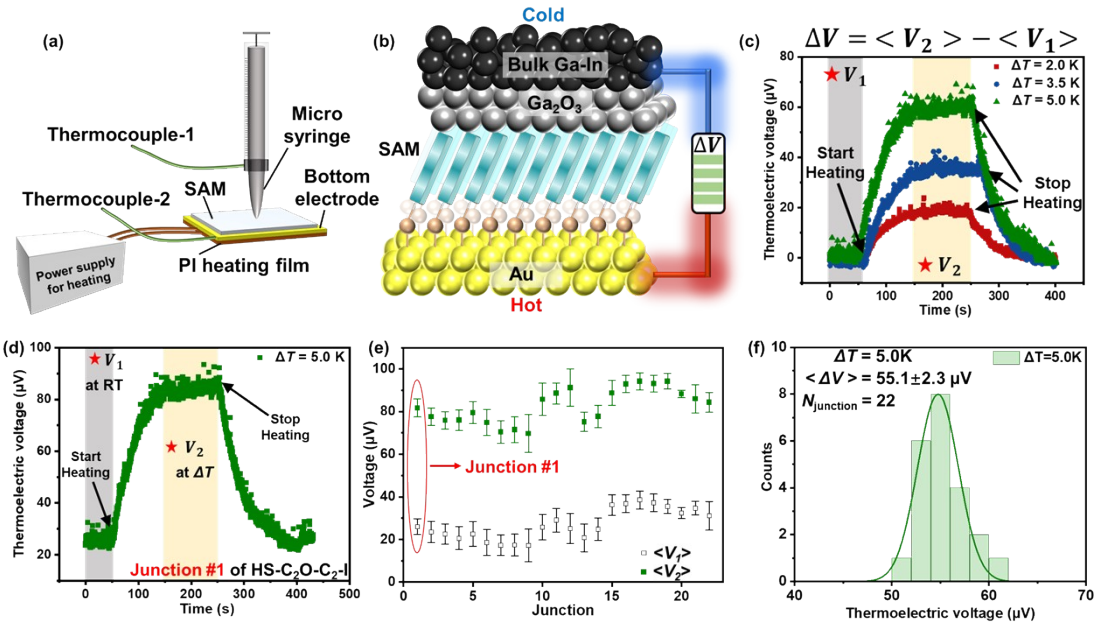

Fig. S83. The demonstrations of thermoelectric measurements conducted by the EGaIn technique. (a) The schematic diagram of the thermoelectric testbed developed from EGaIn technique. (b) The schematic illustration of a SAM-based thermoelectric junction (panel (a) and (b) are cited from our previous work[11]). (c) Thermoelectric voltage of Au^{TS}-S-C_2O-C_2-I//Ga_2O_3/EGaIn junctions at ΔT = 2.0 K (red), ΔT = 3.5 K (blue) and ΔT = 5.0 K (green). (d) Typical thermoelectric-voltage trace for Au^{TS}-S-C_2O-C_2-I (ΔT = 5 K). (e) The plot of ΔV against number of junctions from the SAMs of HS-C_2O-C_2-I at ΔT = 5.0 K. (f) The plot of histograms of $<\Delta V>$ (the mean value of ΔV) over 20 junctions with a Gaussian fit.

Once we heated the bottom electrode, ΔT occurred and the measured voltage was positively shifted. When the junction reached thermal equilibrium, the average of V_2 ($<V_2>$) and its standard deviation were calculated over 100 s test time with a Gaussian fit. Then, the ΔV was obtained by using $<V_2>$ subtracting $<V_1>$ at a certain ΔT for each junction. Fig.. S83c shows that the measured values of ΔV of Au^{TS}-S-C_2O-C_2-I//Ga_2O_3/EGaIn junction were enhanced as ΔT increased, verifiably demonstrating that our method is suitable for testing the thermoelectric effects of molecular junctions with high stability. In order to draw statistically robust results, we collected large amounts of experimental data. Fig. S83d depicts a typical thermoelectric voltage trace for Au^{TS}-S-C_2O-C_2-I (ΔT = 5.0 K). As mentioned above, we

carried out micro-voltage measurements across 400~450 seconds in total for each molecular junction, and each thermoelectric-voltage trace contained three stable sections: the first section started from 0 to 50 s which contained ~500 data points of V_1 (typically ranging from 10.00 μV to 40.00 μV); the second section started from ~150 s to ~250 s which contained ~1000 data points of V_2; the third section started from the time when heating stopped till the voltage dropped to a constant value close to V_1 for another 100s (from 350s to 400s). Fig.. S83e shows ΔV measured with 22 junctions of Au^{TS}-S-C_2O-C_2-I at ΔT = 5.0 K on three samples. For each junction, for instance the junction #1 marked with red ellipse in Fig. S83e, the black empty square represented $<V_1>$ averaged from ~500 data points of V_1, and the green solid square represented $<V_2>$ averaged from ~1000 data points of V_2. We recorded at least 20 junctions for each SAM at each applied ΔT on three samples in order to generate a histogram of ΔV that can be fitted with Gaussians to determine the mean value of ΔV ($<\Delta V>$) and the corresponded standard-deviation, as shown in Fig. S83f.

We proposed that the contact area between the EGaIn tip and the SAMs as well as the details of the shape of the EGaIn conical surface had insignificant influences on the mean values of Seebeck coefficient of the molecular junctions. The reasons were explained as bellow: 1) according to Reddy *et al*. [16], the molecules in a multiple molecule junction acted as independent channels when the intermolecular interactions were weak, indicating that the measured multiple molecule junction (monolayer) Seebeck coefficients were in very good agreement with previous measurements of corresponding single-molecule junctions; 2) the surface area of the heated bottom electrode (> 1 cm^2) was dramatically larger than that of the cold EGaIn tip contacting with the SAMs (~100 μm^2), hence, the small change in the contact area between the EGaIn tip and the SAMs had tiny effect on the amount of heat transferring from the bottom electrode (hot side) to the EGaIn electrode (cold side); 3) the extracted Seebeck coefficient was based on the statistically significant value over 21 different junctions on three samples, which could reduce the error of the experimental data to a considerable degree induced by various shape of the EGaIn surface.

Analysis of relationship between measured ΔV and *S* of the SAMs. As shown in Fig. S84, after the SAMs assembled on Au^{TS} electrode, T_1, V_1 and T_4, V_4 were defined as the temperature (room temperature) and potential of Syringe and tungsten (W) tip away from SAMs, respectively ($T_1 = T_4$). T_2 and V_2 were the temperature measured by thermocouple potential of Syringe close to SAMs. V_3 and T_3 are the potential and temperature of Au surface. We found that the measured T_2 was higher than room temperature and approximately half as T_3 perhaps due to the heat radiation and convection from the bottom electrode to the EGaIn tip. We defined that ΔT was the temperature difference between the temperature of Syringe (T_1, room temperature) or tungsten tip (T_4, room temperature) away from the SAMs and the temperature of the heated bottom electrode, $\Delta T_3 = (T_1 - T_3) = (T_4 - T_3)$; ΔT_1 was equivalent to $(T_1 - T_2)$; ΔT_2 was equivalent to $(T_2 - T_3)$. Considering the measured T_2 was half of T_3, we inferred that the value of ΔT_1 was almost the same as ΔT_2. Then, the temperature difference (ΔT) across the molecular junction could be described as bellow (Equation S1):

$$\Delta T = \Delta T_2 \approx \Delta T_{1=} \frac{1}{2}\Delta T_3 = (T_1 - T_3) \quad \text{(S1)}$$

Therefore, the relationship between *S* and measured ΔV for Au/SAM//Ga_2O_3/EGaIn junctions can be generally depicted as Equation S2-S6.

$$S_{EGaIn} = -\frac{V_1 - V_2}{T_1 - T_2} = -\frac{\Delta V_1}{\Delta T_1} = -\frac{V_1 - V_2}{\Delta T} \quad \text{(S2)}$$

$$S_{SAM} = -\frac{V_2 - V_3}{T_2 - T_3} = -\frac{\Delta V_2}{\Delta T_2} = -\frac{V_2 - V_3}{\Delta T} \quad \text{(S3)}$$

$$S_W = -\frac{V_4 - V_3}{T_4 - T_3} = -\frac{\Delta V_3}{\Delta T_3} = -\frac{V_4 - V_3}{2\Delta T} \quad \text{(S4)}$$

$$S_{EGaIn} + S_{SAM} - 2S_W = -\frac{V_1 - V_2}{\Delta T} - \frac{V_2 - V_3}{\Delta T} - (2 \times \frac{V_4 - V_3}{2\Delta T}) = -\frac{V_1 - V_4}{\Delta T} \quad \text{(S5)}$$

Wherein the $(V_1 - V_4)$ represented the measured ΔV in this work. According to the previous works,[11, 17] the values of thermopower of W tip (S_W) and thermopower of EGaIn (S_{EGaIn}) are ~1.0 μV/K and 3.0μV/K, respectively, hence the S_{SAM} can be extracted as follows.

$$S_{SAM} = -\frac{V_1 - V_4}{\Delta T} - S_{EGaIn} + 2S_W = -\frac{V_1 - V_4}{\Delta T} - 1 \quad \text{(S6)}$$

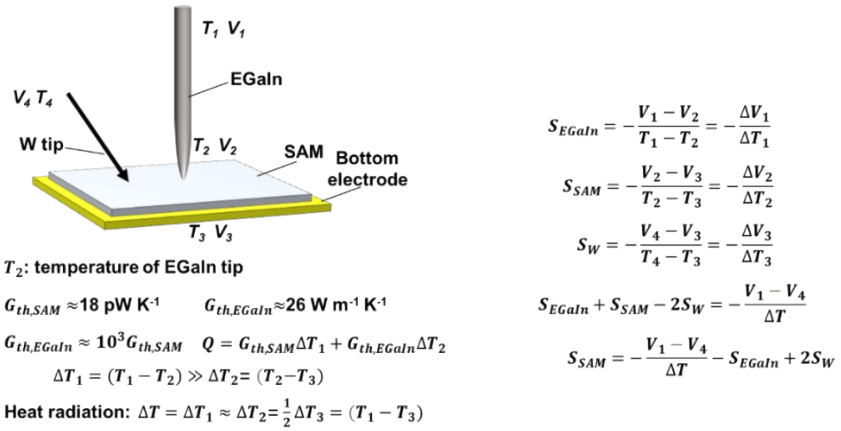

Fig. S84. Schematic diagram of the voltages and temperatures across Au/SAM//Ga_2O_3/EGaIn junction. [11]

Determination of power factor (PF). The values of PF of Au-SAMs//Ga_2O_3/EGaIn junctions were determined by the previously reported procedure. [11, 18] The magnitude of electric field intensity (ε) can be given by:

$$\varepsilon = \frac{V}{l}\,(GV\,m^{-1}) \tag{S7}$$

where V is the applied voltage and l is the molecular length considering the tilt angle (30°) of SAMs. The conductivity (σ) is the inverse of resistivity, and can be obtained as follows:

$$\sigma = \frac{J}{\varepsilon}\,(\mu S\,cm^{-1}) \tag{S8}$$

J (A cm^{-2}) is the current density. Using the calculated σ value and the measured S, the power factor (PF) value was obtained according to the following relationship:

$$PF = S^2\sigma\,(\mu W\,K^{-2}\,m^{-1}) \tag{S9}$$

Mini-discussion about the effects of heteroatom substitutions on *G*, *S* and related PF. S and G are derived from the charge transport in the molecular junctions under the applied temperature field and the electrical field, respectively.[19] Generally, the temperature field can only widen the Fermi distribution of the electrode. While the electrical field can regulate the relative position between the Fermi level of the electrode and the frontier orbitals of the molecules, thereby significantly affecting the potential barrier for electron tunneling in the molecular junctions or allowing more molecular orbitals to participate in charge transport [20-

22], making the *G* of the molecular junctions easier to be enhanced.

The value of *S*, to a greater extent, depend on the nature of the molecules, including the detailed location of the frontier orbitals and coupling strength between the molecules and the electrodes. The molecules designed in this study did indeed have a more pronounced improvement in *G* than *S*. Many previous studies have shown that the increased *G* of the molecular junctions led to a decrease in *S*, and vice versa [23-26] However, this work mainly proposes a molecular design method based on heteroatom substitutions to regulate the PF of the molecular junctions, which could enhance *G* than *S* at the same time and be potential for the further applications of high-efficient nanoscale thermoelectric devices.

According to Whitesides[14] *et al*. reported, the introducing oxygen atoms into the backbone contributed to the high-lying, delocalized molecular orbitals along the molecular skeleton direction, which remarkably improve *G* of the molecular junctions, consistent with our results. In order to improve *S*, it is necessary to simultaneously regulate the position of the frontier orbitals of molecules and the related coupling strength with the electrodes. Comparing with HS-C_n, introducing oxygen atoms into the backbone did not change the coupling strength between the molecules and the electrodes, causing an insignificant effect on *S*. This is why we further introduced iodine atoms as the terminal group of the molecules, which could reduce the interfacial resistance of charge transfer between the molecules and the top electrode by 5 times and dramatically boost the coupling strength between the molecules and the electrodes.[1]

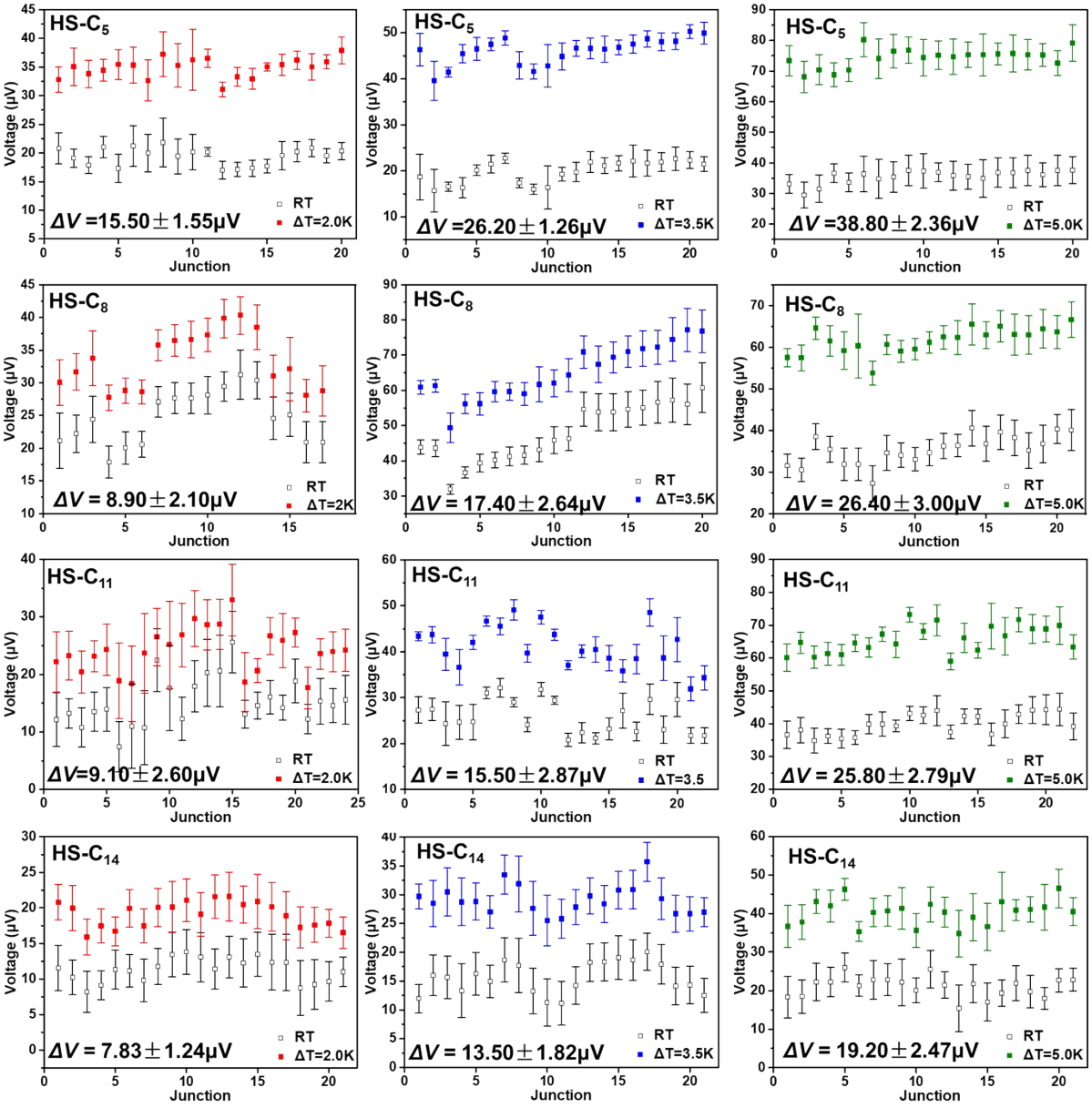

835

836 **Fig. S85.** The potential change of Au-S-C_n//Ga_2O_3/EGaIn junctions for each junction (n =

837 5, 8, 11, 14).

838

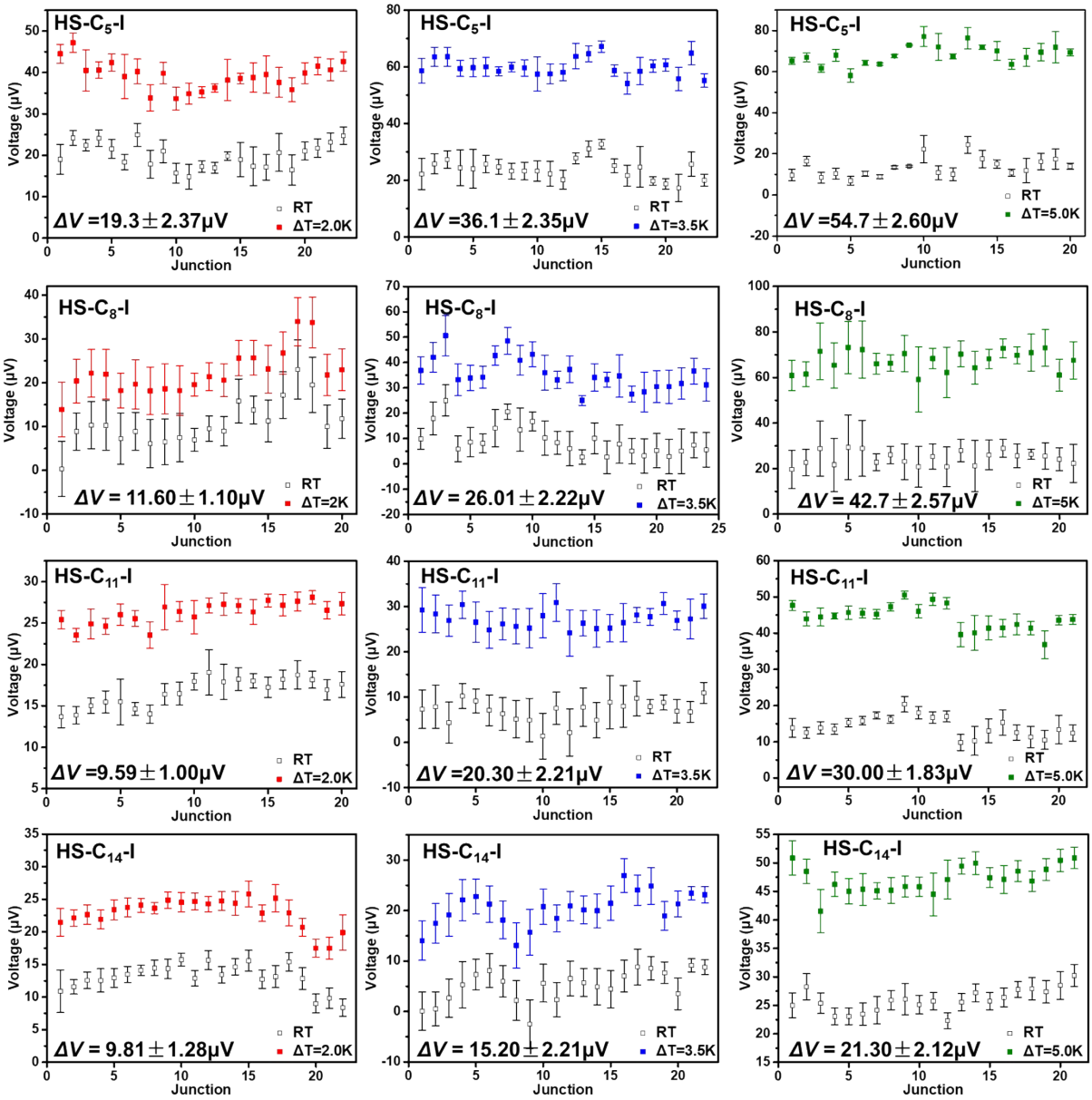

Fig. S86. The potential change of Au-S-C_n-I//Ga_2O_3/EGaIn junctions for each junction (n =5, 8, 11, 14).

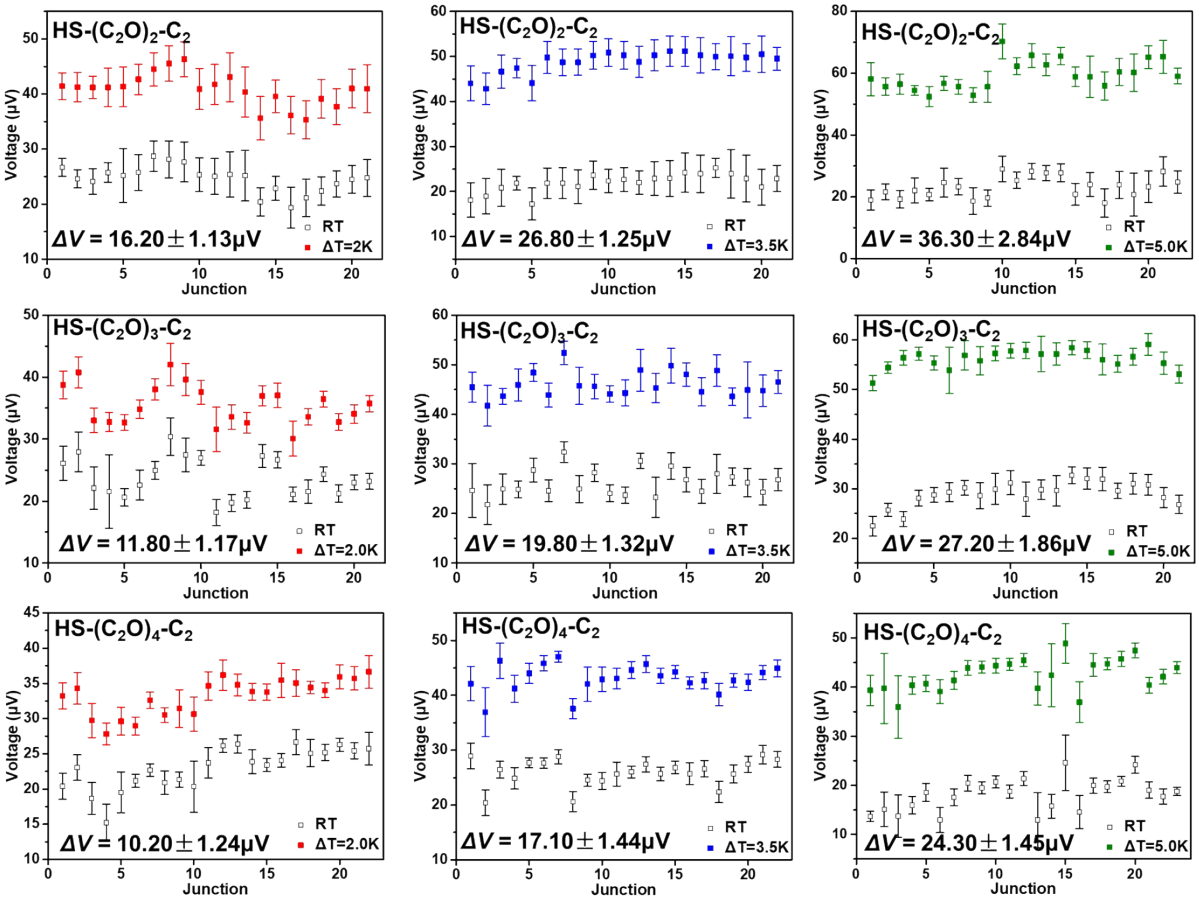

843

844 **Fig. S87**. The potential change of Au-S-$(C_2O)_m$-C_2//Ga_2O_3/EGaIn junctions for each

845 junction (m = 2, 3, 4).

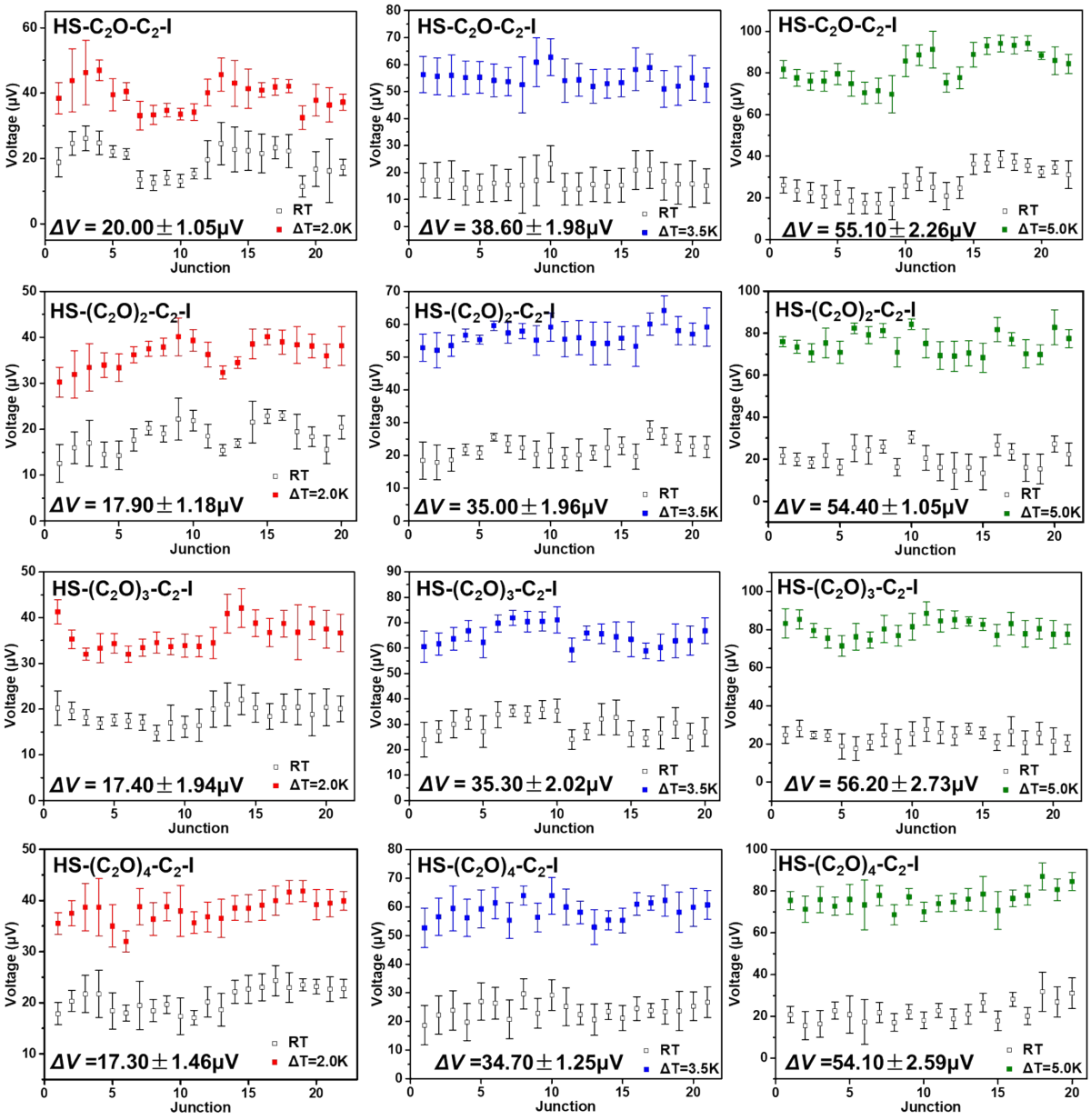

Fig. S88. The potential change of Au-S-$(C_2O)_m$-C_2-I//Ga_2O_3/EGaIn junctions for each junction (m = 1, 2, 3, 4).

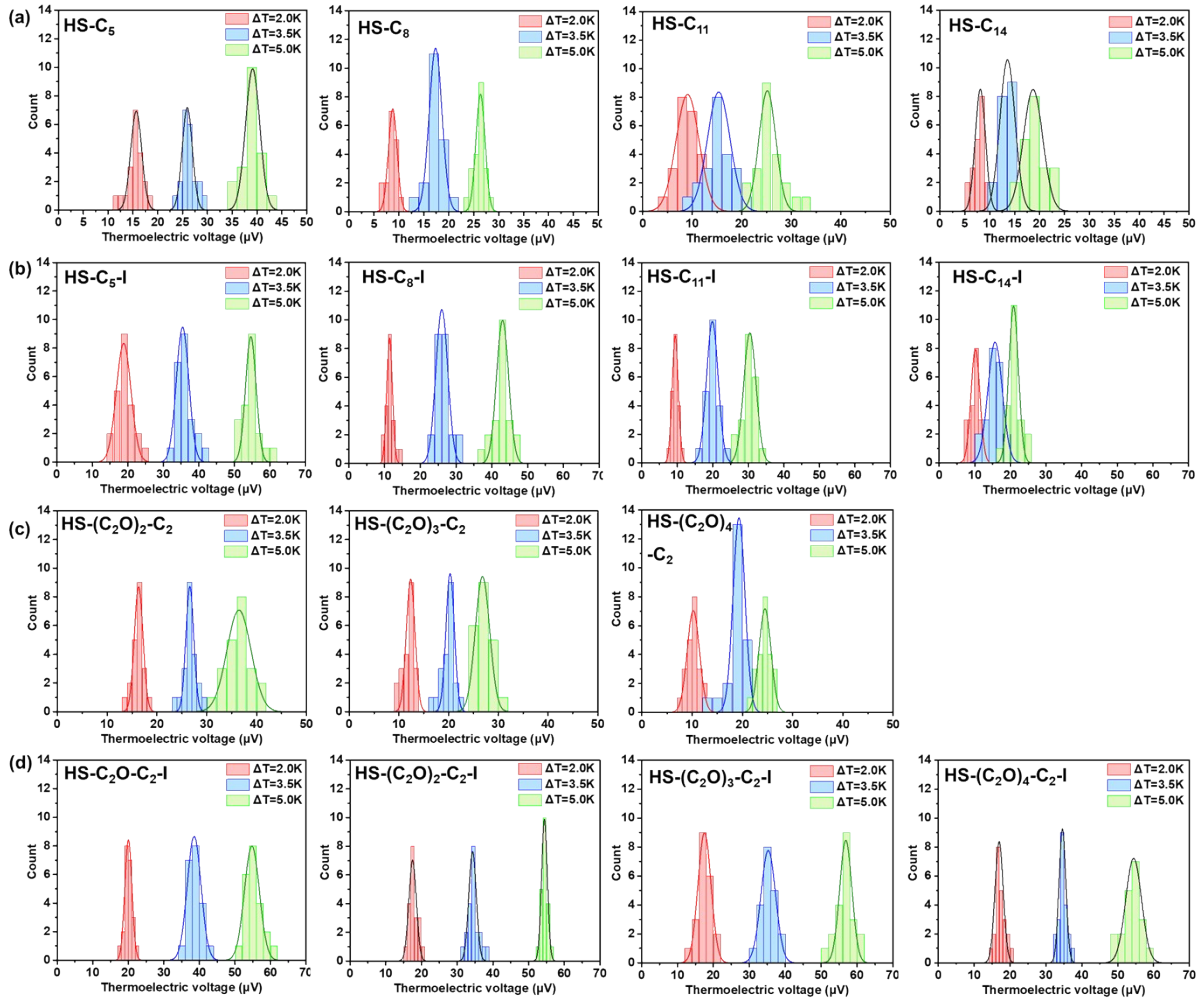

851

852 **Fig. S89.** The ΔV at each applied ΔT and the corresponding histograms of ΔV with a

853 Gaussian fit to these histograms of Au-SAMs//Ga_2O_3/EGaIn junctions with (a) HS-C_n (n = 5,

854 8, 10, 11), (b) HS-C_n-I (n = 5, 8, 10, 11), (c) HS-$(C_2O)_m$-C_2 (m = 2, 3, 4), (d) HS-$(C_2O)_m$-C_2-I

855 (m = 1, 2, 3, 4).

856

857

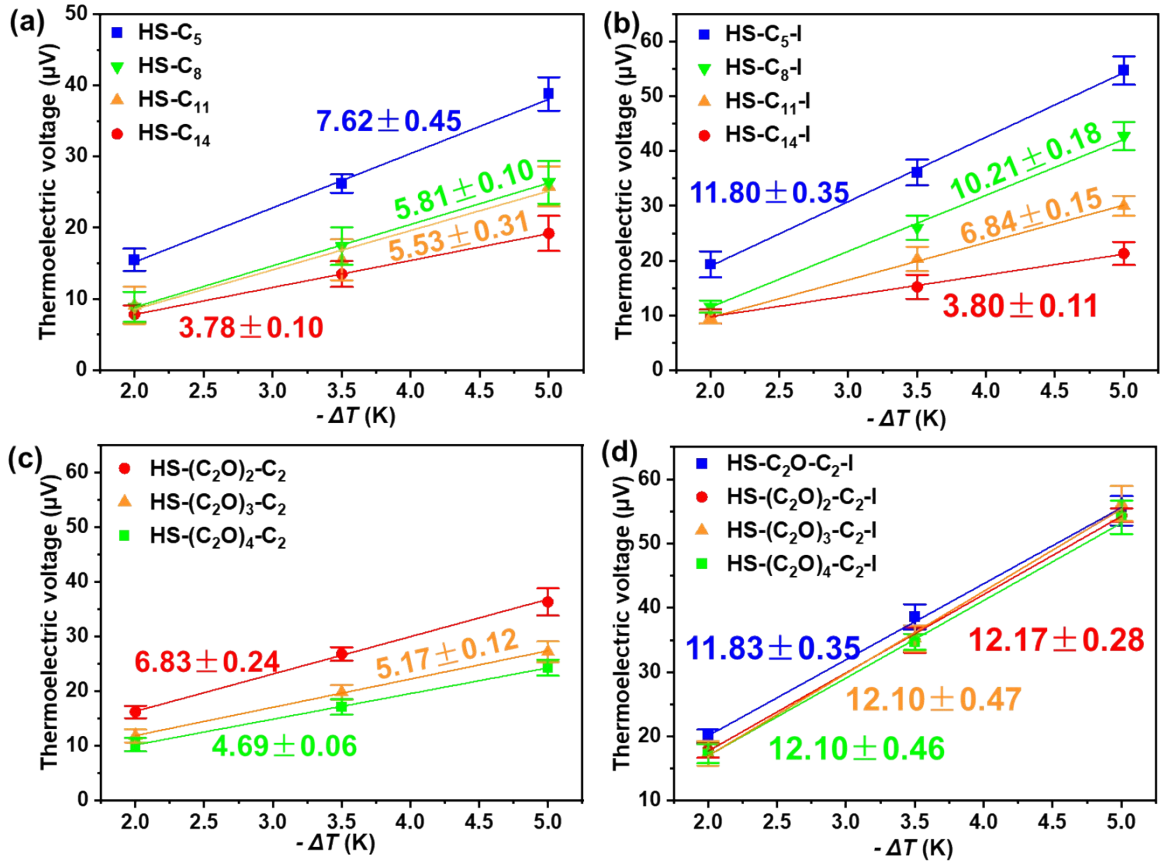

858

859 **Fig. S90**. Plots of thermoelectric voltage verses Δ*T* of Au-SAMs//Ga_2O_3/EGaIn junctions

860 with (a) HS-C_n (n = 5, 8, 10, 11), (b) HS-C_n-I (n = 5, 8, 10, 11), (c) HS-$(C_2O)_m$-C_2 (m = 2, 3,

861 4), (d) HS-$(C_2O)_m$-C_2-I (m = 1, 2, 3, 4).

862

863 **S6. DFT calculation.**

864 **Electronic structure**. The electronic structures of the considered junctions were calculated

865 using the SIESTA package at DFT level. The standard norm-conserving pseudopotentials and

866 a numerical linear combination of an atomic orbital basis set were employed in this package.

867 We used the double-ζ polarized (DZP) basis sets for H, C, O, S and I atoms and single-ζ

868 polarized (SZP) for Au. A real-space grid was defined with an energy cutoff of 200 Ry. All

869 atoms, expect for the Au electrode, were relaxed until the forces acting on them were less than

870 0.02 eV/Å. The temperature used for calculation of thermoelectric coefficient was set as 300

871 K. The optimized structures of molecular junctions are shown in Fig. S91 and S94.

872 **Transmission coefficients.** Upon the electronic structures were obtained from the converged

DFT calculation, we can calculate the transmission coefficients by means of the non-equilibrium Green's function method implemented in TRANSIESTA and the "post-processing" code TBtrans. To eliminate the influence of surface states on top electrode, the wide-band approximation was employed based on the convergent hamiltonian and overlap matrix (Fig. S95).

Thermoelectric coefficients. Based on the calculated transmission coefficients, the electrical conductance (G), Seebeck coefficient (S) and power factor (PF) can be calculated in the framework of a linear response regime. The G, S and PF can be written as follows:

$$G(\mu, T) = \frac{I}{\Delta V}\Big|_{\Delta T = 0} = e^2 L_0 \tag{10}$$

$$S(\mu,T) = -\frac{\Delta V}{\Delta T}\Big|_{I=0} = -\frac{1}{eTL_0}\frac{L_1}{} \tag{11}$$

$$PF = GS^2 \tag{12}$$

Here the coefficient L_n dependent on the transmission coefficient.

$$L_n(\mu,T) = \frac{1}{h}\int_{-\infty}^{\infty}(E-\mu)^n T(E)\left(-\frac{\partial f(E,\mu,T)}{\partial E}\right)dE \tag{13}$$

The Fermi energy also depends on the experimental conditions, such as the adsorbed water, the defects in the electrodes, which gives rise to the discrepancy between experimental and DFT-predicted values. [27-29] Therefore, our calculated Fermi level may not capture the real electronic structure of our junctions. We find that only when the Fermi level is located near these resonant states (E = -1.83 eV), could the theoretical results be consistent with experimental ones, that may because we used the both Au electrodes to simplify the real liquid metal-based junctions.

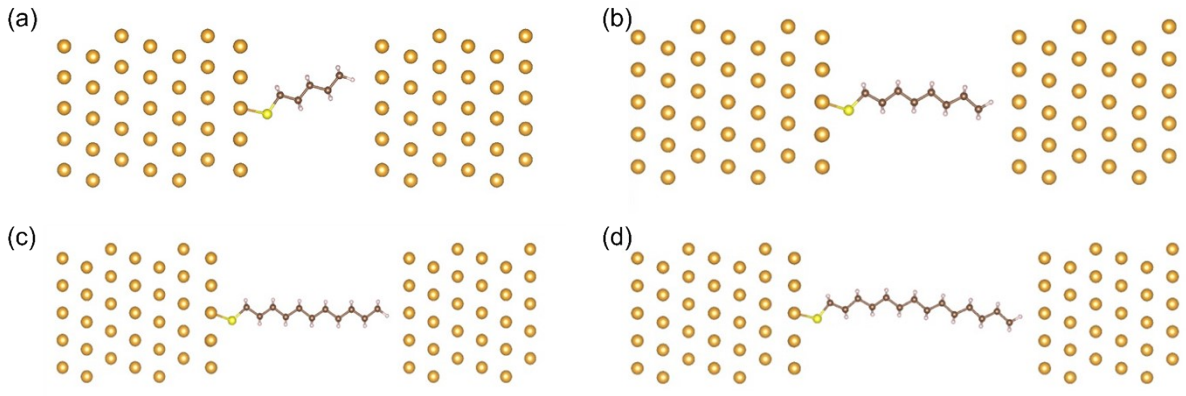

Fig. S91. The optimized structure of molecular junctions for (a) HS-C_5, (b) HS-C_8, (c) HS-C_{11}, (d) HS-C_{14}.

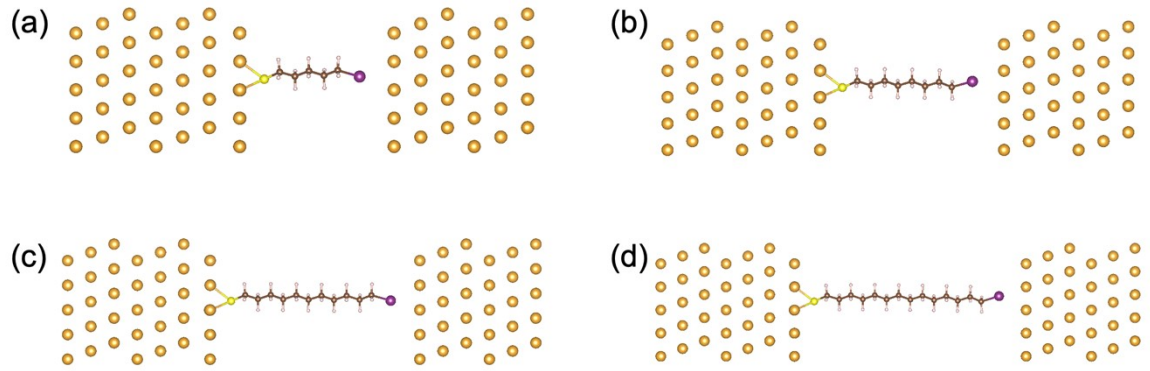

Fig. S92. The optimized structure of molecular junctions for (a) HS-C_5-I, (b) HS-C_8-I, (c) HS-C_{11}-I, (d) HS-C_{14}-I.

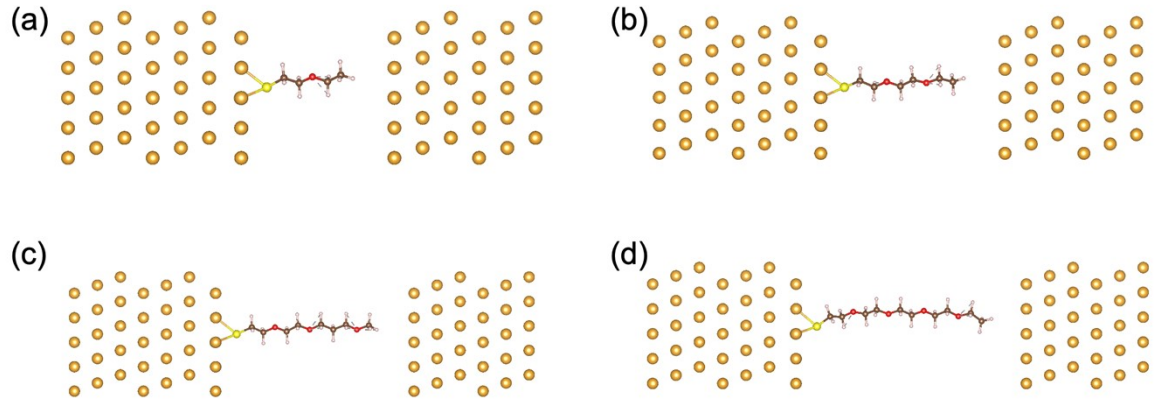

Fig. S93. The optimized structure of molecular junctions for (a) HS-C_2O-C_2, (b) HS-$(C_2O)_2$-C_2, (c) HS-$(C_2O)_3$-C_2, (d) HS-$(C_2O)_4$-C_2.

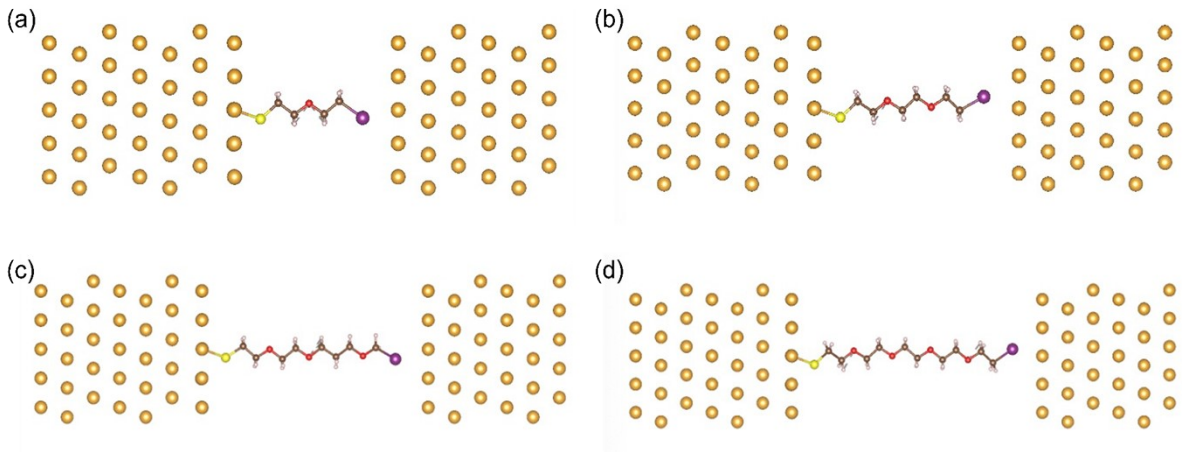

Fig. S94. The optimized structure of molecular junctions for (a) HS-C_2O-C_2-I, (b) HS-$(C_2O)_2$-C_2-I, (c) HS-$(C_2O)_3$-C_2-I, (d) HS-$(C_2O)_4$-C_2-I.

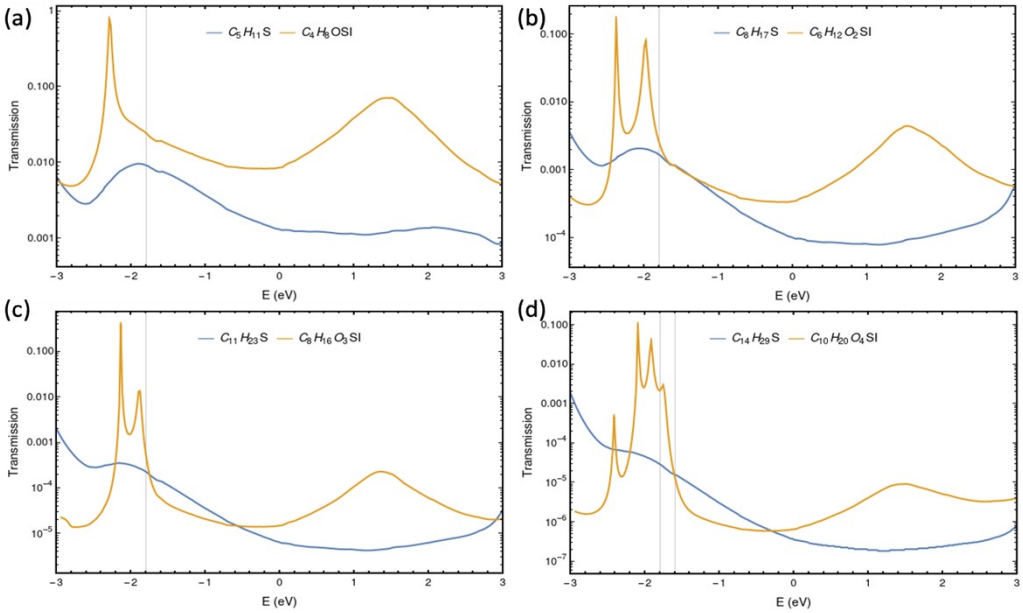

Fig. S95. The calculated transmission coefficient for (a) HS-C_5, HS-C_2O-C_2-I, (b) HS-C_8, HS-$(C_2O)_2$-C_2-I, (c) HS-C_{11}, HS-$(C_2O)_3$-C_2-I, (d) HS-C_{14}, HS-$(C_2O)_4$-C_2-I.

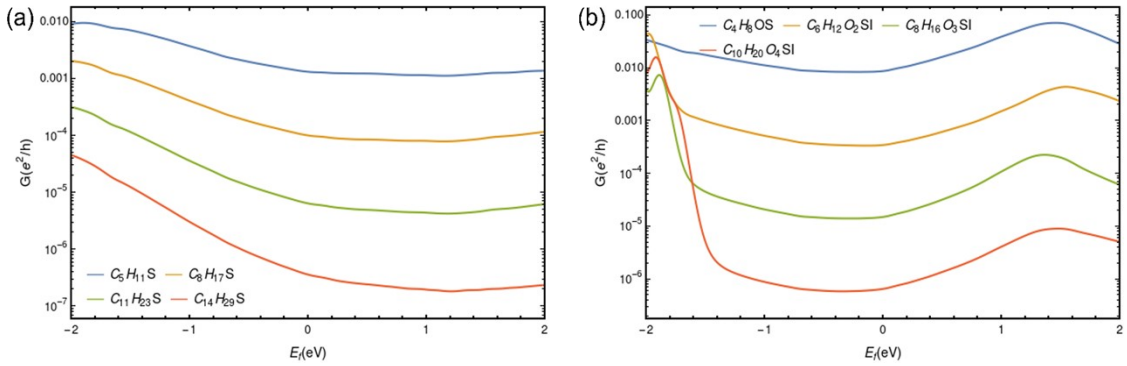

Fig. S96. The calculated electrical conductance (G) with different Fermi energy for (a) HS-C_n, (b) HS-$(C_2O)_m$-C_2-I.

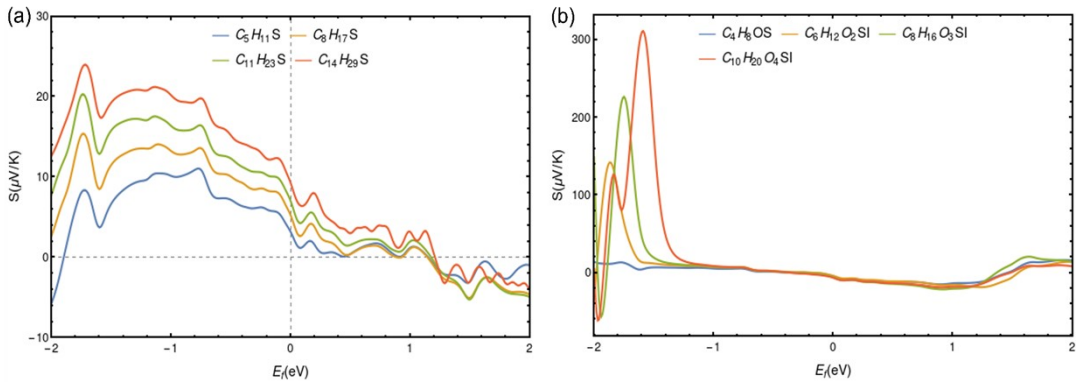

Fig. S97. The calculated Seebeck coefficients (*S*) with different Fermi energy for (a) HS-C_n, (b) HS-$(C_2O)_m$-C_2-I.

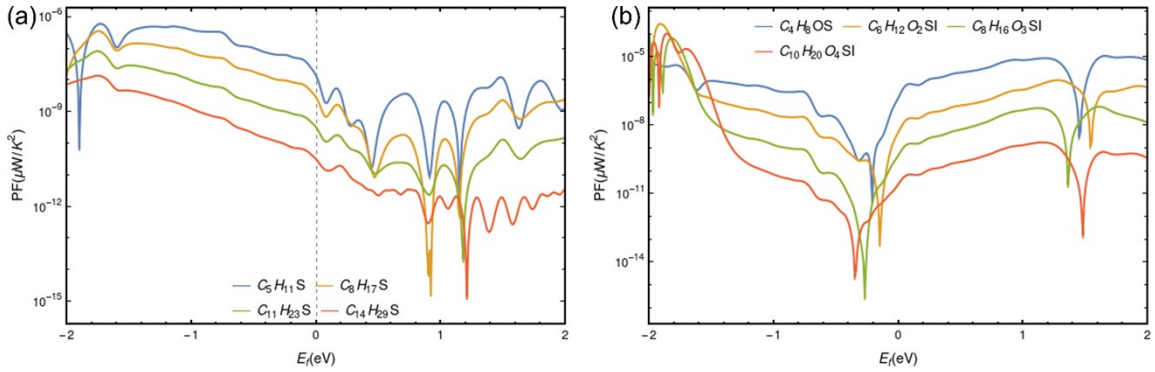

Fig. S98. The calculated power factor (PF) with different Fermi energy for (a) HS-C_n, (b) HS-$(C_2O)_m$-C_2-I.

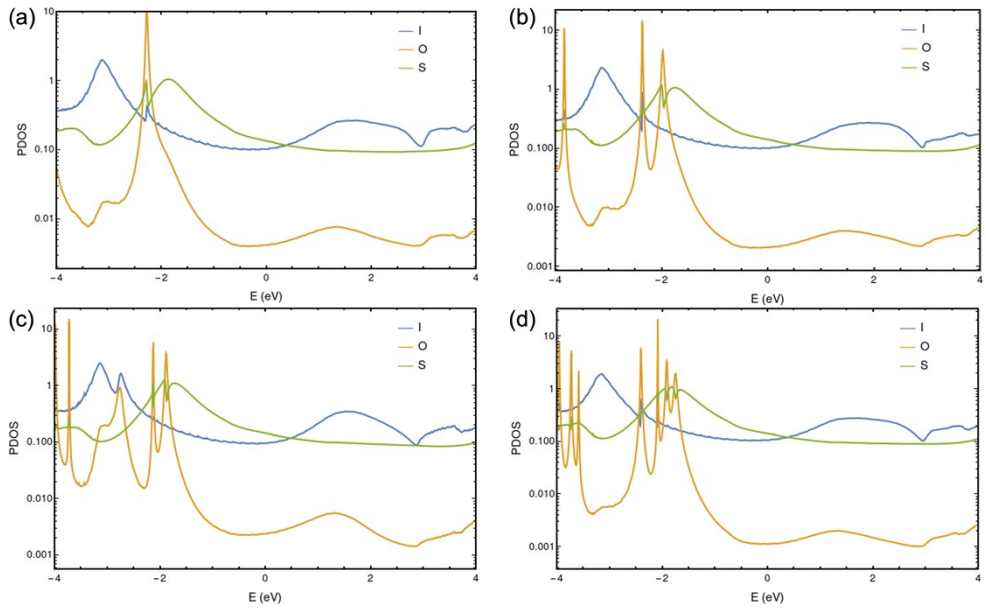

Fig. S99. The calculated projected density of states (PDOS) for (a) HS-C_2O-C_2-I, (b) HS-$(C_2O)_2$-C_2-I, (c) HS-$(C_2O)_3$-C_2-I, (d) HS-$(C_2O)_4$-C_2-I.

References

[1] X. Chen, B. Kretz, F. Adoah, C. Nickle, X. Chi, X. Yu, E.d. Barco, D. Thompson, D.A. Egger, C.A. Nijhuis, A single atom change turns insulating saturated wires into molecular conductors, *Nat. Commun. 12* (**2021**) 3432.

[2] K. Wang, X. Cai, W. Yao, D. Tang, R. Kataria, H.S. Ashbaugh, L.D. Byers, B.C. Gibb, Electrostatic Control of Macrocyclization Reactions within Nanospaces, *J. Am. Chem. Soc. 141* (**2019**) 6740.

[3] M. von Delius, F. Hauke, A. Hirsch, Evaluation of an Intramolecular Approach for the Synthesis of the Elusive C58N2Heterofullerene Family, *Eur. J. Org. Chem.* (**2008**) 4109.

[4] C. Wendeln, S. Rinnen, C. Schulz, T. Kaufmann, H.F. Arlinghaus, B.J. Ravoo, Rapid preparation of multifunctional surfaces for orthogonal ligation by microcontact chemistry, *Chem. Eur. J. 18* (**2012**) 5880.

[5] O. Zenasni, A.C. Jamison, M.D. Marquez, T.R. Lee, Self-assembled monolayers on gold generated from terminally perfluorinated alkanethiols bearing propyl vs. ethyl hydrocarbon spacers, *J. Fluorine Chem. 168* (**2014**) 128.

[6] Y. Cao, M. Zhang, C. Wu, S. Lee, M.E. Wroblewski, T. Whipple, P.I. Nagy, K. Takács-Novák, A. Balázs, S. Torös, J. William S. Messer, Synthesis and Biological Characterization of 1-Methyl-1,2,5,6-tetrahydropyridyl-1,2,5-thiadiazole Derivatives as Muscarinic Agonists for the Treatment of Neurological Disorders, *J. Med. Chem. 46* (**2003**) 4273.

[7] J. Provencher-Mandeville, C. Descoteaux, S.K. Mandal, V. Leblanc, E. Asselin, G. Berube, Synthesis of 17beta-estradiol-platinum(II) hybrid molecules showing cytotoxic activity on breast cancer cell lines, *Bioorg. Med. Chem. Lett. 18* (**2008**) 2282.

[8] Y. Aoki, N. Umezawa, Y. Asano, K. Hatano, Y. Yano, N. Kato, T. Higuchi, A versatile strategy for the synthesis of crown ether-bearing heterocycles: Discovery of calcium-selective fluoroionophore, *Bioorg. Med. Chem. Lett. 15* (2007) 7108.

[9] Y. Li, L. Jiang, B. Zhang, C.A. Nijhuis, Dependency of the tunneling decay coefficient in molecular tunneling junctions on the topography of the bottom electrodes, *Angew. Chem. Int. Edit. 53* (**2014**) 3377.

[10] J.-L. Lin, Z. Cao, X. Bai, N. Chen, C. Li, X. Xiao, L. Wang, Y. Li, Molecular diodes with tunable threshold voltage based on π-extended tetrathiafulvalene, *Adv. Mater. Interfaces 9* (**2022**) 2201238.

[11] W. Peng, Z. Cao, N. Chen, Y. Xie, Y. Li, Dependence of thermoelectric effects in molecular junctions on the topography of the bottom electrodes, *J. Mater. Chem. A 10* (**2022**) 23304.

[12] S. Doniach, M. Sunjic, Many-electron singularity in X-ray photoemission and X-ray line spectra from metals, *J. Phys. C Solid State Phys. 3* (**1970**) 285.

[13] Y. Han, C. Nickle, Z. Zhang, H. Astier, T.J. Duffin, D. Qi, Z. Wang, E. del Barco, D. Thompson, C.A. Nijhuis, Electric-field-driven dual-functional molecular switches in tunnel junctions, *Nat. Mater. 19* (**2020**) 843.

[14] M. Baghbanzadeh, C.M. Bowers, D. Rappoport, T. Żaba, Y. Li, K. Kang, K.-C. Liao, M. Gonidec, P. Rothemund, P. Cyganik, A. Aspuru-Guzik, G.M. Whitesides, Anomalously Rapid Tunneling: Charge Transport across Self-Assembled Monolayers of Oligo(ethylene glycol), *J. Am. Chem. Soc. 139* (**2017**) 7624.

[15] D. Wang, D. Fracasso, A. Nurbawono, H.V. Annadata, C.S.S. Sangeeth, Y. Li, C.A. Nijhuis, Tuning the Tunneling Rate and Dielectric Response of SAM-Based Junctions via a Single Polarizable Atom, *Adv. Mater. 27* (**2015**) 6689.

[16] A. Tan, J. Balachandran, S. Sadat, V. Gavini, B.D. Dunietz, S.Y. Jang, P. Reddy, Effect of length and

964 contact chemistry on the electronic structure and thermoelectric properties of molecular junctions, *J. Am.*
965 *Chem. Soc. 133* (**2011**) 8838.
966 [17] S. Park, H.J. Yoon, New approach for large-area thermoelectric junctions with a liquid eutectic Gallium-
967 Indium electrode, *Nano Lett. 18* (**2018**) 7715.
968 [18] S. Park, S. Kang, H.J. Yoon, Power factor of one molecule thick films and length dependence, *ACS*
969 *Cent. Sci. 5* (**2019**) 1975.
970 [19] K. Wang, E. Meyhofer, P. Reddy, Thermal and thermoelectric properties of molecular junctions, *Adv.*
971 *Funct. Mater. 30* (**2019**) 1904534.
972 [20] H. Xu, H. Fan, Y. Luan, S. Yan, L. Martin, R. Miao, F. Pauly, E. Meyhofer, P. Reddy, H. Linke, K.
973 Wärnmark, Electrical Conductance and Thermopower of *β*-Substituted Porphyrin Molecular Junctions-
974 Synthesis and Transport, *J. Am. Chem. Soc. 145* (**2023**) 23541.
975 [21] Y. Xie, C.-Y. Wang, N. Chen, Z. Cao, G. Wu, B. Yin, Y. Li, Supramolecular memristor based on
976 bistable [2]catenanes: toward
977 high-density and non-volatile memory devices, *Angew. Chem. Int. Ed. 62* (**2023**) e202309605.
978 [22] G.D. Kong, S.E. Byeon, J. Jang, J.W. Kim, H.J. Yoon, Electronic mechanism of *in situ* inversion of
979 rectification polarity in supramolecular engineered monolayer, *J. Am. Chem. Soc. 144* (**2022**) 7966.
980 [23] J. Jang, J.W. Jo, T. Ohto, H.J. Yoon, Seebeck effect in molecular wires facilitating long-range transport,
981 *J. Am. Chem. Soc. 146* (**2024**) 4922.
982 [24] A. Ismael, X. Wang, T.L.R. Bennet, L.A. Wilkinson, B.J. Robinson, C.J. Lambert, Tuning the
983 thermoelectrical properties of anthracene-based self-assembled monolayers, *Chem. Sci. 11* (**2020**) 6836.
984 [25] X. Wang, T.L.R. Bennett, A. Ismael, L.A. Wilkinson, J. Hamill, A.J.P. White, I.M. Grace, O.V.
985 Kolosov, T. Albrecht, B.J. Robinson, N.J. Long, L.F. Cohen, C.J. Lambert, Scale-up of room-temperature
986 constructive quantum interference from single molecules to self-assembled molecular-electronic films, *J.*
987 *Am. Chem. Soc. 142* (**2020**) 8555.
988 [26] R. Miao, H. Xu, M. Skripnik, L. Cui, K. Wang, K.G.L. Pedersen, M. Leijnse, F. Pauly, K. Wärnmark,
989 E. Meyhofe, P. Reddy, H. Linke, Influence of quantum interference on the thermoelectric properties of
990 molecular junctions, *Nano Lett. 18* (**2018**) 5666.
991 [27] S.A. Svatek, V. Sacchetti, L. Rodríguez-Pérez, B.M. Illescas, L. Rincón-García, G. Rubio-Bollinger,
992 M.T. González, S. Bailey, C.J. Lambert, N. Martín, a.N.s. Agraït, Enhanced thermoelectricity in
993 metal−[60]fullerene−graphene molecular junctions, *Nano Lett. 23* (**2023**) 2726.
994 [28] L. Rincón-García, A.K. Ismael, C. Evangeli, I. Grace, G. Rubio-Bollinger, K. Porfyrakis, N. Agraït,
995 C.J. Lambert, Molecular design and control of fullerene-based bi-thermoelectric materials, *Nat. Mater. 15*
996 (**2016**) 289.
997 [29] Y. Hu, J. Li, YuZhou, J. Shi, G. Li, H. Song, Y. Yang, J. Shi, W. Hong, Single dynamic covalent bond
998 tailored responsive molecular junctions, *Angew. Chem. Int. Ed. Engl. 60* (**2021**) 20872.
999